TIME RATE OF CHANGE OF GRAVITY IN NORTH AMERICA AND GREENLAND DUE TO POST GLACIAL REBOUND AND OTHER TECTONIC MOVEMENTS

Franck Olivier KAPOKO KAMTCHANG

A THESIS SUBMITTED TO THE FACULTY OF GRADUATE STUDIES IN

PARTIAL FULFILLMENT OF THE REQUIREMENTS FOR THE DEGREE OF

MASTER OF SCIENCE

GRADUATE PROGRAM IN EARTH AND SPACE SCIENCE

YORK UNIVERSITY

TORONTO, ONTARIO

April 2017

ABSTRACT

In the process to regain isostatic equilibrium following the Last Glacial Maximum, the Earth's crust is experiencing continuous uplift and/or subsidence, a phenomenon called Glacial Isostatic Adjustment (GIA). We determine the time rate of change of gravity (g-dot) due to GIA by estimating it directly from a Least-Squares adjustment of an integrated gravity network covering the continent. Observation equations are created based on historical relative gravity measurements and the network is constrained using g-dot values obtained from absolute gravity measurements. Recognizing that gravity variation is also influenced by other significant continuous geophysical processes (tides, tidal load and hydrology), such effects are removed by correcting all gravity measurements at the pre-adjustment stage. Results are presented in the form of a g-dot map and demonstrate that Canada's National Gravity Data Base (NGDB), with its over 50-year-long history, can provide us with useful constraints for the evaluation/verification and refinement of post-glacial rebound models.

DEDICATION

I will like to dedicate this work to my beloved parents Paul and Valentine Kamtchang whose constant support and most of all love was key to the completion of this thesis.

"I shall forever be in your debt"

ACKNOWLEDGEMENT

I will like to express my deepest gratitude and appreciation to my supervisor, Dr. Spiros Pagiatakis, for his continuous support and guidance and most of all, constant availability through the course of my studies here at York University. His experience, knowledge and expertise provided quality and accuracy to this work. His support and encouragement at different steps of the way made it possible, not only to obtain the best results, but to do so with relative ease.

The other member of my supervisory committee, Dr. Sunil Bisnath is also acknowledged for his support and enlightenment during the evaluation of this work.

I will like to thank Marc Véronneau, Team Leader of Gravity and Height Systems, Canadian Geodetic Survey (CGS), Natural Resources Canada (NRCan) for providing gravity data needed for the completion of this work. His constant ability to quickly provide clarification and additional information was vital for the completion of this work.

This research was financially supported by the Natural Sciences and Engineering Research Council of Canada (NSERC) project entitled “Integrated Geosciences for an enhanced understanding of our planet”.

Table of Content

List of Tables

List of Figures

List of Symbols

A: First design matrices

B: Second design matrices

C_l: Covariance matrix of observations

C_{l_0}: Covariance matrix of pseudo vector of observations

$C_{\hat{x}}$: Covariance matrix of estimated parameters

$\hat{C}_{\hat{x}}$: Estimated covariance matrix of estimated parameters

$C_{\hat{v}}$: Covariance matrix of estimated residuals

$\hat{C}_{\hat{v}}$: Estimated covariance matrix of estimated residuals

D_k^t: Drift of instrument *k* at epoch *t*

G: Universal gravitational constant

H: Height of water at the station

$\dot{g}_i$: Time rate of change of gravity at station *i*

Δg_{ij}^t: Relative gravity measurement between station *i* and station *j* at time *t*

g_i^t: Gravity at station *i* at time *t*

$g_i^{t_0}$: Gravity at station *i* at reference epoch t_0

I: Identity matrix

$\bar{l}$: Vector of observations

l_0: Pseudo vector of observations

k: Standard deviation assigned by analyzing the vector of observations used in previous adjustment

P: Weight matrix

r: Degrees of freedom

ρ: Density of fresh water

σ_0^2: A-priori variance factor

$\hat{\sigma}_0^2$: A-posteriori variance factor

δg_B: Inner zone hydrology effect

S_k^t: Scale of instrument *k* at epoch *t*

Δt_{ij}^t: Time elapsed between reading at station i and j at epoch *t*

t_0: Reference epoch

v: Vector of residuals

$\hat{v}$: Estimated vector of residuals

w: Misclosure vector

$\overline{x}$: Vector of unknown parameters

$\hat{\overline{x}}$: Estimated vector of unknown parameters

x^0: Initial approximation to the solution vector

x: Correction to initial approximation to the solution vector

List of Abbreviations

AG:	Absolute Gravimeter
BIFROST:	Baseline Inferences for Fennoscandia Rebound Observations Sea Level and Tectonics
CACS:	Canadian Active Control System
CBN:	Canadian Base Network
CGS:	Canadian Geodetic Survey
CGSN:	Canadian Gravity Standardization Network
CORS:	Continuously Operating Reference Station
FES:	Finite Element Solution
GIA:	Glacial Isostatic Adjustment
GLONASS:	Global Navigation Satellite System
GNET:	Greenland GPS Network
GNSS:	Global Navigation Satellite System
GOCE:	Gravity Field and Steady-State Ocean Circulation Explorer
GPS:	Global Positioning System
GRACE:	Gravity Recovery and Climate Experiment
GRAVNET:	Gravity Network Software
GSC:	Geological Survey of Canada
g-dot:	Time Rate of Change of Gravity
HRDG:	Higher Reading Difference in Gravity
IGOS:	Integrated Global Observing Strategy
IGSN71:	International Gravity Standardization Network of 1971

K1:	Diurnal Luni-Solar Declinational
K2:	Semidiurnal Luni-Solar Declinational
LGM:	Last Glacial Maximum
LRDG:	Lower Reading Difference in Gravity
LSSA:	Least-Squares Spectral Analysis
L&R:	Lacoste and Romberg Gravimeter
M2:	Semidiurnal Principal Lunar
Mf:	Long-period Lunar Fortnightly
N2:	Semidiurnal Major Lunar Elliptical
NOAA:	National Oceanic and Atmospheric Administration
NGDB:	National Gravity Data Base
NRCAN:	Natural Resources Canada
NSERC:	Natural Sciences and Engineering Research Council of Canada
N-dot:	Time Rate of Change of Geoid Undulation
O1:	Diurnal Principal Lunar
P1:	Diurnal Principal Solar
PGR:	Post Glacial Rebound
POSTGRAVNET:	Post Gravity Network Software
PREGRAVNET:	Post Gravity Network Software
PREM:	Preliminary Reference Earth Model
Q1:	Diurnal Major Lunar Elliptical
R-square:	Coefficient of Determination
S2:	Semidiurnal Principal Solar
VCM:	Vertical Crustal Movement

WGHM:	WaterGAP Global Hydrology Model
WLSR:	Weighted Least-Squares Regression

Chapter 1

Introduction

This introductory chapter provides background information necessary for clear understanding of the work about to be presented. The information here is fundamental and summarizes the objectives of this research. Readers interested in a deeper understanding of phenomena described herein are referred to the references at the end for more literature on specific topics.

In this chapter, Glacial Isostatic Adjustment (GIA) and its influence on Earth's gravity field is described. Moreover, an overview of the Canadian Gravity Standardization Network (CGSN) and the Canadian National Gravity Data Base (NGDB) is presented. We conclude this chapter with two sections: one outlining the research goals and objectives of this thesis and the second describing the main contributions of the research.

1.1 THE ICE AGE AND GLACIAL ISOSTATIC ADJUSTMENT

Geodesy is the science of accurately measuring and understanding three fundamental properties of the Earth: its geometric size and shape, its orientation in space, and its gravity field as well as the changes of these properties with time (NOAA, 2015). Changes to the Earth's geometrical shape, often referred to as deformation, are caused by various forces (e.g. tidal force). Once these forces are removed, the Earth tends to recover its original shape. A medium that behaves in such a fashion (response dependent on the frequency of deforming force) is known as visco-elastic (VANÍCEK AND KRAKIWSKY, 1986). Recovery varies from a fraction of a second to thousands of years depending on the phenomenon and the length of time the force was applied.

Over the past 2.6 million years, the Earth has experienced several ice ages (OCHES, 2009) which have contributed to its shape as we know it today. One such event of utmost importance is the last glacial period, which began 110,000 years ago (MATSON ET AL., 2010) when temperatures in the Northern and Southern Hemispheres dramatically dropped below 0 °C and remained at this level for over 90,000 years (PELTIER, 1994). With sub-zero temperatures all year round, the snow never melted. A major snow storm could drop millions of tons of snow over the cold land surface. The ever increasing weight of the snow compacted into thick layers of solid ice called ice sheets. The ice sheets reached its thickest at the Last Glacial Maximum (LGM) about 20,000 years ago (*IBID, 1994*). In fact, many researchers (e.g. GORDON, 1983; GOSNELL,

2007; SELLA ET AL., 2007 etc.) argue that ice was thickest in the region around Hudson Bay reaching almost 3 km. A large portion of North America was covered with ice of varying thickness which caused the continent to undergo deformation. Naturally, the magnitude of the deformation varied according to ice thickness.

FIGURE 1.1 shows three prominent glaciations that occurred in North America during the LGM. These are the Cordilleran, Laurentide and Greenland ice sheets named historically according to their geographic distribution. Interested readers are referred to DYKE ET AL (2002), BOOTH ET AL.,(2003), GONG ET AL., (2015), etc. for a deeper understanding of the formation of these ice sheets.

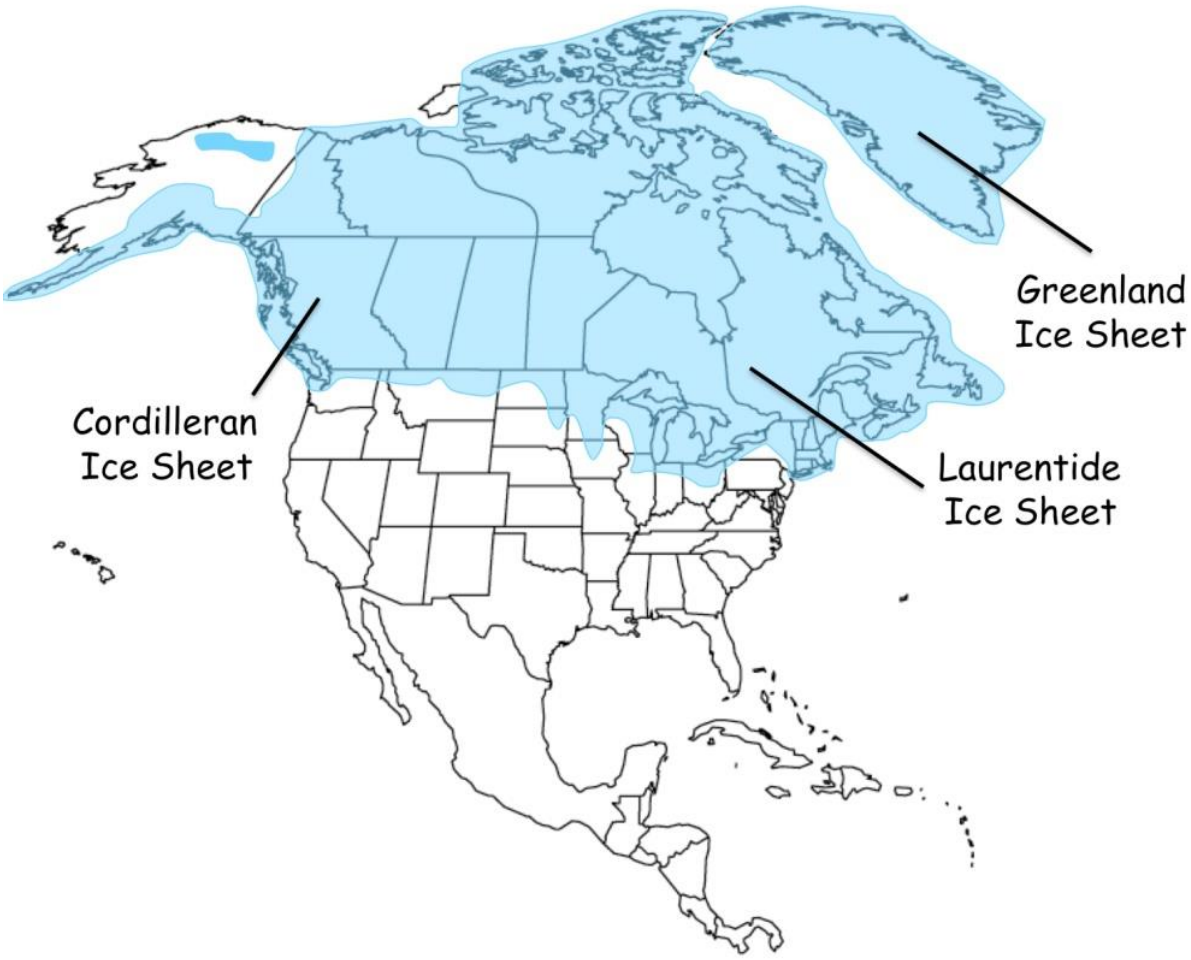

FIGURE 1.1: Ice coverage of North America during the Last Glacial Maximum (LOUGHEED & MORRILL, 2016).

Following the LGM, most of North America was buried deep under ice for over 4000 years. It is only about 17,000 years ago when deglaciation began (HULTON, 2002), exposing slowly the land mass. Melting ice was at the origin of declining pressure on land surface and is one of the major causes of uplift in many areas of the continent. This rise of the land masse that was suppressed by the weight of ice sheet is what is called Post Glacial Rebound (PGR), a phenomenon still in progress and observable today. Glacial Isostatic Adjustment (GIA) is a more precise term that includes the uplift and/or subsidence of land mass, melting or build-up of ice, and mass transfer and redistribution including sea level rise.

Points on the surface of the Earth are within the Earth's gravity field and therefore within the immediate gravitational potential (work done per unit mass to move that point to a reference point) that is inversely proportional to its distance from Earth's centre and proportional to the mass of the Earth. Points of equal gravitational potential are called equipotential surfaces; in fact the geoid is the equipotential surface that best fits the global mean sea level. In regions like North America, where the GIA is in progress, the surface of the Earth changes gradually causing gravity field changes as well. In addition, there is mass redistribution caused by uplift and/or subsidence in different regions, which in turn causes gravity variation in an indirect mode. Therefore, GIA in North America can be studied by observing gravity variation in the area, specifically what is done in this work.

1.2 THE CANADIAN GRAVITY STANDARDIZATION NETWORK (CGSN) AND THE CANADIAN NATIONAL GRAVITY DATA BASE (NGDB)

> "*Otto J. Klotz was the first to use the original Mendenhall pendulum gravimeter in Canada in 1902. He acquired his first readings in Ottawa and later Montreal and Toronto to demonstrate the utility of gravimetry to the Dominion Observatory.*
>
> (NATURAL RESOURCES CANADA, 2016)

The Canadian Gravity Standardization Network (CGSN) was established in the 1950s to provide gravity control, primarily for geophysical exploration purposes. It is defined by more than 1,400 control stations systematically distributed throughout Canada (NRCAN, 2016), 64 of which are primary gravity stations located at very stable sites for high quality gravity measurements. Each of the 64 sites encompasses several gravity stations that form an ''excentre network'' (cluster), whose spatial extent is a few to several kilometres (PAGIATAKIS & SALIB, 2003). Each excentre station in the cluster has been tied to the primary station and other excentre stations by high precision relative gravity measurements. The main objective of excentre stations was to aid in recovery of primary stations in the event of damage or loss. Secondary

stations on the other hand are located on sites that are not as stable and so provide less reliable measurements. The CGSN is linked to the international network at 3 stations; Schefferville, Penticton and Yellowknife making them International Absolute Gravity Base Network (IAGBN) stations.

> *The first regular gravity survey was conducted in 1914-15 and consisted of 18 points. As Canadian activities in gravimetry flourished, a National Gravity Program was created to map the gravity field over all of Canada's lands and offshore. Following the Mendenhall pendulum came the torsion balance, the relative gravimeter and finally the Absolute Gravimeter (AG) that directly determines acceleration due to gravity by precisely measuring the time and distance travelled by a free-falling optical mass in a vacuum chamber.*
>
> (NATURAL RESOURCES CANADA, 2016)

Over the years, both absolute and relative gravity measurements have been observed across the network in response to national and international geosciences requirements. These historical measurements have since then since meticulously stored and have today become part of Canada's National Gravity Data Base (NGDB). The NGDB consists of over 6000 stations, among which 154 are absolute gravity stations, over 85,000 relative gravity measurements and over 1500 absolute gravity measurements.

Though not established for monitoring GIA, the CGSN has, over the years, produced data exploitable for studying GIA and analyzing its effect on the time rate of change of gravity, henceforth called g-dot. This is exactly what makes this work particularly unique and challenging. The NGDB contains not only gravity stations located in Canada but also those in the United States and Greenland. It thus provides an adequate source of information for completion of this project. FIGURE 1.2 depicts a larger number of stations in Canada compared to the rest of the continent because stations displayed are obtained from Canada's NGDB. Note that most stations displayed are secondary stations with lower stability which are only used in this work for investigating their usefulness in the determination of g-dot. Also notice that there are several stations in Hawaii which, for reasons that will soon be clear, are not used in the final adjustment. All stations in the USA and Greenland containing at least one tie are used, including secondary stations, at least at the quality investigation mode. These regions contain fewer stations and would have been too sparse if only primary and excentre stations are considered. This will be treated more in depth later in this work.

Gravity operations were moved within NRCan from the Geological Survey of Canada (GSC) to the CGS in 1995."

(NATURAL RESOURCES CANADA, 2016)

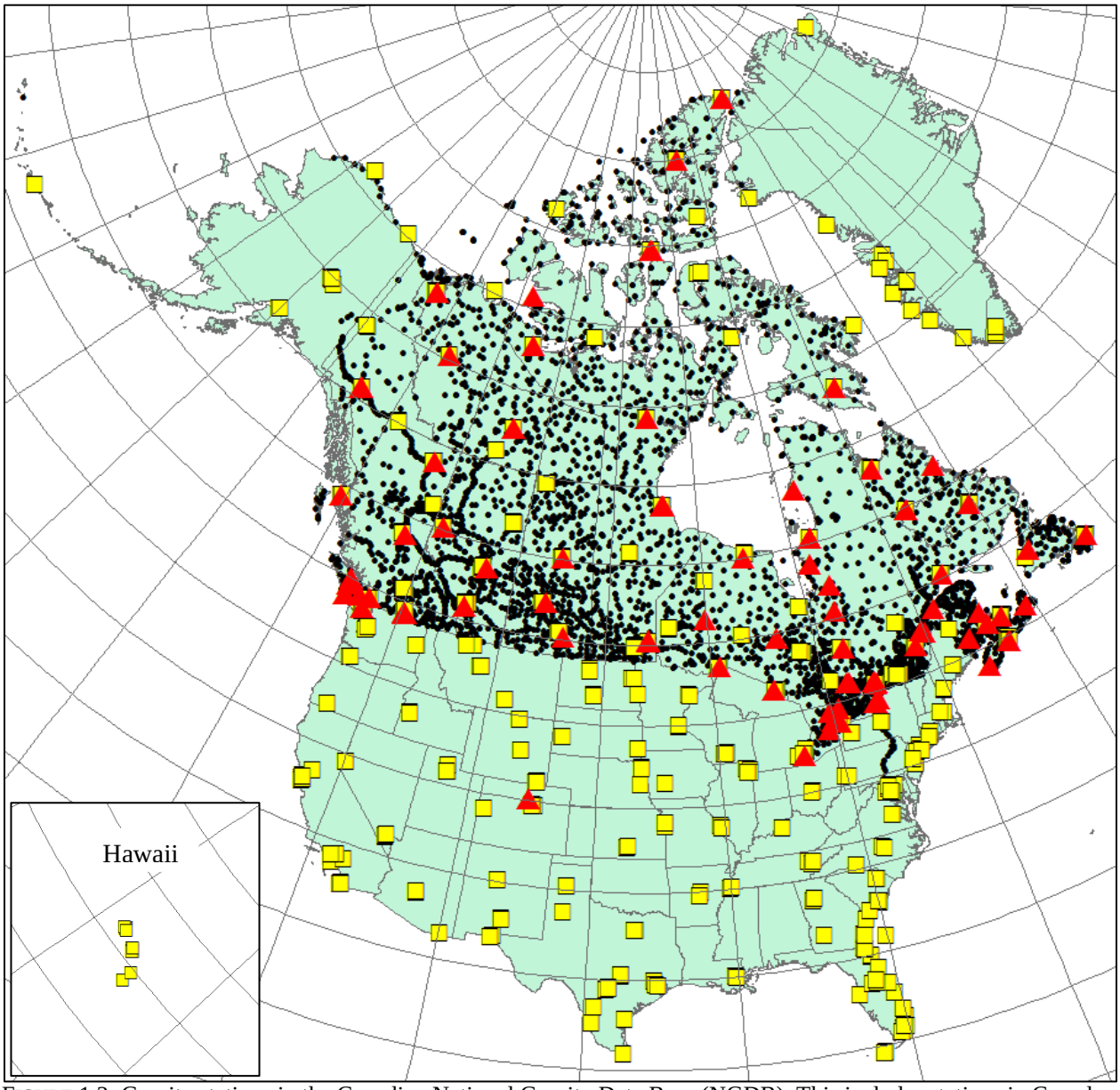

FIGURE 1.2: Gravity stations in the Canadian National Gravity Data Base (NGDB). This includes stations in Canada, USA and Greenland. Red triangles depict sites that have been observed, at least once, with an absolute gravimeter. Yellow squares show sites of excentre network each containing a primary station and several excentre stations. Black circles are secondary and other stations [Base map: NATURAL EARTH, 2013].

1.3 RESEARCH GOALS AND THESIS OUTLINE

Gravity is used to study numerous natural phenomena across the field of Earth Sciences, for example, geoid computation (determination of geoid undulation) in Geodesy. Knowledge of gravity variation in time (g-dot) is therefore imminent in obtaining an accurate geoid undulation variation (N-dot). The geoid is known to vary by 1.5 mm every year in the centre of Hudson Bay (SJÖBERG ET AL., 1990) caused by effects, such as glacial and polar ice sheet mass changes, sea level changes and most importantly, Glacial Isostatic Adjustment (GIA). This variation is quite significant and must be taken into account in very precise geodetic applications.

PAGIATAKIS & SALIB (2003) used the Generalized Least-Squares Constraint Adjustment to investigate the time rate of change of gravity in Canada due to GIA and other tectonic movements. They summarized their findings in the first of its kind g-dot map of Canada. The goal of this research is to expand their work by carefully selecting gravity stations in Alaska, Greenland and continental USA and extending the network to the rest of North America. This expansion is achieved by obtaining relative and absolute gravity measurements, treating them for gross and systematic errors and determining appropriate weight for each. The constraint Least-Squares adjustment may provide the time rate of change of gravity at various stations provided that appropriate observation equations (mathematical models) are developed to account for it. FIGURE 1.3 provides a general overview of the procedure used in this research to determine g-dot values from raw gravity measurements.

The edges of the current g-dot map of Canada (PAGIATAKIS & SALIB, 2003) are simply an extrapolation based on inland stations and may contain artefacts of the gridding algorithm used. Fulfilling the goal of this research will also improve resolution and remove such edge artefacts.

CHAPTER 2 includes a review of work done by researchers in an attempt to investigate the effect of GIA on geodetic measurements. Also, an overview of the optimal estimation method of Least-Squares adjustment that is used in this research to obtain g-dot estimates is presented. We begin by developing the mathematical model required for the adjustment and we describe how each matrix/vector is formed from acquired data. Least-Squares adjustment is based on the assumption that all measurements are free from systematic and gross errors. It is therefore imperative that our measurements be free from such errors. An overview of significant systematic effects, including ocean and body tides, hydrology and ocean tide loading is presented at end of this chapter.

In CHAPTER 3, the source and format of the data used in this project are reviewed. Acquired data are scrutinized and analyzed for possible gross errors; explanations are given as to why certain measurements are flagged as erroneous and dropped from the set. Stations are divided into 4 regions, Alaska, Canada,

Greenland and continental USA, for easy analysis. Finally, acquired data are analyzed quantitatively and qualitatively to determine their sufficiency in conducting an accurate adjustment. Uniformity in distribution of stations and ties across the continent and uniformity in distribution of measurements in time are key to accurate g-dot estimation. These are therefore also analyzed in this chapter.

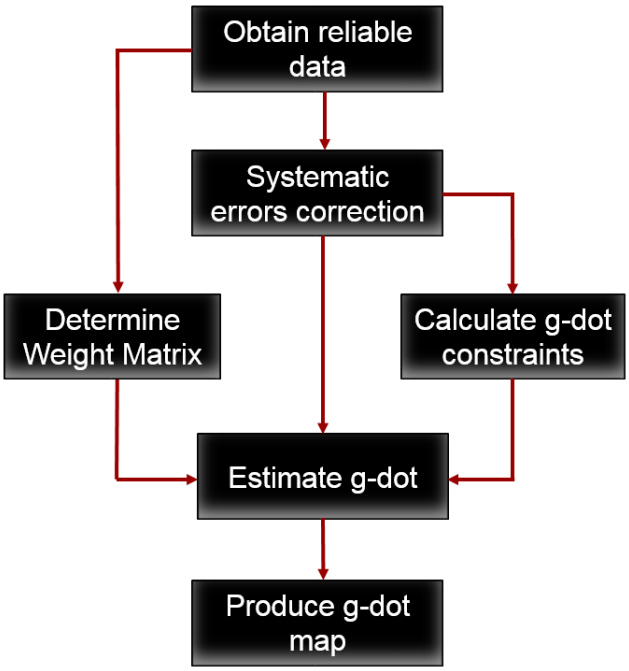

FIGURE 1.3: General overview of process used to determine time rate of change of gravity from gravity measurements.

CHAPTER 4 includes an in depth analysis of the systematic errors (defined in CHAPTER 2), and their effect on gravity measurements. Here (CHAPTER 4), software and/or models used to calculate each effect is/are evaluated. These effects are then used to correct the relative and absolute gravity measurements. Note that all absolute gravity measurements had been corrected for body tide and ocean tide loading prior to this project that is, only hydrological correction was required. On the other hand, relative gravity measurements were raw measurements and therefore had to be corrected for all systematic errors.

In CHAPTER 5, we describe how g-dot constraints are obtained from absolute gravity measurements at selected sites. In addition, we describe how the input files for software GRAVNET are obtained and how the covariance matrix of measurements is formed.

Input files obtained in the previous chapter are used in CHAPTER 6 to estimate g-dots at different stations. These g-dots are used, along with an appropriate gridding algorithm, to produce the g-dot map of North America. A discussion follows in which our results are compared to other previous research, e.g., MITROVICA ET AL., (1994); WU (2002); PAGIATAKIS & SALIB (2003); NIELSEN ET AL., (2014) and others.

Conclusions of our findings are presented in CHAPTER 7. Recommendation on possible future work is given at the end of this chapter.

1.4 CONTRIBUTION OF THIS RESEARCH

This work is conducted as a contribution to "Integrated Geosciences for a better understanding of the Earth system", which implies integration of different geodetic techniques, models, and approaches to ensure long-term monitoring of the geodetic observables in concert with the Integrated Global Observing Strategy (IGOS) (www.ggoc.org). This research projects suggests for an update of the current g-dot map of Canada by selecting new gravity ties between Canada and Greenland and between Canada and the USA to increase resolution and remove artifacts of the g-dot map. The g-dot map of Canada is updated concurrently, with high accuracy gravity networks within the continental USA, Greenland and Alaska used to extend the map to the rest of North America, producing the first of its kind g-dot map of North America.

This research introduces a step-by-step approach for obtaining accurate g-dot solutions from raw measurements. It includes all steps involved: pre-adjustment (statistical analysis of measurements; gross and systematic error corrections and formatting); adjustment and analysis of solutions; and post-adjustment assessment. We summarize this approach in a software package made up of several parts and modules, each designed to complete a specific task, facilitating reproduction of the map and providing an easy but efficient way for updates, when additional data and/or models (e.g., hydrological model) are available. There currently exists no piece of software capable of systematically achieving this.

1.5 SUMMARY

In this chapter, we described the ice age, the origin of the Glacial Isostatic Adjustment and their effect to current day gravity variations in North America. We described the Canadian Gravity Standardization Network (CGSN) and the Canadian National Gravity Data Base (NGDB), which constitute the primary source of measurements used to complete this work. We concluded the chapter with a thesis outline and contributions of this research.

In the following chapter, we provide an overview of previous work related directly or indirectly to this research. We also describe the optimal estimation method of Least-Squares (adjustment technique used by software GRAVNET – see APPENDIX A) and the mathematical model used and provide a brief overview of systematic errors commonly present in gravity measurements.

Chapter 2

The State of the Art in the Field of GIA Studies

2.1 INTRODUCTION

GIA has been studied and investigated from numerous perspectives, one of utmost importance to geodesists being its effect on varying gravity and crustal deformation. This chapter provides a detailed overview of research works conducted in an attempt to evaluate the effect of GIA on the vertical motion of the crust. Selected works, directly or indirectly related to this research, are presented to provide the reader with a general idea of the existing problem and create a framework through which the motivation for this research is established.

In the second part of this chapter, we provide background information on the principle of Least-Squares, used in this work. The mathematical model used is then developed based on available measurements and required parameters. Note that Least-Squares adjustment makes the assumption that observed quantities are free from any systematic and gross (blunders or outliers) errors. For this reason, we conclude by presenting an overview of common systematic errors present in gravity measurements which must be corrected before the adjustment.

2.2 PREVIOUS WORK

Over the years, various scientists have conducted research in an attempt to study and understand paleoclimate that had resulted to a number of glaciation and deglaciation periods, the future movement of the present ice and its impact on climate as well as its effect on the height systems. Glaciology, Geophysics and Geodesy are just a few branches of Earth Sciences interested in the phenomenon of GIA. Unlike other branches, in Geodesy, we investigate the effect of GIA on the shape and size of the Earth by evaluating its effect on gravity variation or on crustal deformation. Gravity and GNSS measurements are therefore the backbone of all geodetic investigations when it comes to Glacial Isostatic Adjustment. These measurements are obtained on the ground using gravimeter/GPS receivers and/or from space using satellites. An overview of previous work conducted on GIA from terrestrial and space measurements are provided below.

2.2.1 GIA from terrestrial measurements

The BIFROST (Baseline Inferences for Fennoscandia Rebound Observations Sea Level and Tectonics) project is a project conducted with joint efforts from the Scandinavian countries in an attempt to investigate crustal deformation caused by Glacial Isostatic Adjustment (GIA). It consists of a network of GNSS stations across Fennoscandia continuously observed since 1993 (JOHANSSON ET AL., 2002; SCHERNECK ET AL., 2002; & LIDBERG ET AL., 2010). These measurements have been processed using various algorithms and methodologies to model the GIA signature in the area to show that GIA contributes over 1 cm/year crustal displacement in some sites with only one site showing subsidence (LIDBERG ET AL., 2010). These significant uplift rates bring into question the effect of GIA on crustal deformation in other regions of the northern hemisphere, especially North America. In this work, we attempt to answer this very important concern. EKMA ET AL., (1996) also investigated the recent Glacial Isostatic Adjustment of Fennoscandia; however, they used sea-level, levelling and gravity data. Their results showed that a viscous inflow of mantle is a necessary part of the ongoing uplift process. Like EKMA ET AL., (IBID, 1996), gravity measurements are used in this project to study rebound/subsidence rates in North America.

In an attempt to constrain present day ice thickness change, WAHR ET AL (1995) predicted crustal uplift rates of several mm/year and up to 10-15mm/year in Antarctica and Greenland respectively. That research was followed by a series of investigations including BEVIS ET AL., (2012), in which the authors used the Greenland GPS Network (GNET) to measure the displacement of bedrock exposed near the margins of the Greenland ice sheet. They discovered that the entire network was uplifting in response to past and present-day changes in ice mass. Also, KHAN ET AL., (2015) used satellite altimetry, airborne altimetry, interferometry, aerial photographs and gravimetry data sets to review the Greenland ice sheet mass balance while KHAN ET AL., (2016) used geodetic measurements (GPS) to determine the GIA signature in Greenland. Results from the later findings agreed with the ICE-5G ice model which models the global GIA signature (PELTIER, 2004). NIELSEN ET AL (2014), on the other hand, investigated the GIA signal in Greenland based on seven different Earth models. They showed that the GIA gravity signal in Greenland is less than 1 µGal/year and proposed the use of future repeated absolute gravity measurements from Greenland Network (GNET) GPS stations (initiated in 2009) to further constraint the network. Results of these independent studies are compared to our results in CHAPTER 6.

PAGIATAKIS & SALIB (2003) used Generalized Least-Squares Constraint Adjustment to investigate the time rate of change of gravity in Canada due to GIA and other tectonic movements. They showed that the area around Hudson Bay experiences the highest negative rate (g-dot in Kuujjuarapik = -2.35 ± 0.06 µGal/year) while Dawson, Yukon Territory, witnesses the highest positive rate (g-dot = 1.86 ± 0.73 µGal/year). A comparison between their g-dot map and deformation maps produced by MITROVICA ET AL., (1994) and

WU (2002) showed high degree of consistency (PAGIATAKIS & SALIB, 2003): the zero line (g-dot equal zero) followed similar paths and areas of negative and positive g-dots overlapped on all three maps.

As shown in FIGURE 2.1, SELLA ET AL., (2007) analyzed the motion of 360 GPS sites across North America and determined a present-day uplift of roughly 10 mm per year around Hudson Bay with smaller values elsewhere. They also located the hinge line, the line that separates uplift and subsidence, to be along the Great Lakes showing uplifts along the northern shores and subsidence along the southern ones. These results are compared to ours in CHAPTER 6.

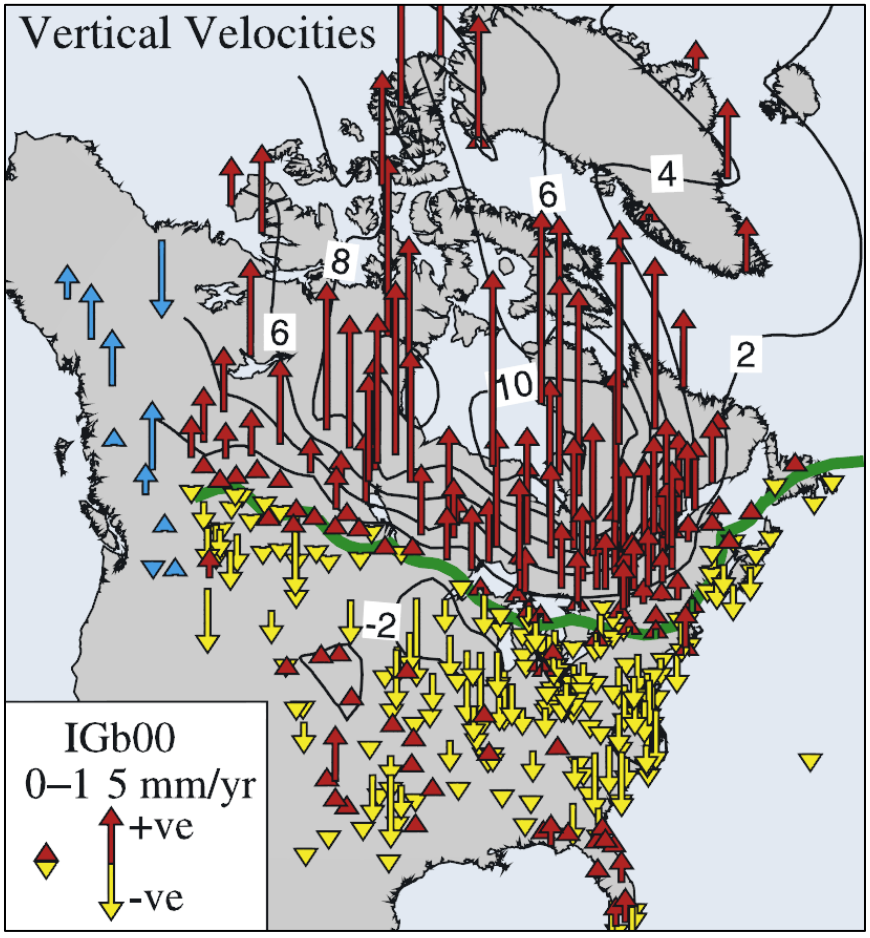

FIGURE 2.1: Vertical motion of GPS stations across North America (SELLA ET AL., 2007). The green line is the hinge line which depicts the line of zero vertical movements.

SATO ET AL., (2012) investigated the GIA signal in South East Alaska by setting up a gravity network composed of 6 sites at which gravity measurements were observed for a period of 3 years. They obtained a mean time rate of change of gravity of -4.5 ± 0.76 µGal/year over the area. Again, these results are compared to ours in CHAPTER 6.

2.2.2 GIA from satellite measurements

VELICOGNA & WAHR (2002) used time variable gravity measurements from Gravity Recovery and Climate Experiment (GRACE) space mission to isolate the GIA signal, which they then used to estimate the Earth's viscosity structure. Though not able to differentiate between viscosities of the transition zone and those of the upper mantle from GRACE measurements, such measurements were able to provide viscosities of these layers to within ±30-40%. Wahr was involved in several investigations in which geodetic measurements were used to examine the vertical movement of the crust (BEVIS ET AL., 2012; SHEPHERD ET AL., 2012; KHAN ET AL., 2015 & KHAN ET AL., 2016). Some of these involved using variable gravity measurements from the GRACE satellite to investigate GIA. For example, in SHEPHERD ET AL., (2012), the authors combined different satellite data sets (satellite altimetry, interferometry, and gravimetric data sets) with GIA models to estimate the mass balance of the Earth's polar ice sheet. In fact, WAHR & VELICOGNA (2003) presented an overview of possible GRACE data contributions to the study of GIA. They examined the expected sensitivity of GRACE measurements to GIA signals and concluded that GRACE will improve GIA resolution and an improved estimates of the Earth's viscosity profile.

BARLETTA ET AL., (2008) used level 2 data from GRACE to isolate the GIA signal in Antarctica and Greenland in an attempt to investigate its impact of mass balance in the regions. On the other hand, CHEN ET AL., (2006) used time-variable gravity measurements from GRACE satellite mission to estimate ice mass changes over Greenland during the period April 2002 to November 2005 and obtained an estimated value of -239 ± 23 km^3 per year. This significant change in ice mass directly affects vertical crustal movement (uplift) and is a primary contributor to Glacial Isostatic Adjustment in Greenland and most of North America.

2.3 LEAST-SQUARES ADJUSTMENT AND THE MATHEMATICAL MODEL

As mentioned earlier, the main objective of this work is to determine the time rate of change of gravity from historical relative and absolute gravity measurements. One way the time rate of change of gravity is determined is by adjusting a network consisting of gravity stations linked together by repeated relative gravity measurements. Repeated absolute measurements are used to determine g-dot values at selected sites which are in turn used to constrain the network. A more in-depth description of how these measurements are exploited is presented later in CHAPTER 5 and APPENDIX B.

2.3.1 The Principle of Least-Squares

The principle of Least-Squares is based on the concept that the best estimate to an unknown parameter is the one that minimizes the sum of the squares of weighted residuals, which is equivalent to the minimization of the variance of the estimated parameters. An appropriate mathematical model that describes the relationship between unknown parameters and observables is required. Determining such a matrix is perhaps the most crucial step in an adjustment.

For $\bar{x}$ being the vector of parameters (unknown quantities) and $\bar{l}$ the vector of observed quantities, 3 types of Least-Squares adjustments are possible depending on the mathematical model (VANÍCEK & KRAKIWSKY, 1986):

a) Combined Adjustment is the most general case in which the observed quantities cannot be explicitly expressed as a function of the parameters

$$F(\bar{x}, \bar{l}) = 0. \tag{2.1}$$

b) Parametric Adjustment is used when the observed quantities can be explicitly expressed as functions of the parameters

$$F(\bar{x}) = \bar{l}. \tag{2.2}$$

c) Conditional Adjustment is used when the mathematical model consists of conditions among the observed quantities. There are no unknown parameters involved in the model:

$$F(\bar{l}) = 0. \tag{2.3}$$

A necessary requirement for performing Least-Squares adjustment is that the mathematical model be linear. This is seldom the case in Geodesy. Linearization is performed using Taylor series about the point defined by the initial approximation to the solution vector (x^0) and the vector of observations $\bar{l}$. Note that $\bar{x} = x + x^0$ and $\bar{l} = l + v$, where x is the unknown correction to x^0 and l is the vector of observations.

Using the most general case of combined adjustment (Equation (2.1)) and considering only the linear terms, the model becomes

$$F(\bar{x}, \bar{l}) = w + Ax + Bv = 0. \tag{2.4}$$

A and B are, respectively, called first and second design matrices and are equal to the partial derivatives of the mathematical model with respect to the unknowns and observables at x^0 and l, v is the vector of residual; and w is the misclosure vector $w = F(x^0, l)$.

The covariance matrix of observations C_l, consists of variances and covariances of observations arising from measuring instruments and observational procedures. It is usually possible to assign relative variances and covariances to observations that is, C_l is known only to within a scale factor σ_0^2, known as a-priori variance factor. Since variances and covariances determine the quality of one observation compared to the other, a rational choice for the weight matrix of observation is therefore

$$P = \sigma_0^2 C_l^{-1}. \tag{2.5}$$

The principle of Least-Squares can be applied by generating the following variation function

$$\Phi = v^T P v = \min. \tag{2.6}$$

Linearization of a non-linear model imposes a constraint given by Equation (2.4) to the variation function. Using Lagrange's method and for K multiplier, Equation (2.6) becomes

$$\Phi = v^T P v + 2K^T (w + Ax + Bv) = \min. \tag{2.7}$$

WELLS & KRAKIWSKY (1971) and VANICEK & KRAKIWSKY (1986) showed that after minimizing of this variation function, estimated parameters, $\hat{\hat{x}}$, and estimated residuals, $\hat{v}$, can be obtained as follows

$$\hat{\hat{x}} = -(A^T (BP^{-1}B^T)^{-1} A)^{-1} A^T (BP^{-1}B^T)^{-1} w + x^0 \tag{2.8}$$

$$\hat{v} = -P^{-1}B^T (BP^{-1}B^T)^{-1} (A\hat{\hat{x}} + w). \tag{2.9}$$

Their covariance matrices are respectively

$$C_{\hat{x}} = \sigma_0^2 (A^T (BP^{-1}B^T)^{-1} A)^{-1} \text{ and} \tag{2.10}$$

$$C_{\hat{v}} = \sigma_0^2 P^{-1}B^T (BP^{-1}B^T)^{-1} [BP^{-1} - A(A^T (BP^{-1}B^T)^{-1} A)^{-1} A^T (BP^{-1}B^T)^{-1} BP^{-1}]. \tag{2.11}$$

For parametric adjustment, B = ±I. Therefore,

$$\hat{\hat{x}} = -(A^T PA)^{-1} A^T Pw + x^0, \tag{2.12a}$$

$$\hat{v} = A\hat{\hat{x}} + w, \tag{2.12b}$$

$$C_{\hat{x}} = \sigma_0^2 (A^T PA)^{-1} \text{ and} \tag{2.12c}$$

$$C_{\hat{v}} = \sigma_0^2[P^{-1} - A(A^T PA)^{-1}A^T]. \tag{2.12d}$$

Similarly, for conditional adjustment, $A = 0$. Therefore

$$\hat{\bar{x}} = x^0 \tag{2.13a}$$

$$\hat{v} = -P^{-1}B^T(BP^{-1}B^T)^{-1}w \quad \text{and} \tag{2.13b}$$

$$C_{\hat{v}} = \sigma_0^2[P^{-1}B^T(BP^{-1}B^T)^{-1}BP^{-1}]. \tag{2.13c}$$

The a-posteriori variance factor, $\hat{\sigma}_0^2$, which is an estimate of the a-priori variance factor, σ_0^2, is an essential statistic required in post adjustment statistics. If r are the degrees of freedom, the a-posteriori variance factor can be computed as follows

$$\hat{\sigma}_0^2 = \frac{\hat{v}^T P\hat{v}}{r}. \tag{2.14}$$

From this, the estimated covariance matrix of estimated parameters and estimated residuals are, respectively

$$\hat{C}_{\hat{x}} = \frac{\hat{\sigma}_0^2}{\sigma_0^2} C_{\hat{x}}, \tag{2.15a}$$

$$\hat{C}_{\hat{v}} = \frac{\hat{\sigma}_0^2}{\sigma_0^2} C_{\hat{v}}. \tag{2.15b}$$

Interested readers are referred to WELLS & KRAKIWSKY (1971) AND VANICEK & KRAKIWSKY (1986) for more formulas and details on how the above equations are derived.

2.3.2 Mathematical Model

Available in this work are relative gravity measurements obtained in time at gravity stations across the continent. In addition, absolute gravity measurements have been historically obtained at a few selected stations. Our objective here is to determine a mathematical model linking these observed quantities to unknown parameters.

Before developing this mathematical model, a few definitions are in order: Relative gravity measurements are measurements obtained using a relative gravimeter, such as a Lacoste and Romberg (L&R), Burris or Scintrex gravimeters, which measures the difference in gravity (gravity tie) between two points. The instrument is placed over the first point and a reading (Reading 1) is recorded. It is then placed over the

second point and a second reading (Reading 2) is recorded. The difference between these two readings gives the difference in gravity between the two points in an "instrumental" unit called delta g, denoted as Δg . L&R instruments come with conversion tables from which the scale factor for converting readings from "instrumental" units to gravity units (mGal or μGal). Absolute gravity measurements on the other hand are measurements taken with an absolute gravimeter, such as JILA, FG-5 or A10. These instruments are much more expensive and much more difficult to transport and operate. They measure the absolute gravity value over a point in gravity units.

Consider two gravity stations i and j given in FIGURE 2.2 below for which time rates of change $\dot{g}_i$ and $\dot{g}_j$, respectively, are required

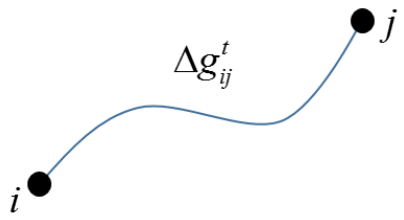

FIGURE 2.2: Gravity tie over which relative gravity measurement Δg_{ij}^t was obtained using a relative gravimeter.

Repeated relative gravity measurements Δg_{ij}^t have been observed between these stations at different epochs, *t*. A simple relationship between Δg_{ij}^t and gravity values at stations i and j (g_i^t and g_j^t) at time of observation, *t*, is given by

$$g_i^t - g_j^t = \Delta g_{ij}^t . \tag{2.16}$$

Gravity variation due to GIA is a very slow process and is known to vary approximately linearly over a short period of time (PAGIATAKIS & SALIB, 2003). For this reason, g_i^t and g_j^t are linear functions of time with slopes $\dot{g}_i$ and $\dot{g}_j$, respectively, and can each be computed as follows

$$g_i^t = g_i^{t_0} - \dot{g}_i (t - t_0), \tag{2.17a}$$

$$g_j^t = g_j^{t_0} - \dot{g}_j (t - t_0), \tag{2.17b}$$

where t_0 is the reference epoch for which, $g_i^{t_0}$ and $g_j^{t_0}$ are computed. Note that the estimated g-dot is independent from the choice of t_0. For sake of comparison, the year 2000 was chosen to represent the reference epoch. The year 2000 is the year during which the second adjustment of the Canadian gravity

network was performed (IBID, 2003). Δg_{ij}^{t} is observed gravity difference between stations i and j in units of acceleration. For L&R instruments, Δg_{ij}^{t} is obtained by multiplying the instrument reading (unitless) by a scale factor provided by the manufacturer. This scale factor is known to vary with time due to material fatigue and needs frequent calibration.

Gravimeters change their null reading value gradually with time. This drift results mainly from creep in the springs (TELFORD ET AL., 1990) and environmental changes, such as temperature and pressure. This effect is significant when sub-microgal g-dot values are sought and should therefore be accounted for in the model (PAGIATAKIS & SALIB, 2003). For Δt_{ij}^{t} being the time range within which Δg_{ij}^{t} was observed and D_k^t and S_k^t being unknown drift and secondary scale factor of instrument k at time of observation t, Equation (2.16) is fully written as

$$g_i^{t_0} - \dot{g}_i(t-t_0) - g_j^{t_0} + \dot{g}_j(t-t_0) - D_k^t \Delta t_{ij}^t - S_k^t \Delta g_{ij}^t = 0, \tag{2.18}$$

where $g_i^{t_0}$ and $g_j^{t_0}$ are the gravity values at point i and j at reference epoch t_0; and $\dot{g}_i$ and $\dot{g}_j$ are time rates of change of gravity at i and j stations, respectively.

2.3.3 Defining the variables

According to SUB-SECTION 2.3.1, the first step in every Least-Squares adjustment is to design an appropriate mathematical model relating the observed quantities to unknown parameters. After doing so, each variable in Equation (2.8) will now be defined as it relates to our present situation.

Unknown parameters to our optimum point estimation problem include gravity at each station at a reference epoch, g-dot at each station and instrument scales and drifts. These form the vector of unknowns $\overline{x}$, provided in Equation (2.19) and estimated in Equation (2.8) as $\hat{\overline{x}}$.

$$\overline{x} = \begin{bmatrix} g_i^{t_0} \\ \dot{g}_i \\ g_j^{t_0} \\ \dot{g}_j \\ D_k^t \\ S_k^t \end{bmatrix} \tag{2.19}$$

Its initial approximate value (x^0) is defined by

$$x^0 = \begin{bmatrix} g_{i_0}^{t_0} \\ \dot{g}_{i_0} \\ g_{j_0}^{t_0} \\ \dot{g}_{j_0} \\ D_{k_0}^{t} \\ S_{k_0}^{t} \end{bmatrix}. \tag{2.20}$$

The only observed quantities are relative gravity measurements Δg_{ij}^{t} thus, the vector of observations, l , is given by

$$l = \left[\Delta g_{ij}^{t} \right]. \tag{2.21}$$

Using generalized adjustment (SCHMID & SCHMID, 1965), Equations (2.20) and (2.21) can be lumped together in a pseudo-observation hypervector l_0

$$l_0 = \begin{bmatrix} l \\ x^0 \end{bmatrix} = \begin{bmatrix} \Delta g_{ij}^{t} \\ g_{i_0}^{t_0} \\ \dot{g}_{i_0} \\ g_{j_0}^{t_0} \\ \dot{g}_{j_0} \\ D_{k_0}^{t} \\ S_{k_0}^{t} \end{bmatrix}, \tag{2.22}$$

from which the misclosure vector can be obtained from

$$w = g_{i_0}^{t_0} - \dot{g}_{i_0}(t - t_0) - g_{j_0}^{t_0} + \dot{g}_{j_0}(t - t_0) - D_{k_0}^{t} \Delta t_{i_0 j_0}^{t} - S_{k_0}^{t} \Delta g_{i_0 j_0}^{t}. \tag{2.23}$$

For k_1 and k_2 equal individual a-priori variance factor of Δg and x^0 , respectively, the covariance matrix of l_0 is defined as

$$C_{l_0} = \sigma_0^2 \begin{bmatrix} k_1 C_{\Delta g} & 0 \\ 0 & k_2 C_{x^0} \end{bmatrix}. \tag{2.24}$$

The first design matrix is the partial derivative of the mathematical model (Equation (2.18)) with respect to unknown parameters

$$A = \left[\frac{\partial F(\bar{x}, \bar{l})}{\partial x} \right]_{/x^0, l} = \left[\frac{\partial F}{\partial \dot{g}_i} \quad \frac{\partial F}{\partial \dot{g}_j} \quad \frac{\partial F}{\partial g_i^{t0}} \quad \frac{\partial F}{\partial g_j^{t0}} \quad \frac{\partial F}{\partial D_k^t} \quad \frac{\partial F}{\partial S_k^t} \right]_{/x^0, l}, \tag{2.25a}$$

which when applied to our mathematical model yields

$$A = \left[-(t - t_0) \quad (t - t_0) \quad 1 \quad -1 \quad -\Delta t_{ij}^t \quad -\Delta g_{ij}^t \right]. \tag{2.25b}$$

For NM being the number of observations, NS being the number of instrument and NSTN being the number of stations on the network, the first design matrix has a size of NM by 2*(USTN+NS) that is, *A* has as many rows as the number of observations and as many columns as twice the sum of the number of stations and the number of instruments. Looking at individual matrices that make up matrix *A*, $\pm(t - t_0)$ is NM by USTN, ±1 is NM by USTN, $-\Delta t_{ij}^t$ is NM by NS and $-\Delta g_{ij}^t$ is NM by NS. The second design matrix is the partial derivative of the mathematical model (Equation (2.18)) with respect to observed quantities

$$B = \left[\frac{\partial F(\bar{x}, \bar{l})}{\partial l} \right]_{/x^0, l} = \left[\frac{\partial F(\bar{x}, \bar{l})}{\partial \Delta g_{ij}^t} \right]_{/x^0, l}, \tag{2.26a}$$

which yields

$$B = \left[-S_k^t \right]. \tag{2.26b}$$

Similarly, the second design matrix (B) has a size of NM by NM with diagonal elements representing instrument scales and off diagonal elements all being zero.

2.3.4 Least-Squares and Systematic Errors

From the rise and fall of tides to the continuous variation of the rotational axis of our planet, the Earth is known to be a dynamic system. The constant internal mass redistribution of the Earth (Earth deformation) caused by such events affects its gravity field. These signals appear in gravity measurements and are therefore considered systematic errors. The principle of Least-Squares operates on the assumption that only random errors are present in measurements that is, systematic effects have all been eliminated otherwise, the solution will be biased. Significant systematic effects usually present in gravity measurements (in

descending order of magnitude) include body tides, hydrology, ocean tide loading and polar motion. A brief overview of these systematic effects is given along with their effect on gravity measurements.

2.3.4.1 Tides

In addition to causing the rise and fall of sea levels, the gravitational pull of the Moon and the Sun and the rotation of the Earth cause the rigid crust to move up and down by a few decimetres. Deformation of the solid Earth caused by the attraction of the celestial bodies, but primarily from the Moon and the Sun is called body tide. Part of this deformation (about 10% of the total tide) is also due to the variations coming from the varying ocean tide which produces the so called "load tide" or “ocean tide loading” (PAGIATAKIS, 1988). The effect of tides causes deformation in the shape of the Earth and perturbation in Earth’s gravity field. Perturbation magnitudes are location dependent, they are present in gravimetric measurements and constitute major systematic errors.

2.3.4.2 Ocean tide loading

Ocean tide can be defined as the rise and fall of sea levels caused by the gravitational pull of the Moon and the Sun and the rotation of the Earth. In order words, they are very long-wavelength waves that move through the oceans in response to the forces exerted by the Moon and Sun (NOAA, 2015). Ocean tide loading is clearly observed at shorelines through variation of water heights. This rise and fall of tides causes the redistribution of ocean mass relative to their equilibrium state which in turn induces gravity variation, especially in regions along coastlines. The elastic response of the crust underneath the ocean to this mass redistribution causes crustal deformation called ocean tide loading. Ocean loading is therefore a secondary tidal response of the ocean floor which causes surface displacement of the adjacent land. This redistribution in land mass causes a variation in gravity, an effect noticeable in all gravity measurements around the world. Global ocean tide loading can be expected to produce total tidal variations of 5-10 µGal in amplitude and total height variations of the solid surface of 10-20 mm in amplitude over large parts of eastern and western North America (LAMBERT ET AL., 1998). This variation constitutes significant systematic effect to gravity measurements; correction of this effect is of utmost importance for the completion of our current task.

2.3.4.3 Hydrology

The mass of water around a gravity station affects its local gravity field. In other words, a variation in the water table around a gravity station will cause a variation in its local mass which in turn causes a variation in local gravity field. In fact, local water storage variations within 10km of a station alter the local mass field and thus can significantly affect gravity measurements (LAMPITELLI & FRANCIS, 2010). In recent years, the effect of hydrology (or local water storage variation) on gravity measurements has gained importance in a wide range of geophysical research issues. Gravimetric measurements have now been used to study variation is gravity due to hydrology (e.g. CREUTZFELDT ET AL., 2010; HASAN ET AL., 2005; LAMPITELLI & FRANCIS, 2010). Signals generated by perturbation in Earth's gravity field due to local water storage variation are observable by absolute and relative gravimeters (KRONER ET AL., 2007; NAUJOKS ET AL., 2010).

2.3.4.4 Polar motion and other deformations

The North and South Poles are not fixed with respect to the Earth's crust, but rather constantly change as the Earth rotates on its axis. The Earth's rotation axis, which passes through both poles, is therefore constantly changing causing the Earth to wobble around. This is called polar motion, describing the motion of the rotation axis of the Earth relative to the crust caused by the changing location of the poles. The Earth, by virtue of it axial rotation, experiences a centrifugal force; force which contributes to its gravity field. Variations in either the rate of rotation or in the geocentric position of the rotation axis (i.e., polar motion) will perturb the centrifugal force (IBID, 1985). Polar motion therefore causes disturbance of Earth's gravity field, which affects surface gravity measurements whose effect can be as large as 10-13 μGal peak-to-peak (IBID, 1985). Fortunately, polar motion is a very slow process and as explained in SECTION 4.5, there will be no need to correct such effect, at least for gravity ties that are measured over relatively short distances and short periods of time.

The above effects are just a few of a long list of effects that cause Earth deformations, whose signals are present in gravity measurements. Others, including crustal deformation and plate tectonic are also present but are of much smaller magnitudes. Simply stated, the Earth's gravity field would have been constant in time if no systematic effects, e.g. from GIA, ocean and body tide, hydrology, ocean tide loading, polar motion, plate tectonics, crustal deformation etc., existed. In order to effectively model the time rate of change of gravity due to Glacial Isostatic Adjustment and tectonic movements, it is required that measurements be corrected of all other systematic effects.

2.4 SUMMARY

In this chapter, a brief review of previous work related to our research was presented, including investigations on GIA using gravity measurements from gravimeters and GRACE satellite specifically stated. Investigations on GIA using GNSS measurements from GPS networks and investigations using a combination of gravity and GNSS measurements were reviewed. The method of Least-Squares adjustment was also described, the mathematical model used in the adjustment was derived and a brief overview of systematic errors commonly present in gravity measurements was provided.

In the next chapter, we describe the data used in the adjustment process. This includes the source, type and content of acquired data. A qualitative and quantitative analysis of these data is then performed in an attempt to investigate their suitability in performing the current task.

Chapter 3

Absolute and Relative Gravity Measurements

3.1 INTRODUCTION

A mathematical model linking observed quantities to unknown parameters was derived earlier in SECTION 2.3. In that same section, all variables involved in the Least-Squares Adjustment procedure were defined in SUB-SECTION 2.3.1 including the first and second design matrices, vector of unknown parameters, vector of observations, covariance matrix of observations and misclosure vector. As previously mentioned, data required to populate these matrices/vectors, originate from Canada's National Gravity Data Base (NGDB). This database contains relative gravity measurements as well as absolute gravity measurements systematically observed in time since the establishment of the Canadian Gravity Standardization Network (CGSN). According to our mathematical model, relative gravity measurements as well as their characteristic parameters (station names and numbers, dates and times of measurement, instrument number, instrument scale factor and project number), are the only observed quantities required to perform the adjustment. Absolute gravity measurements on the other hand are used to directly compute g-dots at selected stations which are then used to constrain the network during the adjustment. Again, details of this are given later in CHAPTER 5 and APPENDIX B.

The purpose of this chapter is to describe the data used in this research and the analyses that were performed before the adjustment. Outlined here are a description of the source, form and format of the data; methods used to detect/eliminate gross errors and a step-by-step description of qualitative and quantitative investigations performed on the data.

3.2 DATA ACQUISITION

In order to achieve the goals of this research, it is imperative to obtain repeated relative gravity measurements linking the gravity stations together in a network. In addition, repeated absolute gravity measurements are also essential as they will be used to provide g-dot constraints to the network. Repeatability is key for successful completion of this research because the g-dot signature is based on repeated measurements; these weak signals can only be detected from repeated measurements obtained over an extended period of time.

Considering a maximum rebound rate of approximately 2 µGal per year, and relative gravity measurements obtained mainly with LaCoste-Romberg gravimeters (with typical precision of about 20–30 mGal, single gravity tie) (PAGIATAKIS & SALIB, 2003), several decades of measurements are needed to observe the GIA signal. The same applies to Canadian, Scintrex and Worden meters, which were used to measure a few ties on the network. The NGDB with its over 6600 gravity stations, 85000 relative gravity measurements and 1500 absolute gravity measurements meticulously observed since the establishment of the CGSN in the 1950s provides an important source of information for successful completion of this work.

At the onset of this research, gravity data were requested and obtained from Natural Resources Canada's (NRCan) NGDB (MARC VÉRONNEAU, PERSONAL COMMUNICATION, 2015) and delivered in the following formats:

- *base.dat*, henceforth called "station file" contains all 6661 gravity stations in the NGDB. This includes Canada, Greenland and the US stations, each defined by station number, position (latitude, longitude and height), adjusted gravity (based on IGSN71), location (city/town) and base code. Adjusted gravity values, base codes and positional information are very useful in this work.

- *absoluteG.dat*, henceforth called "absolute gravity file" contains 1705 processed absolute gravity measurements obtained at 154 stations. Each line in the file includes an absolute gravity measurement and its estimated error, date and time of observation as well as the instrument used. All this information is used in g-dot constraint calculation. As we shall see later, only five (5) of the aforementioned stations contain sufficient measurements for accurate g-dot constraint estimation.

- *tie.dat*, henceforth called "tie file" contains 97457 relative gravity measurements obtained over gravity ties on the network. Each line in the file contains stations (names and numbers), dates and times of measurements, readings, project number, instrument, instrument scale factor and reference to field book. Note that readings are raw and uncorrected as obtained from the instruments.

- *GravityTies_Format2015* contains a format descriptor for each of the above files that is, what each column and row represents.

We emphasize that the NGDB is the sole source of data used in this work for reasons that will soon be clear.

3.3 DATA SCRUTINY - GROSS ERROR DETECTION AND ELIMINATION

Measured quantities are subject to errors of different types: random, systematic and/or blunders. Unlike the first two, blunders, also called gross errors, are non-systematic errors (and often large) that originate from carelessness of the observer, improper equipment functioning etc. Only large obvious gross errors are usually detectable at the pre-adjustment stage and statistical tests are used at the post-adjustment stage to confirm the absence (or insignificance) of possible small gross errors. Metadata proved very useful in this process as some provided direct indication as to the poor nature of the measurement. This section provides the reader with a brief description of the approach used to flag outliers.

3.3.1 Relative gravity measurements

A quick analysis of the tie file shows that many measurements were obtained on January 1st. No measurement on the Canadian network was performed on January 1st and this date was often used when the true day of measurement was unknown (MARC VÉRONNEAU, PERSONAL COMMUNICATION, 2015). For this reason, all measurements with readings on January 1st are flagged as outliers and removed from the set of measurements.

We also notice that for many ties, the time difference between reading 1 and reading 2 (readings at each station) are, in some instances, as short as 1 minute. No matter how close the stations were to each other or how quick an operator was, it will take sufficiently longer than one minute to record a reading at a station, move and setup the instrument over the second station to record the second reading. As a rule of thumb, all gravity ties obtained in less than 3 minutes are fagged as outliers and eliminated from the set.

Moreover, we notice that many station pairs have measurements observed on different days, but at exactly the same times. For example, 5 ties between stations 96441963 and 96231949 were obtained on different days but exactly at 06:01 and 06:02, respectively, on each of those days. Not only are these measurements taken within a minute, but they are also taken at exactly the same time every day, making them very suspicious. All such measurements are thus considered outliers and also taken out of the set.

After this quick gross error analysis, 85866 (of 97457) relative gravity measurements remain. The routine used to clean relative gravity measurement was developed during this study and it is included in the software called INPUTGRAVNET. More information on this software is given later in APPENDIX A.

3.3.2 Absolute gravity measurements

Of all 154 absolute gravity stations obtained from the NGDB, 99 lack positional information (latitude and longitude information) that is, they are not included in the station file. In addition, a quick examination shows that none of these stations is tied to the rest of the network by relative gravity measurements making them irrelevant to this work. 55 stations with 1173 absolute gravity measurements remain after their exclusion.

JILA-002 was the first absolute gravimeter purchased by the government of Canada in the late 1980s. At that time, field personnel had not been exposed to such an instrument or the instrument had not been properly calibrated thereby making early measurements questionable. For this reason and for the purpose of reliability, all absolute measurements obtained before 1990 are ignored.

In order to obtain g-dots from weighted Least-Squares regression of repeated absolute gravity measurements over long periods of time, a minimum of 3 observational epochs per station are necessary. Due to the slow rate of GIA, an epoch is considered to be one year. As a rule of thumb, stations with fewer than 5 epochs of measurements will not be considered, leaving only 13 absolute stations with adequate number of measurements for reliable g-dot estimation.

Preliminary analysis of the absolute gravity measurements obtained at the Ottawa stations showed no definite pattern. It is worth mentioning that Ottawa was the home of JILA-002 absolute gravimeter and all tests on the instrument were done at nearby stations. Several uncertainties existed about the quality of the measurements at this location. To err on the side of caution, all Ottawa absolute gravity measurements were neglected. After these 3 Ottawa stations were eliminated, only 10 absolute stations with adequate number of measurements remained.

3.4 QUANTITATIVE AND QUALITATIVE ANALYSIS OF DATA

In the previous section we described how gross errors were detected and removed based on characteristics such as time and duration of measurements. Note that the actual readings were never subjected to any statistical test and may therefore still contain gross errors. For this reason, post adjustment statistical testing will be used to flag outliers. Nevertheless, an important pre-adjustment step requires that we perform thorough evaluation of the data in an attempt to assess their quality in accomplishing the task at hand. Data are evaluated based on the following characteristics:

- Number of absolute/relative stations and uniformity in their distribution.
- Type of station.

- Number of ties and uniformity in their distribution.
- Range, repetition and spread of absolute gravity measurements.
- Range, repetition and spread of relative gravity measurements.

To ease this process, we begin by grouping stations and measurements based on their locations (regionalization).

3.4.1 Regionalization

In order to produce the g-dot map of North America, it is essential that selected stations be uniformly distributed across the continent. PAGIATAKIS & SALIB (2003) used all primary and excentre stations (437) in Canada to produce the first g-dot map of Canada. Unfortunately, only 249 (227 obtained and 22 recovered) of these could be retrieved. Also, these stations do not uniformly cover inland Canada; there exists a sparse area in the region west of Hudson Bay. To remedy this problem, 343 secondary stations located in this region were carefully selected and added to the network. The large number comes from the fact that most ties to these stations had no repetition. As seen in subsequent chapters, two absolute sites (Ucluelet and Nanoose) not previously included, were found to have adequate number of absolute gravity measurements from which g-dot constraints can be computed. The excentre networks at Ucluelet and Nanoose include 4 and 5 stations (primary and excentre), respectively, for a total of 9 additional stations. The network therefore contains a total of 601 stations located in Canada (cf. TABLE 3.1).

ArcGIS is used to extract all Alaska, Greenland and continental USA stations (primary, excentre and secondary) from the acquired station file. As shown in TABLE 3.1 and later in FIGURE 3.1, relative gravity measurements are available at 24 Alaska, 48 Greenland and 357 USA (continental) stations, which together with Canadian stations total 1030 gravity stations that are used in the final adjustment. Note that stations in Hawaii are not included as being far away.

TABLE 3.1: Number of stations, area and station density of each region.

Region	Number of Stations	Area (sq. km)	Points per 100000 sq. km
Alaska	24	1704217	1.4
Canada	601	9984670	6.0
Greenland	48	2166086	2.2
USA	357	7898891	4.5

Gravity ties are also grouped based on the location of stations involved (e.g. Greenland-USA ties, Alaska-Canada ties etc.) and provided in TABLE 3.2. This was done using an algorithm written by us and included in INPUTGRAVNET (See APPENDIX A).

The distributions of all stations (cf. TABLE 3.1) and all ties (cf. TABLE 3.2) used in the final adjustment are graphically shown in FIGURE 3.1.

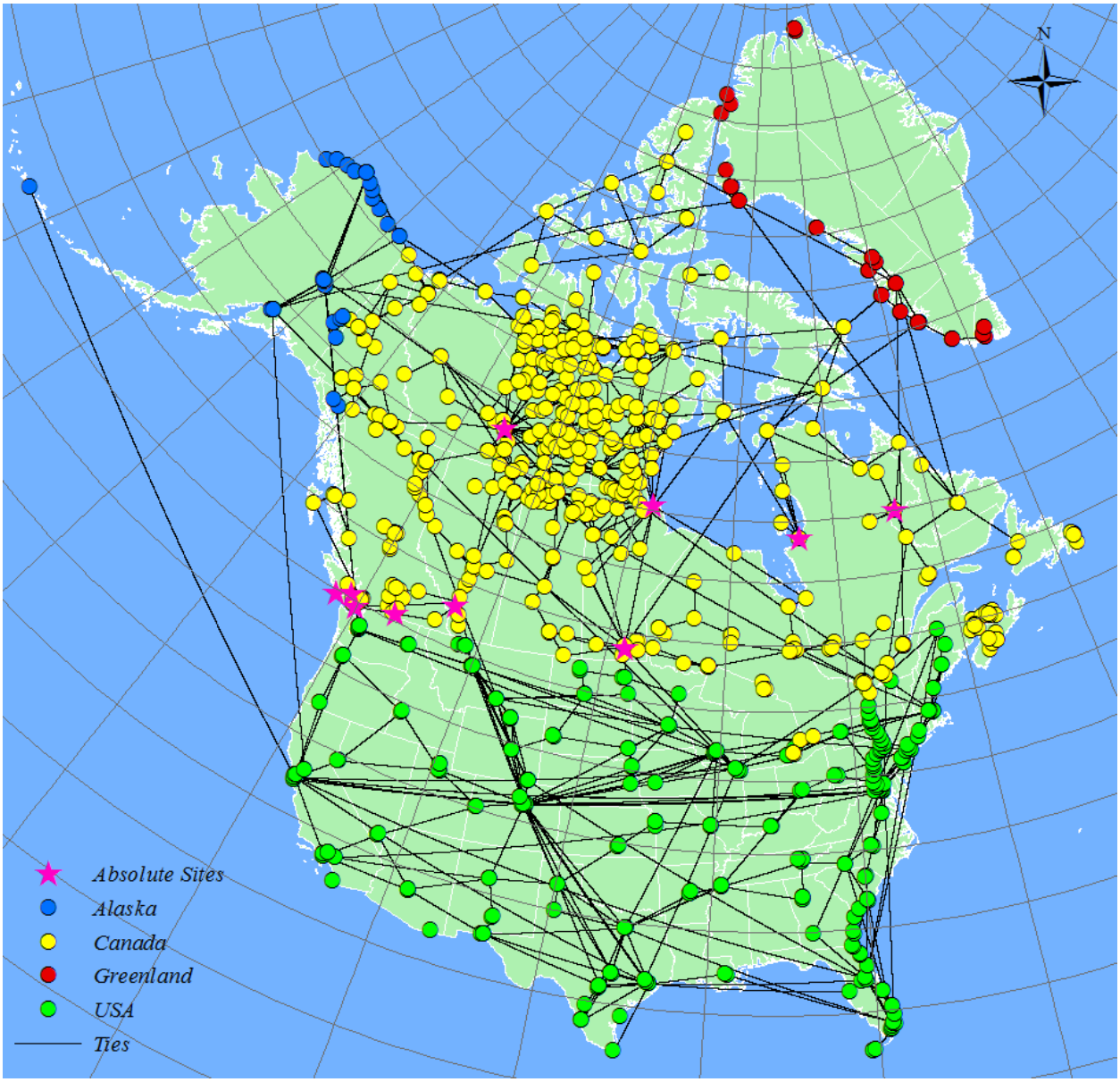

FIGURE 3.1: Distribution of stations used in the final adjustment into Alaska (blue), Canada (yellow), Greenland (red) and continental USA (green), including absolute stations (pink stars). Gravity ties are displayed as black lines [Base map: NATURAL EARTH, 2013].

TABLE 3.2: Distribution of ties and relative gravity measurements.

Type	Number of Ties	Number of relative gravity Measurements
Alaska-Alaska	48	565
Alaska-Canada	4	27
Alaska-Greenland	1	2
Alaska-USA	6	17
Canada-Canada	862	4422
Canada-Greenland	13	51
Canada-USA	21	127
Greenland-Greenland	70	338
Greenland-USA	0	0
USA-USA	634	4552

We will realize that not only is it important to have a sufficient number of measurements but it is vital that they be uniformly distributed across the continent. This prevents bias, of any kind, towards a particular region of the network.

A more in-depth evaluation of this FIGURE 3.1 as well as TABLES 3.1 and 3.2 is performed later in this chapter.

3.4.2 Analysis - number and distribution of stations

TABLE 3.1 shows the distribution of all 1030 stations that are used in the final adjustment across the four regions. The area of each of these regions, according to the UN DEPARTMENT OF ECONOMIC AND SOCIAL AFFAIRS (2012) and WORLD ATLAS (2016), is also shown on the same table along with computed station density (number of stations per unit area). Notice that we have roughly the same number of primary and excentre stations in Canada (258) and USA (383), two regions of roughly equal land area. The low density in Alaska and Greenland comes from the fact that most of the land is inaccessible hence stations are concentrated only in certain regions along the edges of Alaska and along the west stretch of Greenland. FIGURE 3.1 shows that all stations used in the final adjustment are evenly distributed across the continent.

Also shown in FIGURE 3.1 are the available absolute stations (pink stars). Notice that even though no absolute stations from other regions are used, those in Canada show uniformity in their spread across the country, and most importantly, around Hudson Bay. It is important to have constraints evenly distributed across the network as it reduces possible bias. We conclude that the network comprises sufficient number of stations (both relative and absolute) uniformly distributed across the continent ensuring a reliable and robust network adjustment.

3.4.3 Analysis - base class

Recall from CHAPTER 1 that primary gravity stations are those stations located at easily accessible and very stable sites for high precision gravity measurements; excentre stations are located a few to several kilometers from the primary stations and tied to primary stations by relative gravity measurements while secondary stations are located on sites that are not as stable as those of primary stations and so provide less precise reference. Some stations are designated "Absolute" to simply distinguish them as being stations over which absolute gravity measurements have been observed. Stations used in the final adjustment are distributed, according to base codes, as shown in TABLE 3.3 below.

TABLE 3.3: Distribution of stations according to base class.

	Base Class Description	**Base Class**	**Alaska Stations**	**Canada Stations**	**Greenland Stations**	**USA Stations**	**Total**
Relative	Unknown	0	0	1	0	0	**1**
	Primary	1	5	43	14	89	**151**
	Excentre	2	18	182	34	266	**500**
	Secondary	3	1	345	0	0	**346**
	Special Project	4	0	13	0	0	**13**
Absolute	Fundamental	10	0	1	0	2	**3**
	Primary	11	0	4	0	0	**4**
	Secondary	12	0	4	0	0	**4**
	Other	13	0	8	0	0	**8**
Total:			**24**	**601**	**48**	**357**	**1030**

TABLE 3.3 shows that only one "unknown" station will be used in the final adjustment. Unknown stations are those whose base class was not specifically known, consequently, measurements from them are considered the least accurate. In addition, relative gravity stations include 13 special project stations. As the name indicates, these stations were setup and observed for a particular project other than mere gravity control. Relative gravity measurements obtained over these stations are therefore considered as accurate as well as those of excentre stations (and primary stations). In addition to primary and secondary absolute gravity stations, the network consists of two other types: "fundamental" and "other" absolute stations. Fundamental absolute stations are stations which were built for the purpose of obtaining absolute gravity measurements. TABLE 3.3 shows two in the US and one in Canada. Further investigations show that the two USA fundamental absolute stations are located in Boulder, Colorado, same as the storage facilities of USA's absolute gravimeter while the Canadian fundamental absolute station is located in Cantley PQ just outside of Ottawa, also where the storage facilities of JILA-002 gravimeters is located. Lastly, "other" absolute stations are those absolute stations that do not fall in any of the other 3 categories.

Notice again from TABLE 3.3 that only about 35% of the relative stations are classified as secondary while only about 20% of absolute stations are classified as secondary making most of the network consist of primary, excentre and other very stable stations. Also note that most ties to secondary stations were observed only once. In fact, only 2923 secondary relative gravity measurements are included in the adjustment, which is just 29% of all measurements. At this point, it is safe to say that our network consists of stable stations from which high quality measurements were obtained.

3.4.4 Analysis - number and distribution of ties

In order to estimate the time rate of change of gravity from relative gravity measurements, it is imperative to have a large number of uniformly distributed measurements. TABLE 3.2 gives the number of ties within and between regions while FIGURE 3.1 presents a visual representation of the distribution of these ties. These show that we have a network with uniformly distributed relative gravity observation, which most importantly cover almost the entire region.

Notice the large number of stations in northern USA, east Alaska and west Greenland having ties between themselves and to Canadian stations: roughly 200 relative gravity measurements (from 45 ties) link regions together ensuring rigidity of the network (cf. TABLE 3.2). Greenland-Canada and Alaska-Canada are respectively linked together by only 51 and 27 relative gravity measurements making the network relatively weak in these regions. Fortunately, there exist a large number of Canada-Canada ties in these regions (eastern and western Canada) which compensate for such shortcomings, supporting the evidence that there exist a large number of uniformly distributed ties (or measurements) across the network which is critical when high accuracy is sought.

3.4.5 Analysis - duration of measurements

The time interval between the first and the second reading of any tie observation is critical in analyzing the adequacy of that observation in obtaining reliable g-dot estimates. Two stations could be far apart that requires several hours of driving, sometimes on rough terrain, to obtain readings between them. This travel distance can negatively affect the accuracy of such observation, in fact we believe that measurements obtained within a few minutes are likely to be more accurate that longer ones. It is therefore crucial that measurements have minimum time between readings. TABLE 3.4 below gives the number of relative gravity measurements obtained within different time intervals while FIGURE 3.2 shows a graphical representation of such distribution.

TABLE 3.4: Distribution of relative gravity measurements according to length of observation (time interval between the first and second reading).

Time Between Readings (Hours)	No of Measurements	Relative Frequency
[0 , 1)	2932	29.03%
[1 , 2)	3135	31.04%
[2 , 3)	1621	16.05%
[3 , 4)	844	8.36%
[4 , 5)	420	4.16%
[5 , 6)	249	2.47%
[6 , 7)	194	1.92%
[7 , 24)	654	6.49%
OVER 24H	52	0.51%
TOTAL	**10101**	**100.00%**

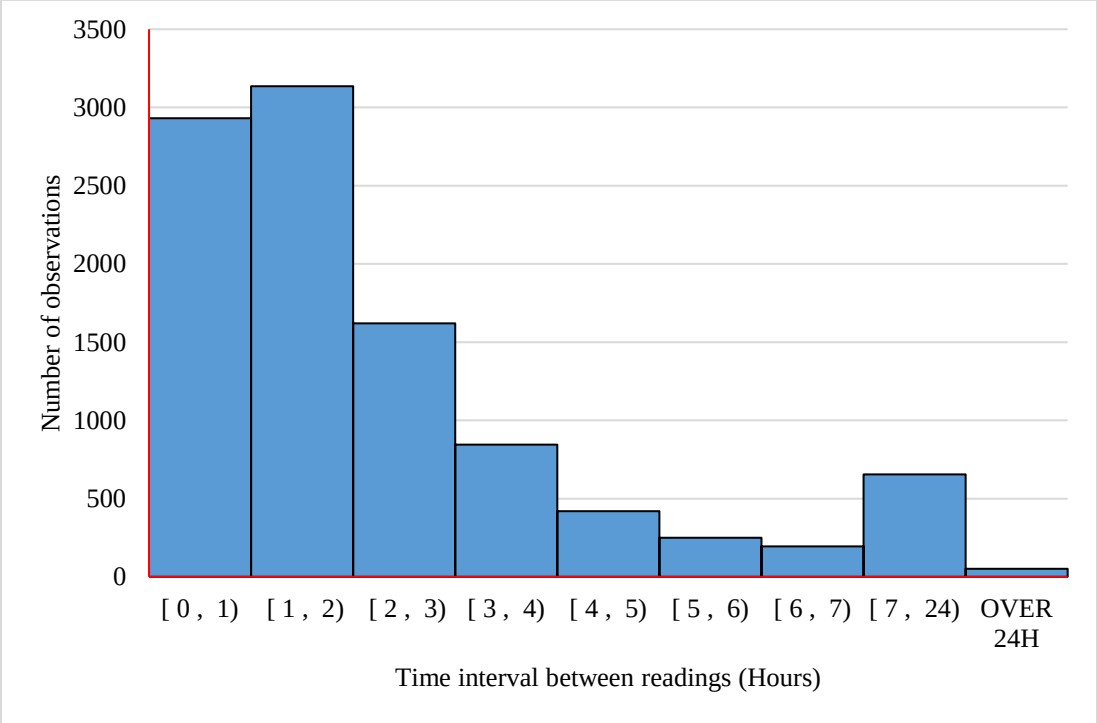

FIGURE 3.2: Histogram depicting the distribution of relative gravity measurements according to the length of observation (time interval between the first and the second reading).

TABLE 3.4 (and FIGURE 3.2) shows that 52 measurements were obtained in over 24 hours; in fact the longest observation took 157 hours, which is almost a week. These particular measurements are assigned very high standard deviations to account for their duration, during which they might have become erroneous. Notice

that over 85% of measurements are obtained within 4 hours while 60% are obtained within less than 2 hours. These large proportions provide additional evidence towards the adequacy of measurements in performing a reliable adjustment.

3.4.6 Analysis - range, repetition and spread of absolute gravity measurements

Reliability of absolute gravity measurements will be treated in depth in the next chapter. Here a few ideal characteristics of such measurements are discussed. First and foremost, absolute gravity measurements are used to obtain g-dot constraints from the solution of a Weighted Least-Squares Regression (WLSR). As with every Least-squares study, WLSR requires at least one degree of freedom. In fact, a minimum of three absolute gravity measurements is necessary to form an over-determined system. Repetition of absolute gravity measurements at different epochs was therefore vital to accurately and reliably accomplish our task. Recall that only stations with at least 5 epochs (years) of absolute gravity measurements are considered (TABLE 3.5).

TABLE 3.5: Absolute gravity stations from which g-dot constraints are computed.

Station	Years of observation	Observation Range (years)	Number of observations
Calgary	2002 - 2007	5	5
Churchill	1995 - 2009	14	17
Nanoose	1997 - 2006	9	32
Ucluelet	1997 - 2007	10	59
Victoria	1997 - 2008	11	144

As shown in TABLE 3.5, g-dot constraints are computed at 5 absolute stations with many repeated measurements obtained within a minimum of 5 epochs. It is important to note that even though 10 g-dot constraints were used in the final adjustment (cf. FIGURE 3.1), only 5 were directly computed in this work. The other 5, which were used in the adjustment of the CGSN (PAGIATAKIS & SALIB, 2003), were recomputed after absolute gravity measurements were corrected for hydrology (MOHAMMED EL-DIASTY, PERSONAL COMMUNICATION, 2015).

With a weak g-dot signal, it is crucial to have long range measurements. TABLE 3.5 shows that absolute gravity stations have an average observational range of 10 years during which g-dot signals can clearly be detected. The same table shows that all measurements used were obtained after 1994. At this point in time, JILA was seldom used; instead, the more accurate FG-5 gravimeter was used to obtain absolute gravity measurements. The long observational range and high accuracy the absolute gravimeter explains the high degree of trust we placed on these measurements.

The uniform distribution of absolute stations across the continent (cf., FIGURE 3.1) and the large number of absolute gravity measurements per station are imperative when high quality g-dot constraints are sought. In addition to these, it is important that the measurements be uniformly observed in time. An analysis of the spread of absolute gravity observation at each absolute station is performed and the results show that all selected stations have excellent observational spread. Victoria station is presented here as an example (FIGURE 3.3).

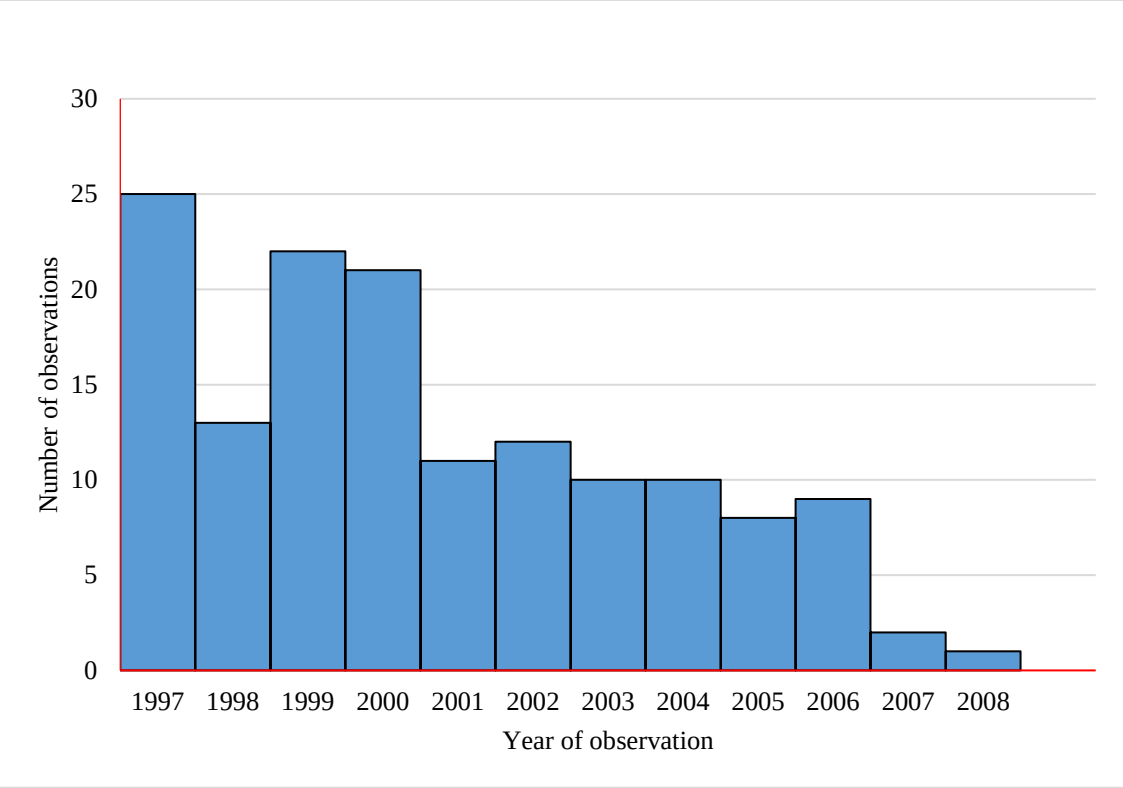

FIGURE 3.3: Histogram depicting uniformity in the distribution of absolute gravity measurements according to year of observation at Victoria station.

Notice from FIGURE 3.3 that, with some exceptions, 8 to 13 measurements were observed each year with an average of 12 measurements per year. This shows uniformity in the spread of measurements ensuring reliable g-dot computation. Similar analysis was conducted for the other 4 absolute stations whose g-dot constraints were computed in this work and comparable results were obtained. We therefore concluded that all selected stations have sufficient absolute gravity measurements, uniformly observed over a long range of time, making them adequate for constraint adjustment.

3.4.7 Analysis - range, repetition and spread of relative gravity measurements

The final network consists of 1659 ties or station pairs from which 10101 relative gravity measurements were collected over the years. Most ties were observed within a year but for a few ties, repeated measurements were obtained over a series of years.

Recall that the CGSN was set up for gravity control, as such, it was not observed uniformly in time but on as need basis. FIGURE 3.4 shows that for most ties (1446 ties), all relative gravity measurements were recorded within a year. It is worth noting that it is not necessary to have individual ties recorded over many years. The entire network was observed between 1958 and 2010 (TABLE 3.7) producing over 46 years of measurements. For an expected g-dot of 2 µGal/year, in some regions, our observation presents a more than adequate time range for g-dot detection. G-dot signals are very weak and observable only over a long period of time.

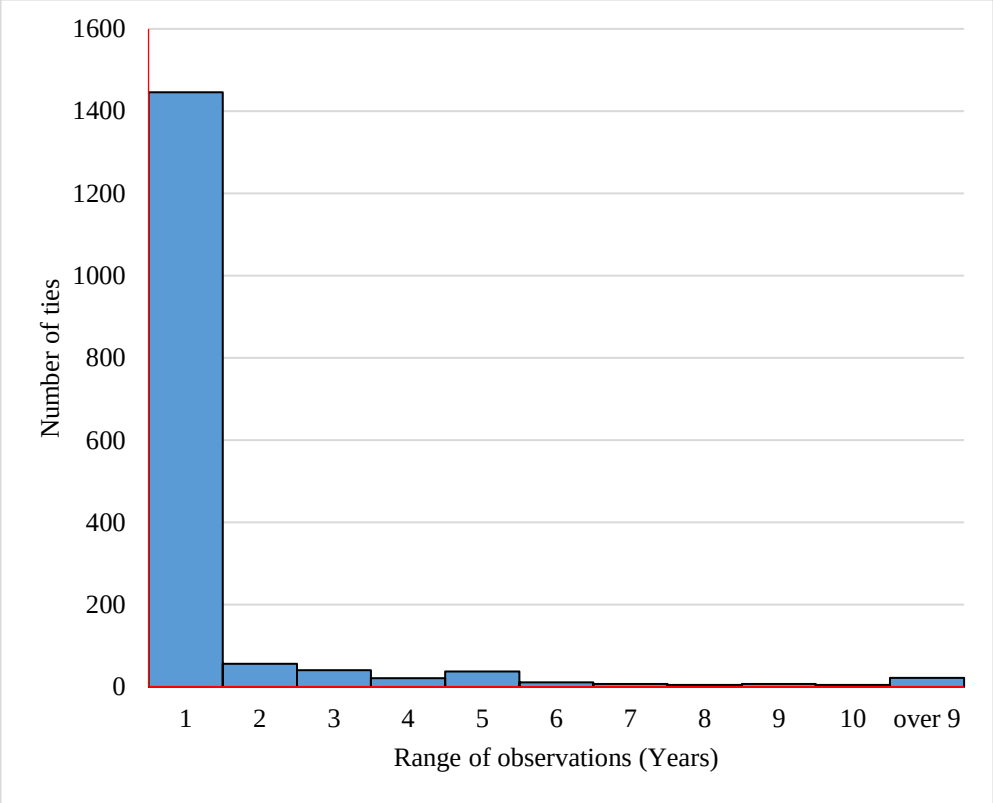

FIGURE 3.4: Histogram depicting the distribution of ties observed within different time epochs.

Repetition of relative gravity observations is even more essential for g-dot estimation. Here however, not every tie needs to have repeated observation and there is no minimum number of measurements per tie

required. It is very important to have sufficient ties with repeated measurements. The term "sufficient" is really just a matter of perspective and this requirement cannot be guaranteed before the adjustment. A true quantification of the sufficiency of measurements is determined post-adjustment. TABLE 3.6 shows the distribution of ties according to the number of times they were observed. Notice that only 337 ties were observed only once, the rest had at least one repetition; in fact, some were observed as many as over 10 times. Single observation ties consisted mainly of secondary ties (ties involving at least one secondary station) and concentrated within Canada due to the elevated number of secondary stations in the area (notice the 281 ties in Canada observed only once). On the other hand, almost 80% of all ties in the network were observed at least twice. In fact, 17% were observed 4 times, 16% 8 times and 10% more than 10 times. It therefore seems fair to say that our measurements pass the test for sufficiency and no additional ties are necessary at this stage.

TABLE 3.6: Distribution of ties according to the number of times they were observed.

No obs. per tie	**Number of ties**						
	Alaska	**Canada**	**Greenland**	**USA**	**Others**	**Total**	**%**
1	2	281	3	44	7	337	20.31%
2	6	165	7	70	16	264	15.91%
3	1	68	4	22	1	96	5.79%
4	5	125	37	107	6	280	16.88%
5	0	19	1	7	0	27	1.63%
6	4	55	5	34	3	101	6.09%
7	5	18	3	12	0	38	2.29%
8	4	63	4	210	2	283	17.06%
9	1	8	0	11	3	23	1.39%
10	2	7	4	15	1	29	1.75%
10+	18	53	2	102	6	181	10.91%
TOTAL	**48**	**862**	**70**	**634**	**45**	**1659**	**100.00%**

In addition to having sufficiently uniformly distributed gravity ties, accurate g-dot estimates are achieved only if these measurements are obtained at regular time intervals. A huge gap in measurements could bring bias in the form of datum shift. It is therefore imperative that for many ties, repeated measurements be roughly evenly obtained in time. Now, it is almost impossible to analyze each of the 1659 ties so what we present here is an analysis of all measurements obtained over the entire network. This analysis is summarized in TABLE 3.7 and graphically represented in the form of a histogram in FIGURE 3.5.

TABLE 3.7 shows the distribution of relative gravity measurements in time between 1958, when the earliest measurement was recorded, and 2010, when the last observation was recorded, grouped in two year periods. This together with the histogram in FIGURE 3.5 shows, reasonable distribution of measurements from 1958 to 2010.

TABLE 3.7: Distribution of relative gravity measurements according to year of observation.

Years of Observation	**No of Observations**	**Relative Frequency (%)**
[1958 , 1960)	12	0.12
[1960 , 1962)	251	2.48
[1962 , 1964)	723	7.16
[1964 , 1966)	1638	16.22
[1966 , 1968)	3085	30.54
[1968 , 1970)	287	2.84
[1970 , 1972)	476	4.71
[1972 , 1974)	303	3.00
[1974 , 1976)	98	0.97
[1976 , 1978)	118	1.17
[1978 , 1980)	289	2.86
[1980 , 1982)	354	3.50
[1982 , 1984)	419	4.15
[1984 , 1986)	80	0.79
[1986 , 1988)	573	5.67
[1988 , 1990)	543	5.38
[1990 , 1992)	456	4.51
[1992 , 1994)	114	1.13
[1994 , 1996)	60	0.59
[1996 , 1998)	14	0.14
[1998 , 2000)	2	0.02
[2000 , 2002)	197	1.95
[2002 , 2004)	1	0.01
[2004 , 2006)	0	0.00
[2006 , 2008)	0	0.00
[2008 , 2010)	8	0.08
SUM	**1010**	**100.00%**

In FIGURE 3.5, a class interval of 2 years is taken for convenience. Notice that over 45% of the measurements were obtained between 1964 and 1968. This was the time interval during which CGSN

operations were at their peak. The number of measurements dropped after 1992 with only 9 measurements recorded between 2002 and 2010; in fact, there was a 4 year gap (2004-2008) during which no observation was recorded. Omitting a few time intervals, an average of 258 measurements were recorded every 2 years. With the exception of the 4-year peak period, the histogram shows reasonable uniformity, clearly seen in FIGURE 3.5 where the bins are of roughly equal heights. One can satisfactorily say that adequate relative gravity measurements are available for reliable g-dot estimation.

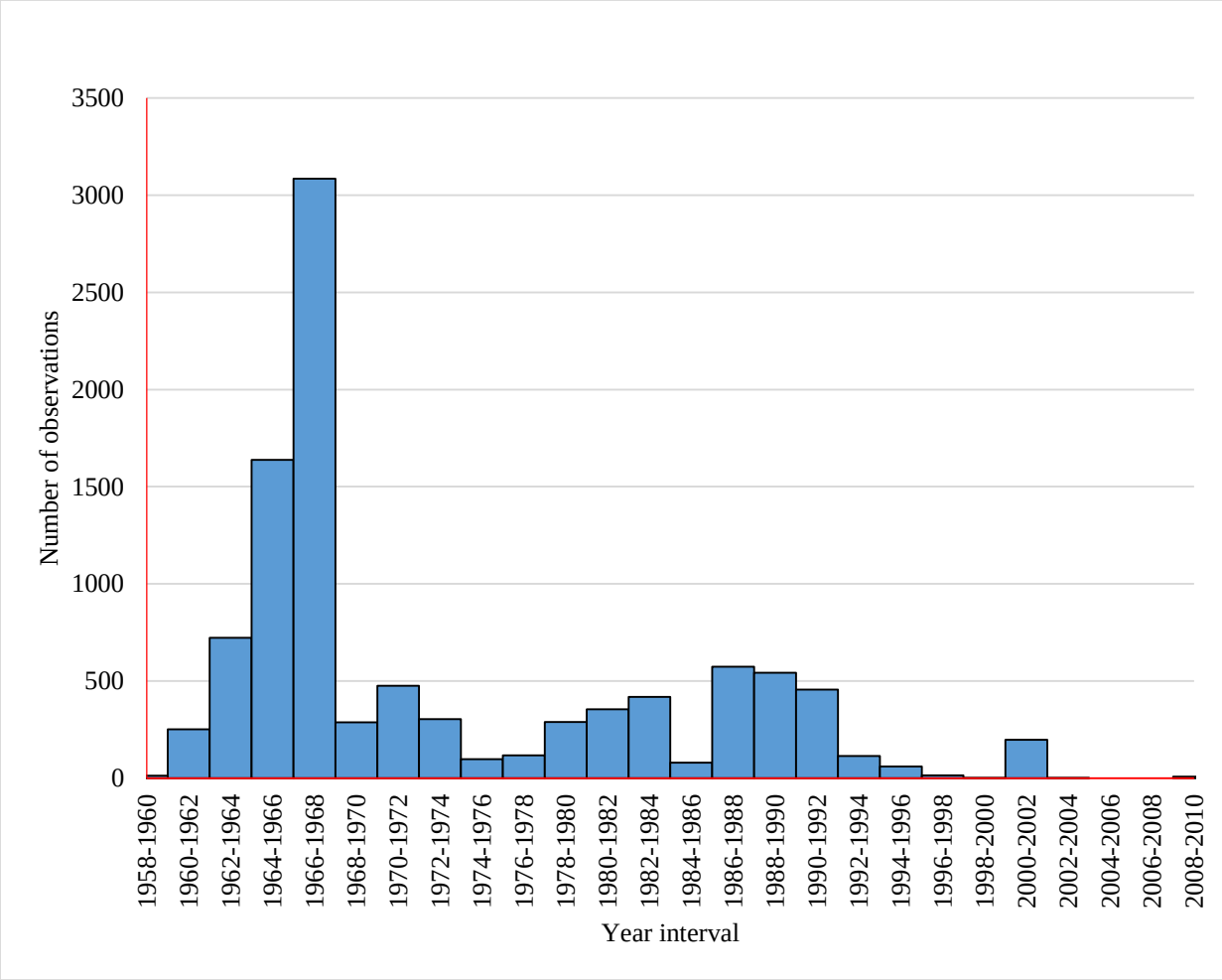

FIGURE 3.5: Histogram depicting the distribution of relative gravity measurements according to year of observation.

After thorough analysis of the data, we conclude that the quality and quantity of measurements used in the adjustment are high. The process of data scrutiny, followed by qualitative and quantitative analysis of residual data is in fact one of the major contributions of this research. In the next chapter we describe the various systematic errors that are expected in the measurements, what models and software are used to

correct them, and what parameters are chosen. We also determine the maximum influence of each effect on measurements and their effect on the final solution.

3.5 SUMMARY

In this chapter we described the source and format of the data used in this work. This includes an overview of relative and absolute gravity measurements as well as time of observation and instrument used. We then performed a qualitative and quantitative analysis of the data in an attempt to investigate their sufficiency and reliability in accomplishing the objectives of this work.

In the next chapter, we provide an in-depth overview of systematic effects expected to be present in gravity measurements. These effects are considered errors and must be corrected before the adjustment. We therefore describe how these effects are computed (what software and/or models are used) and eliminated from the measurements prior to the least squares adjustment of the network.

Chapter 4

Systematic Effects and Corrections

4.1 INTRODUCTION

Systematic effects, as used here, are those physical phenomena that cause perturbation in Earth's gravity field and can be observed with an absolute or relative gravimeter. As mentioned earlier, three phenomena produce systematic effects of significant magnitudes; body tides, ocean tide loading and hydrology. Body tides can reach a magnitude of up to 250 µGal (PERTSEV, 2007) making it the largest systematic effect. Hydrology and ocean tide loading on the other hand have amplitudes as high as 54 µGal (LEIRIÃO, 2009) and 5-10 µGal (LAMBERT ET AL., 1998), respectively. In projects like this one, where sub-µGal g-dots are sought, it is imperative that these effects be eliminated from the measurements. Systematic errors, unlike random or gross errors can, to a high degree of accuracy, be modelled. A lot of effort has been put in the modeling of the systematic errors (e.g. DOLL ET AL., 2003; & HASAN ET AL., 2003**)** and several models exist for each. In this chapter we present a brief summary of the methods used to calculate each systematic effect and we describe what models, parameters and/or the software is/are used to correct such effects.

4.2 BODY TIDES

Notice that only the Sun and Moon are used in the definition of tides; tides normally include gravitational pull from other celestial bodies but for most applications, only contributions from the Sun and the Moon are significant. The small sizes and/or long distances of other celestial bodies from the Earth make their contributions negligible. In fact each tidal signal is represented by a combination of various components called tidal constituents of varying amplitudes and periods. Each constituent is given a 2 or 3 character name (usually a letter and a number). The letter usually represents the principal source of the tide, while the number represents its rate of occurrence (diurnal, semi-diurnal, etc.) (HICKS, 2006), for example, tidal constituent M2 is caused by the attraction of the Earth by the Moon (M) whose occurrence is semi-diurnal, i.e., twice a day, hence M2.

The rise and fall of sea levels due to ocean tides cause perturbation in Earth's gravity field the magnitude of which is usually proportional to the proximity of the observation point from the tide location. Ocean tides is a complex phenomenon whose magnitude depends on several factors including the alignment of the Moon and Sun relative to the Earth, the rotation of the Earth, the altitude of the Moon, etc. (HICKS, 2006).

The amplitude of the tides also depends on the shape of coastal lines and near shore bathymetry. Therefore, tide gauges have been installed at many coastlines around the world where tides are measured. These measurements are combined with satellite measurement to produce numerical ocean tide models (LE PROVOST ET AL., 1998).

GWAVE is a gravity tide prediction program (MERRIAM, 1994) used to remove the gravity tide signal from gravity measurements with predictions accurate to about 40 nGal in the direct attraction and indirect effect of the Sun and Moon. It is based on the Xi Qinwen series of 3070 tidal constituents, including the most common and significant tidal constituents M2, S2, K1, O1, N2, P1, K2, Q1 and many more of lower amplitude, making it ideal for accurate completion of the data analysis of this research. It is therefore the most appropriate software for correcting body tides.

GWAVE is used to calculate the effect of body tides on each measurement taken over the entire network. In this research, only relative gravity measurements require tidal correction as the absolute gravity measurements provided to us by Natural Resources Canada had already been corrected for this effect.

FIGURE 4.1 shows a histogram depicting the magnitude of systematic effects due to body tides on relative gravity measurements. Note that 3958 ties included in the final adjustment came from the previous adjustment for the g-dot map of Canada (PAGIATAKIS & SALIB, 2003) and had previously been corrected for all systematic effects.

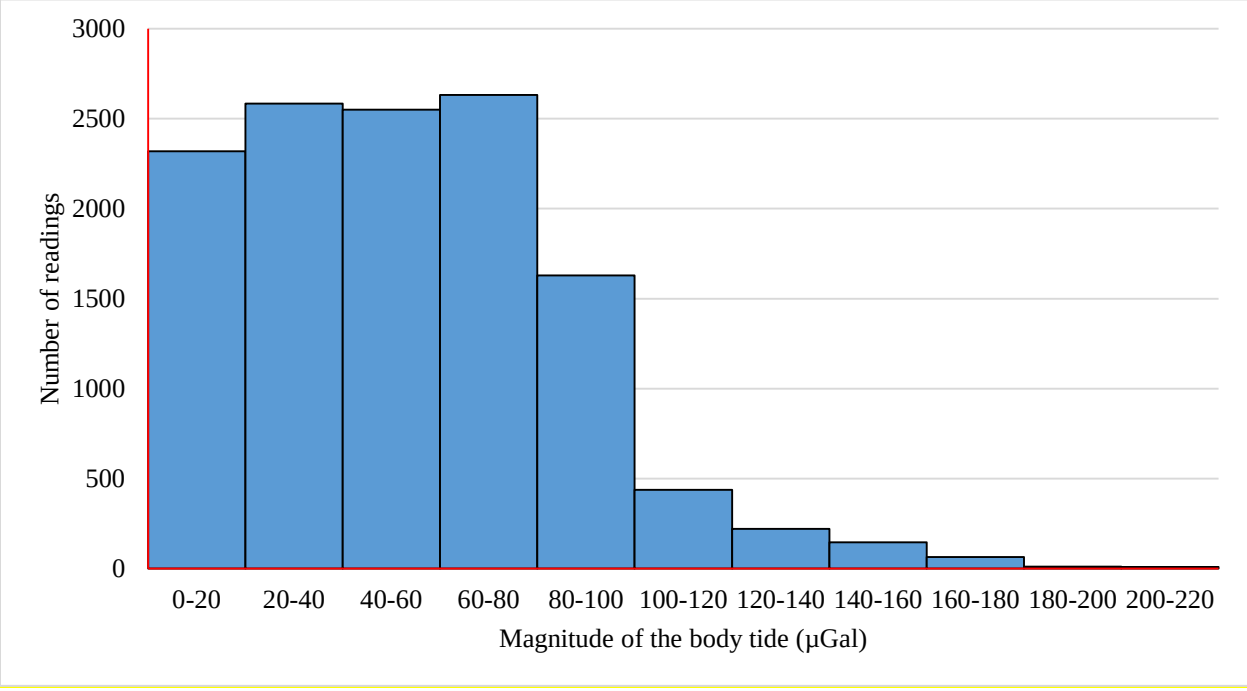

FIGURE 4.1: Histogram depicting the distribution of systematic effect due to body tides for all measurements at the time each gravity reading was recorded.

We therefore calculate here body tides effects for 6143 new relative gravity measurements. Recall that the measurements were recorded primarily using LaCoste-Romberg gravimeters with typical precision of about 20-30 µGal. Body tides therefore introduce significant effects to gravity measurements which must be removed before the adjustment. Each relative gravity observation consists of 2 readings, one at each station. The effect of body tides is different at each station by virtue of their locations and/or times of observation. Such effect is therefore calculated at each station for each observation and used to correct the corresponding reading, which explains the large number (12286) of corrections obtained.

4.3 OCEAN TIDE LOADING

The effect of ocean tide loading on gravity at any location depends on tidal waves around the globe, the principal ones being M2, S2, K1, O1, N2, P1, K2, Q1 and Mf. These waves are the most significant contributors to gravity perturbation around the Earth. Organizations/research groups have dedicated time and effort to develop global models for ocean tide loading which are used by scientists for various purposes. In this work, we use one of such models to compute phasor (that is, amplitudes and phases of each tidal wave) for stations on the network from which the effect (in µGal) of ocean tide loading was computed. We therefore use 2 pieces of software: the first, LOADSDPv5.03 (PAGIATAKIS, 1990), to compute phasors and the second, GENLOAD (IBID, 1990), to compute ocean load effect at the time of the observations.

Several ocean load models have been developed over the years, some of which have been used by scientists to calculate the effect of ocean load on gravity e.g. Schwiderski's Ocean Tide Model (PAGIATAKIS, 1982); FES95.2 (PAGIATAKIS & SALIB, 2003; LAMBERT ET AL, 1998); CSR4.0, GOT99.2b, NAO.99b, FES2004, TPXO7.1, and TPXO7.2 (KIM ET AL., 2011); in fact, KIM ET AL., (IBID, 2011) compared the effect of ocean load obtained from 6 models and found only small discrepancies. These uniformly distributed global ocean tide models have been developed from satellite altimetry and refined with data from tide gauges, bottom-pressure gauges and from GRACE space gravity mission (IBID, 2011). The accuracy in the computation of the ocean loading effect mostly depends on the Earth model (Green's functions) and ocean tide model (forcing). Any of these models would have been adequate for accurate completion of this work. The FES2012 model is chosen here because it is the most recent model. The previous version FES95.2, which uses the same format as FES2012, was used in the previous adjustment and software GENLOAD was written to read input model in that format.

FES2012 or Finite Element Solution 2012 is a fully revised version of the global hydrodynamic tide and the current tidal model. It uses longer altimeter time series, improved modelling and data assimilation techniques, and more accurate ocean bathymetry (NOVELTIS ET AL., 2012). The model comprises of 32

tidal components on 1/16° grids (amplitude and phase). For the purpose of this research, only the 9 most significant (high amplitude) tidal constituents are used.

FES2012, like many global ocean models, does not usually perform well close to the shore, in fact it does not cover the near shore areas with high tides. To maintain high accuracy, a local ocean model is used to compute phasors for a few regions along the east coast, west coast and the area around Hudson Bay. Interested readers are referred to LAMBERT ET AL., (1991; 1998) for more information on this model and methodology. A masking file is used when calculating amplitudes and phases from the global model to mask the coastal regions mentioned above. This file defines the geographical cells (of varying sizes) to be excluded from the global model and for which phasors would be computed using local ocean models. Phasors obtained from each model for different regions are then added vectorially to obtain accurate phasor for all stations on the network.

As mentioned earlier, two software are used to compute the ocean load effect that is, LOADSDPv5.03 and GENLOAD. These software were originally written by PAGIATAKIS (1982) using elastic Green's functions (Farrell, 1972) and later modified to compute the ocean load effect driven by FES95.2 ocean tide model. The latest ocean tide load software (LOADSDPv5.03) is adapted in this work to compute the ocean load effect using the most recent FES2012 ocean model. LOADSDPv5.03 computes phasors at a location (given by its latitude and longitude) using the Green's function method. The Green's functions provided for this work were derived by PAGIATAKIS (1988) on the Preliminary Reference Earth Model (PREM) considering a viscoelastic, anisotropic, and rotating Earth (IBID, 1988). Evaluation of the load effect is done through a convolution integral by convolving FES2012 ocean tide model with these Green's functions (PAGIATAKIS, 1988).

The effect of ocean tide loading (in µGal) on observed relative gravity obtained by GENLOAD is summarized in FIGURE 4.2. FIGURE 4.2 shows that the magnitude of the systematic effects introduced by ocean tide loading ranges from 0 µGal to 12.6 µGal with a mean of about 1.7 µGal. Again, this effect is computed for only 6143 new relative gravity measurements. Though small, this effect is significant when µGal level g-dot are sought and must be removed from the gravity measurements before the adjustment. Each gravity tie consists of 2 readings, one at each station. The load effect is different at each station by virtue of their locations and/or times of observation. Such effect is therefore calculated at each station for each observation and used to correct the corresponding reading, which explains the large number (12286) of corrections obtained.

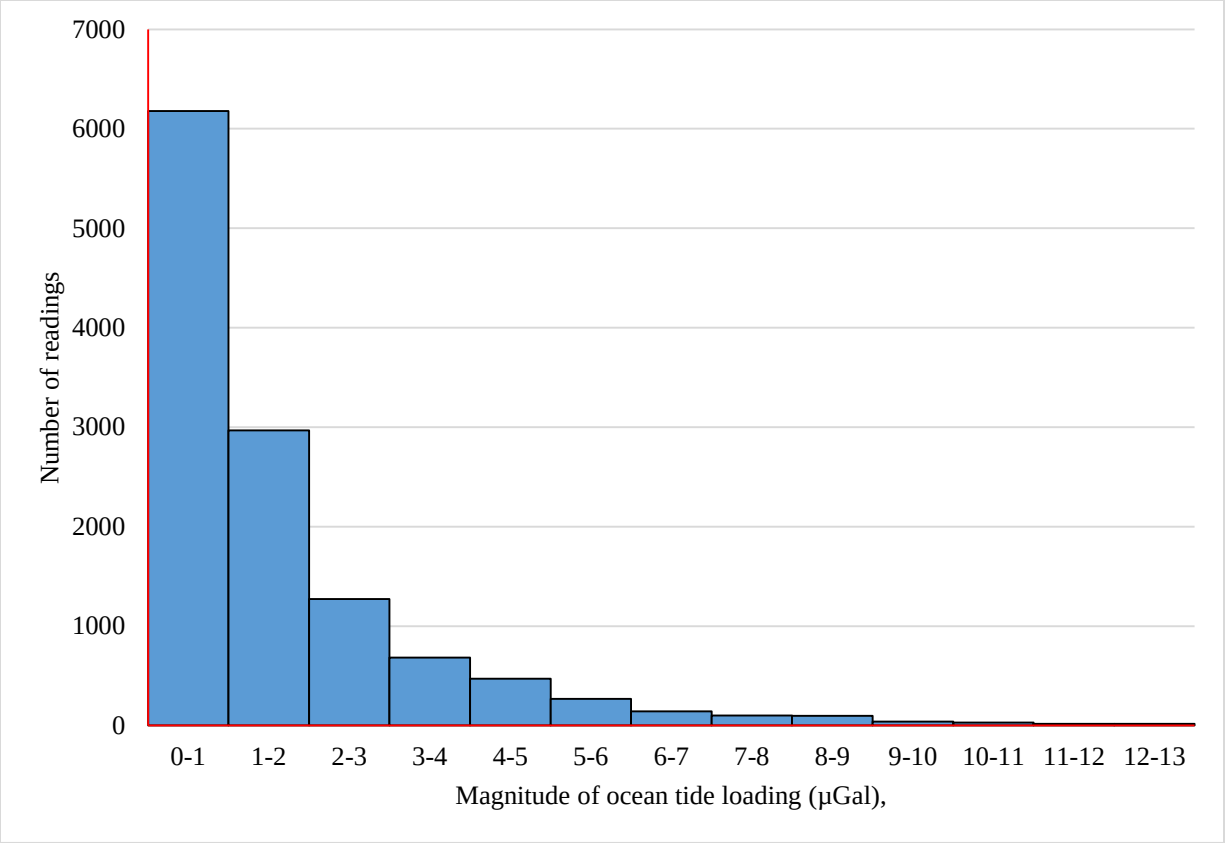

FIGURE 4.2: Histogram depicting the distribution of systematic effect due to ocean tide loading for all measurements at time a reading at each station was recorded.

4.4 HYDROLOGY

The effect of hydrology at a gravity station depends on the height of ground water in a large region around the station. This water height consists of both vertical water balance (water table) and total water runoff (surface water runoff and groundwater recharge). These variations induce substantial perturbations to Earth's gravity field and therefore constitute a significant systematic error to observed gravity. Research groups have dedicated time and effort to develop global models for water availability and water use, one of such models being WaterGAP. In this research, WaterGAP (WGHM2.2a) is used to compute the hydrology effect on gravity (in µGal). The software to calculate this effect is based on LOADSDP and described later in this section.

WaterGAP is a global model of water availability and water use developed to assess the current water resources regime and to estimate the impact of global change on water scarcity. It was developed by the Centre for Environmental Systems Research at the University of Kassel in 1996 and is now maintained

with contributions from The University of Frankfurt (ALCAMO ET AL., 1997). WaterGAP Global Hydrology Model WGHM2.2a, a sub-model of WaterGAP 2 (the most current WaterGAP model), computes surface runoff, groundwater recharge and river discharge at a spatial resolution of 0.5° (DOLL ET AL., 2003). For each cell, the daily vertical water balance and the total runoff are calculated. This model is calibrated against measured discharge at 724 gauging stations, which represent 50% of the global land area (IBID, 2003).

The effect of hydrology on Earth's gravity field can be divided into two parts; the inner zone or gravitational attraction effect and the outer loading effect (MIKOLAJ, 2015). The outer loading effect is evaluated through a convolution integral by convolving water heights (provided by the hydrology model – WGHM2.2a) with appropriate Green's functions. Cubic spline interpolation is first used to determine the coefficients of the discrete Green's functions values provided (PAGIATAKIS, 1990), which are in turn used in an integration kernel for input angle ψ to obtain Green's functions. This effect is very small and almost invariant, therefore insignificant.

The second part, the inner zone effect, is simply the Bouguer plate approximation equivalent to the total water storage. It is also computed using the hydrology model (WGHM2.2a) where the Bouguer plate approximation is implemented using the density of the water to estimate the equivalent gravity. This is done using the following formula (HEISKANEN & MORITZ, 1967)

$$\delta g_B = 2\pi G \rho H \,, \tag{4.1}$$

where δg_B is the inner zone hydrology effect, G is the universal gravitational constant, ρ is the density of fresh water and H is the height of water at the station obtained from WGHM2.2a. The inner zone effect has high variability and is very significant, therefore constitutes the bulk of the hydrology effect.

Routines to calculate the inner and outer zone effects of hydrology were programmed into software – LOADSDP and used here to calculate the effect of hydrology on absolute gravity measurements as the algebraic sum of the inner and outer effect. Variation of the total effect of hydrology on gravity as well as the variation in water heights for regions around Calgary station are summarized in FIGURE 4.3.

FIGURE 4.3 shows the effect on gravity due to hydrology (blue) caused by variation of water height (orange) at Calgary station from 2002 to 2007. Notice that, as expected, both quantities vary proportionately that is, an increase in water height leads to an increase in water mass around the station which in turn leads to an increase in gravity around that station and vice versa. In fact, water heights varying from 31.2 to 52.4 cm introduce systematic effects ranging from 19.7 to 28.7 µGal. We can say that, with no doubt, variation in water storage in a region affects the gravity field appreciably. For absolute gravimeters (JILA or FG-5) with typical precision of about 2-5 µGal, hydrology introduces significant effects to the gravity measurement

which must be removed prior to the network adjustment. The same analysis was conducted for all absolute stations and a similar pattern was observed.

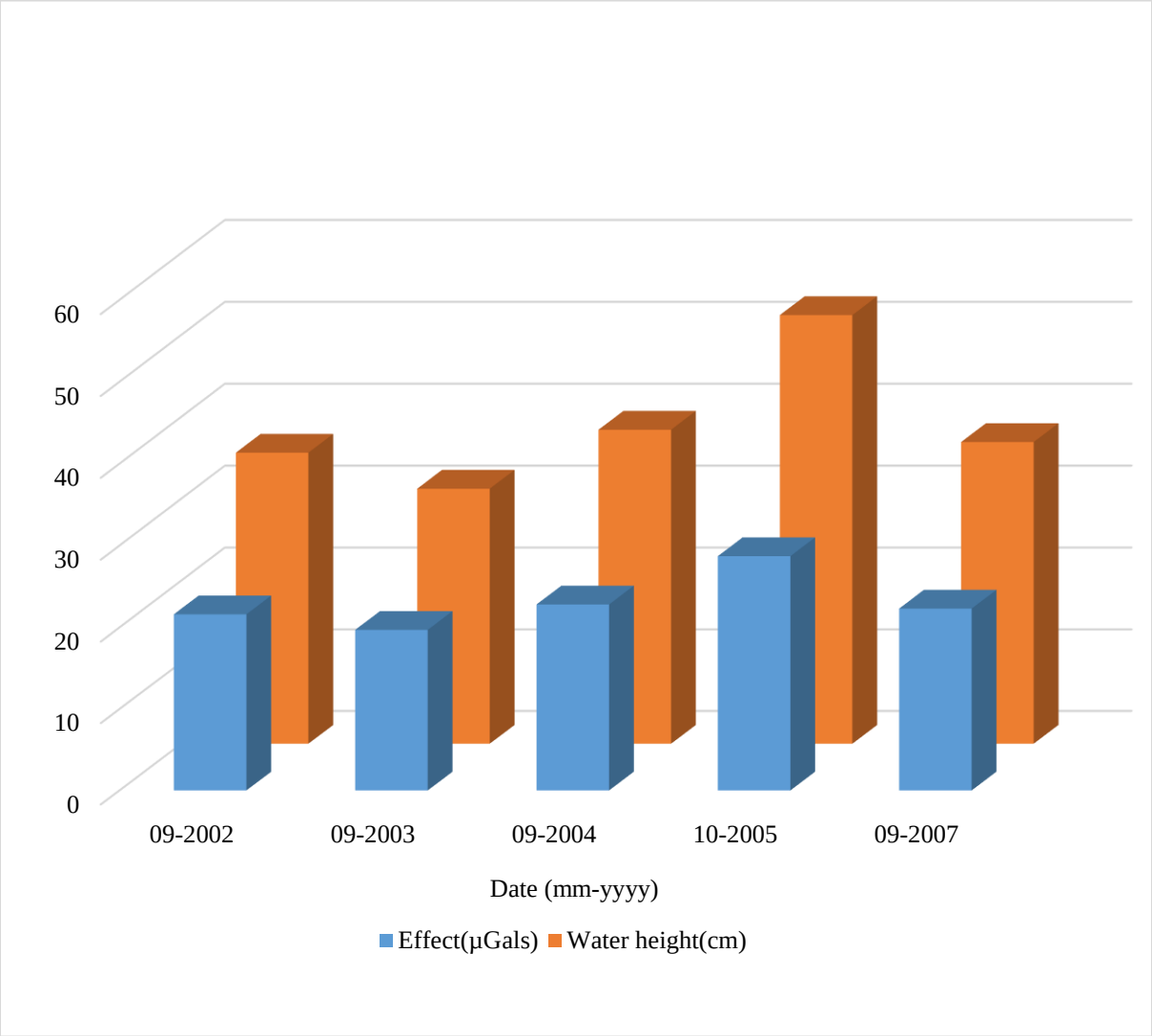

FIGURE 4.3: Bar graph showing yearly variation in water height (orange) and corresponding variation in total effect of hydrology (blue) on gravity at Calgary station.

Notice from TABLE 4.1 that even though the hydrology effect on gravity is the strongest at Churchill (65.4 to 73.6 µGal), it seldom varies (0.6 µGal variation per year). The stability of hydrology at Churchill can be explained by the fact that the water storage around the Churchill station is high but does not change very much in time due to permafrost, therefore gravity does not change as much as in other stations. Ucluelet on the other hand experiences the largest variation followed by Nanoose, Victoria and Calgary. These significant magnitudes make the correction for the effect of hydrology imperative.

TABLE 4.1: Relationship between water height and gravity variation at absolute gravity site.

Station	Years of Observation	Range (years)	Water Heights (cm)			Effect (μGal)			
			Min	Max	Range	Min	Max	Range	Yearly Av.
Calgary	2002 - 2007	5	31.26	52.40	21.14	19.7	28.7	9.0	1.8
Churchill	1995 - 2009	14	139.72	158.49	18.77	65.4	73.6	8.2	0.6
Nanoose	1997 - 2006	9	7.33	54.16	46.83	9.5	29.4	19.9	2.2
Ucluelet	1997 - 2007	10	20.93	77.30	56.37	15.3	39.1	23.8	2.4
Victoria	1997 - 2008	11	5.19	53.81	48.62	8.4	29.2	20.8	1.9

FIGURE 4.4 uses absolute gravity measurements at Victoria station to show the pattern before and after the hydrological correction is applied. Notice how the hydrological correction brings considerable change in the magnitude (notice the offset of roughly 15 μGal) but only a slight change in the trend of absolute gravity measurements. Respectively, these considerable and slight changes to the magnitude and trend of the data can be explained by the fact that the hydrology around the Victoria stations is high but fairly constant (cf. TABLE 4.1).

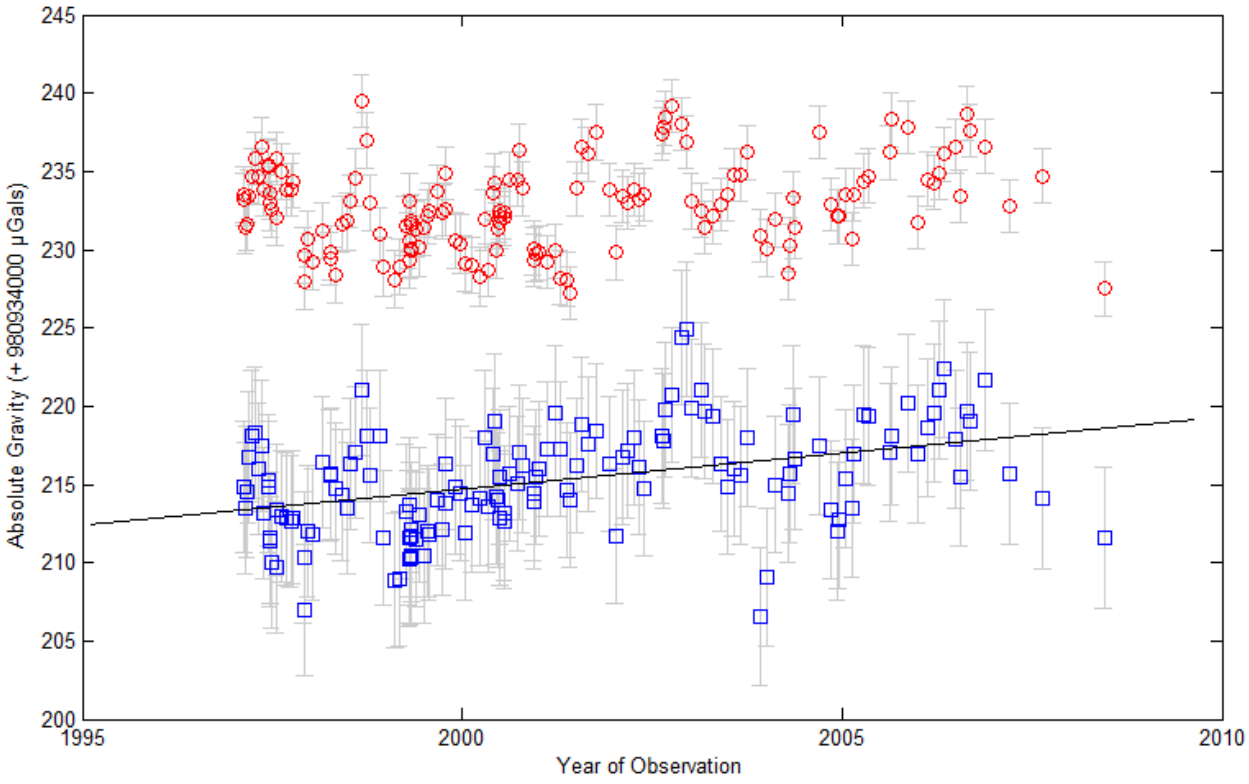

FIGURE 4.4: Absolute gravity measurements before (red circle) and after (blue squares) hydrological correction for Victoria station. Linear trend (black line) defines increasing gravity.

Also, we will see later in SECTION 5.2 that absolute gravity measurements at most absolute gravity sites contain an annual term of unknown origin (notice the sinusoidal pattern in the red circles in FIGURE 4.4). In addition to hydrological correction, this annual term will be suppressed before g-dot constraints computation.

Note that hydrological corrections will not be applied to relative gravity measurements for obvious reasons; ties were observed within a few hours, time during which hydrology is constant. Also, stations forming a tie are normally within 10 to 50 km, and any difference in water level between the two locations cannot be detected using our hydrology model (WGHM2.2), which provides water heights on a 0.5° by 0.5° grid (low resolution).

4.5 POLAR MOTION

The Earth, by virtue of its axial rotation, experiences a centrifugal force; force which contributes to its gravity field. Variations in either the rate of rotation or in the position of the rotation axis (i.e., polar motion) will perturb the centrifugal force (WAHR, 1985). Polar motion therefore causes disturbance of Earth's gravity field which affects surface gravity measurements. We deem unnecessary to correct measurements for polar motion as such correction would not affect the outcome of this work. Relative gravity measurements were recorded within a few hours, from stations that are not very far apart (normally within 10 to 50 km). Therefore, the effect of polar motion, which is very slow with periods of one year (annual period) and about 14 months (Chandler period), will be identical at both stations and cancel out in Δg.

4.6 SUMMARY

An in-depth description of the methodology used to correct significant systematic effects in the gravity measurements that is, body tide, ocean tide loading and hydrology was presented in this chapter. This includes a description of the models, software and procedure undertaken for each effect. The framework through which systematics errors can be calculated and eliminated from gravity measurements is in fact another significant contribution of this research.

In the next chapter, g-dot constraints are calculated from corrected absolute gravity measurements; input files required by GRAVNET are set up; and a realistic covariance matrix is determined using techniques similar to those in PAGIATAKIS & SALIB (2003).

Chapter 5

Weighted Constraints, the Weight Matrix and Associated Vectors

5.1 INTRODUCTION

Early on in this work, we reckoned to constrain our network at those stations with the adequate number of absolute gravity measurements from which high accuracy g-dots could be estimated. In the first part of this chapter, we therefore describe how these g-dot constraints are calculated using the method of Weighted Least-Squares Regression (WLSR).

As stated earlier, GRAVNET is a piece of software initially written to adjust the Canadian Gravity Standardization Network (CGSN) and later adapted to also compute the time rate of change of gravity (g-dot) (PAGIATAKIS & SALIB, 2003). This computation is done via the method of Least-squares using the vector of observations and the vector of initial approximations to unknown parameters along with their associated covariance matrices (cf. SUB-SECTION 2.3.3). SECTIONS 5.3 to 5.6 therefore include a description of how each of these vectors/matrices was formed. Entries of the vector of observations are directly obtained from the tie and/or base files (obtained from the National Gravity Data Base), while those of the covariance matrices of observations and of initial approximations to unknown parameters are based on instrumentation used, instrument calibration, observational evidence and experience of the investigator.

These vectors and matrices are supplied to GRAVNET using three input files SPC, TIE and NX-1 files, and one SPEC (or specification) file. In the last section, we therefore describe the piece of software that was written as a result of this work to aid create these input files from the tie and station files and set parameters.

5.2 G-DOT WEIGHTED CONSTRAINTS

Weighted Least-Squares Regression (WLSR) here is a line fitting methodology, just like simple linear regression. Its major advantage over the latter is that it assigns weights to each observation inversely proportional to its variance. For each given station, the slope of such regression line of a set of absolute gravity measurements defines the time rate of change of gravity (g-dot) while its y-intercept represents

gravity at a defined epoch. We set our model such that this epoch is the year 2000 for reasons that will soon be clear. As a result, the mathematical model describing our system is given by

$$g^t = g^{2000} + \dot{g}(t - 2000), \tag{5.1}$$

where g^t is gravity at year t, g^{2000} is gravity in the year 2000 and $\dot{g}$ is the time rate of change of gravity (g-dot).

At the outset of this research, computer code was written to perform regression analysis for each absolute site. In addition to computing the line of best-fit (in weighted Least-Squares sense), the software computes the coefficient of determination or r-squared (R^2) which, in addition to the a-posteriori variance factor, describe how well the regression line fits the measurements. The outcome of this analysis reveals that most of the measurements still contain uncorrected periodic signals from one or more systematic effects described earlier. Plots of time series at each absolute site shows a sinusoidal pattern and later confirmed by analysis with Least-Squares Spectral Analysis (LSSA). As an example, FIGURE 5.1 represents a plot of absolute gravity measurements (before hydrological corrections) recorded at Victoria station.

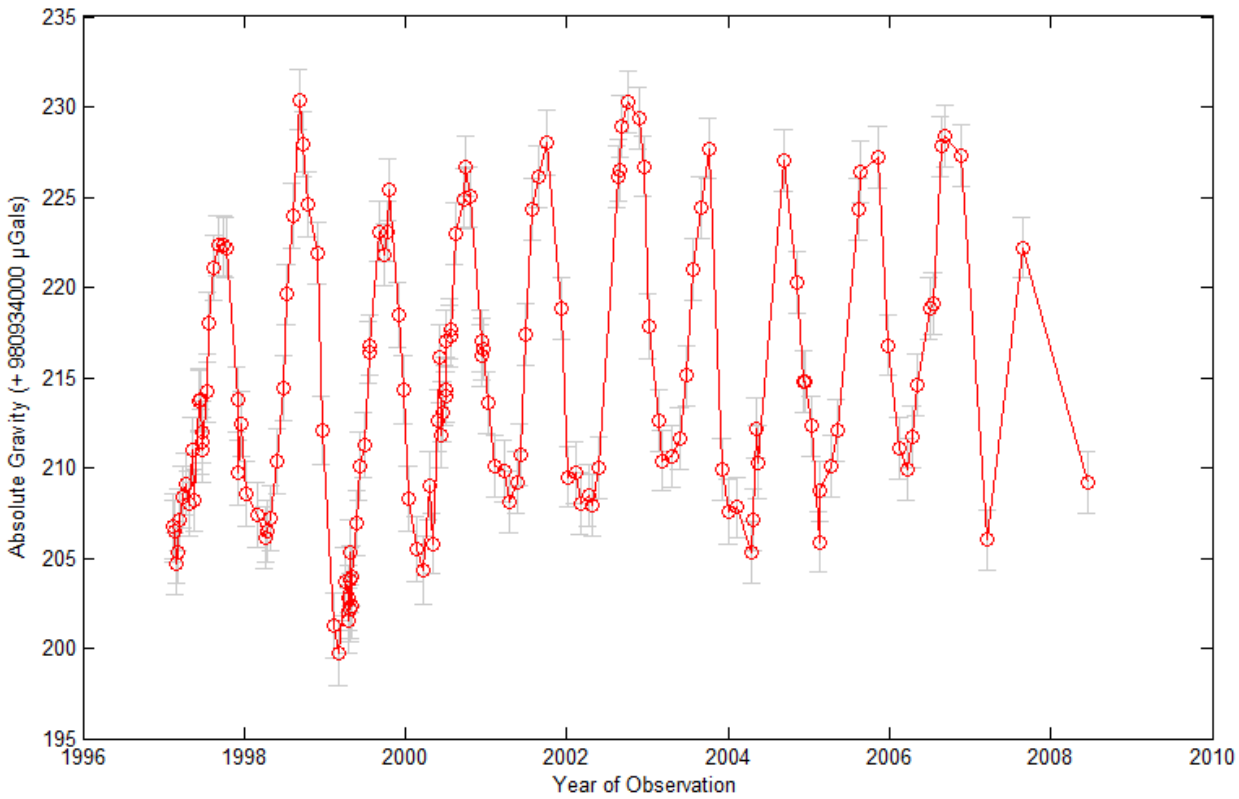

FIGURE 5.1: Time series of absolute gravity measurements at Victoria station.

Notice that, unlike an expected linear trend, the figure clearly displays a sinusoidal pattern in absolute gravity measurements which suggests the presence of a periodic signal. Note that this pattern was maintained after corrections for hydrology were applied (cf. FIGURE 4.4). Based on field procedures [SPIROS PAGIATAKIS, PERSONAL COMMUNICATION, 2016] and information obtained from field books, all absolute measurements are corrected for body tide and ocean tide loading. Unfortunately, the procedures or models used for correcting body tides remains unknown. It is therefore possible that the correction model excluded at least one significant tidal constituent.

To remedy this problem and remove undesirable signals, we perform a spectral analysis of measurements at each site using Least-Squares Spectral Analysis (LSSA). The choice of LSSA over Fourier Transform sprung from the fact that Fourier Transform requires equally spaced data with no datum shifts, which was not the case here. Decimating the data was also not ideal especially since μGal level g-dots are sought. An alternative to Fourier analysis, which most importantly does not require an evenly spaced data set is LSSA. Interested readers are referred to WELLS ET AL., (1985), PAGIATAKIS (1999), PAGIATAKIS (2000) and PAGIATAKIS ET AL., (2007) for more details about this method and its advantages over classic Fourier Transform. In fact, WELLS ET AL., (1985) led to the advancement of software LSSA whose main function is to decompose a signal into its various components using the principle of Least-Squares Spectral Analysis.

FIGURE 5.2 shows one periodic signal of frequency 0.9985 cycles per year (period 365.8 days) whose amplitude is 9.8 μGal. This signal is significant and it is the principal contributor to the sinusoidal nature of the signal as observed in FIGURE 5.1. The only possible explanation to this is that corrections applied to absolute gravity measurements did not include this annual term of unknown origin.

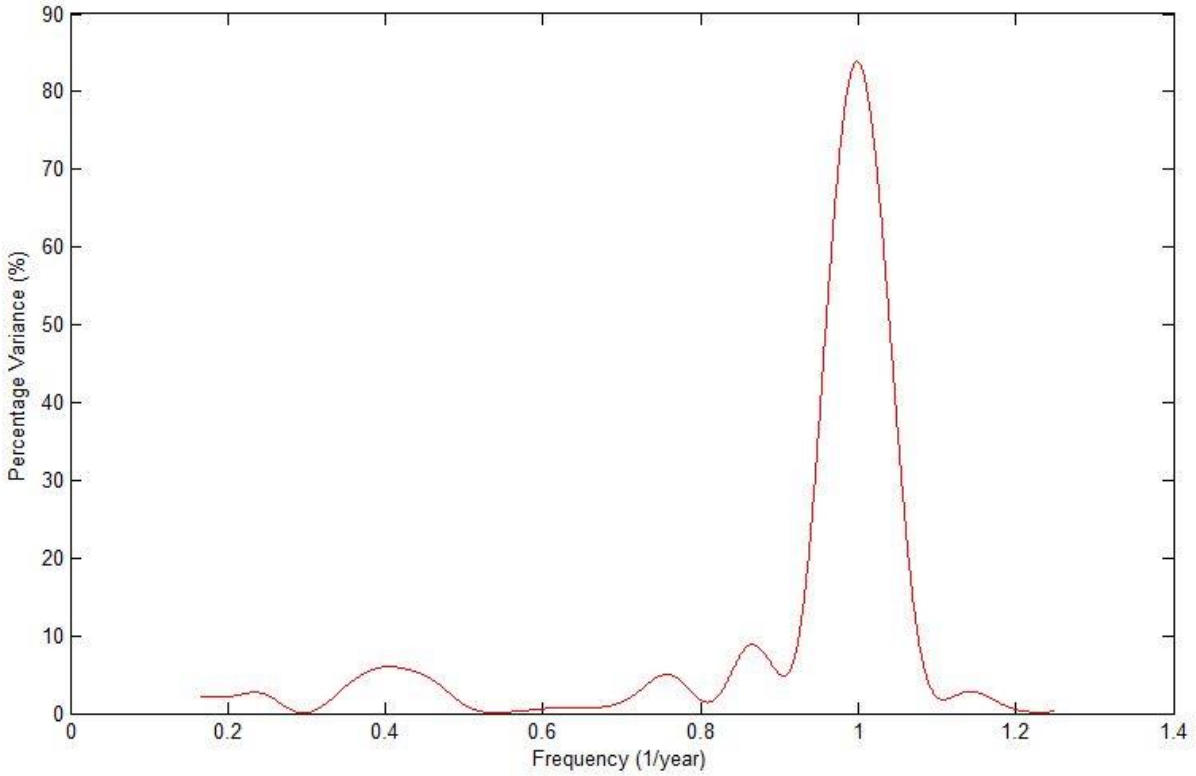

FIGURE 5.2: Least-Squares spectrum of absolute gravity measurements at Victoria stations.

FIGURE 5.3 shows measurements before and after this signal was suppressed. The R-square (coefficient of determination) of these absolute gravity measurements with the annual term (red circles in FIGURE 5.3) is 0.06. After suppressing the annual term (blue squares in FIGURE 5.3), the R-square increases to 0.17, implying that indeed signal suppression brings about a better linear fit. Further spectral analysis of this residual spectrum showed no significant peaks. WLSR is then applied to the corrected signal and a line is obtained (blue line in FIGURE 5.3) with slope (0.46 ± 0.05) μGal/a representing g-dot from which gravity in 2000 is computed as (980934214.8 ± 3.9) μGal. FIGURE 5.3 also shows the line of best fit (red line) that would have been obtained if WLSR was used on the raw measurements. This line has a slope of (0.60 ± 0.05) μGal/a and estimated gravity value of g=980934213.8 ± 3.9 μGal in 2000. Notice that these results are only slightly different because, in this particular case, the annual term has a relatively stable amplitude and a mean approaching zero.

A pattern similar to FIGURE 5.1 was observed at most of the other absolute sites. In the same way, LSSA was used to analyze the absolute gravity signals at each of these sites and the results are summarized in APPENDIX B. Note that APPENDIX B does not include the sites which showed poor fit even after suppressing multiple signals.

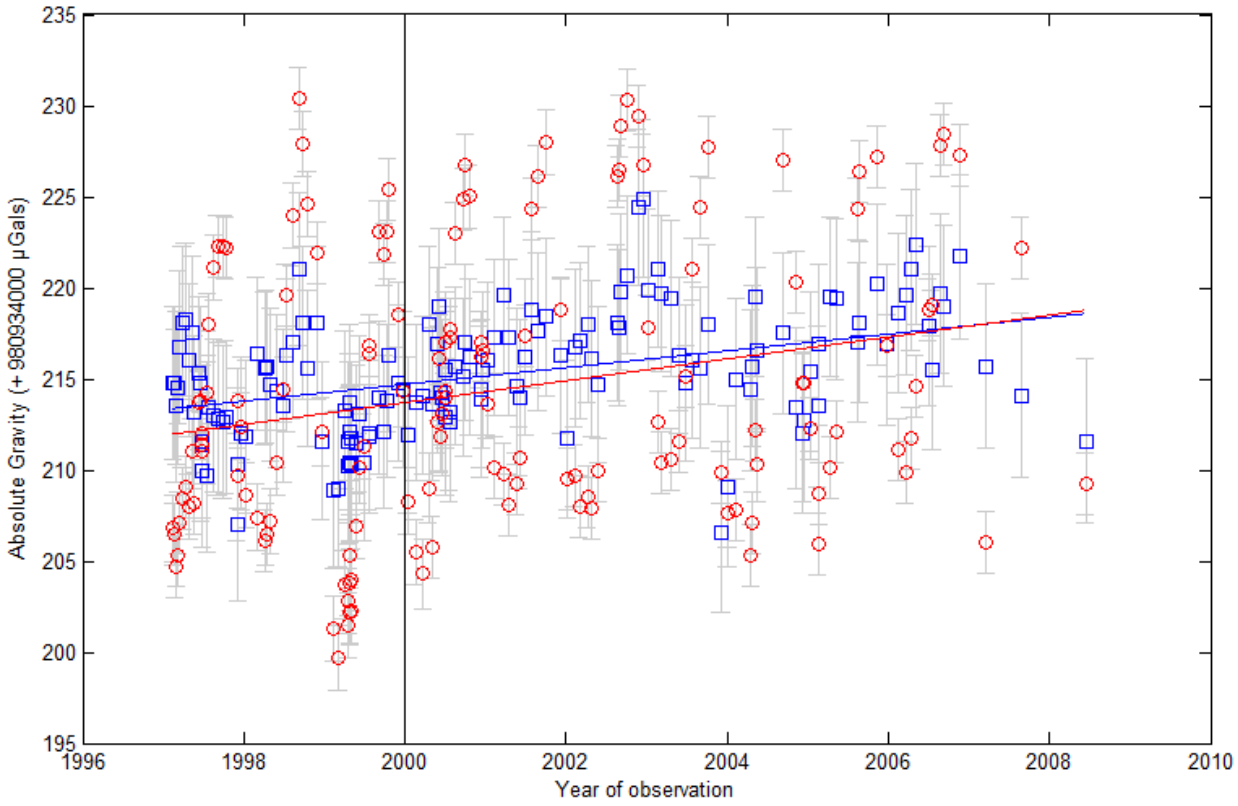

FIGURE 5.3: Absolute gravity measurements before (red) and after (blue) suppressing the signal of period 365.8 days and amplitude of 9.8 µGal at Victoria station. Best fit line of raw (red line) and corrected signals (blue line) are also shown. Black line represents the reference epoch (Year 2000).

Recall from CHAPTER 3 that, albeit the large number of the absolute gravity sites, only ten (10) have the minimum number of observational epochs (5) required for high accuracy g-dot estimation. Of these, only five (Calgary, Churchill, Nanoose, Ucluelet and Victoria) have adequate number of measurements with an acceptable linear fit from which additional constraints are computed. Note that, shortly after the g-dot map of Canada was published, all absolute gravity observations were corrected for hydrology and published g-dot constraints recomputed (MOHAMMED EL-DIASTY, PERSONAL COMMUNICATION, 2015). These newly computed constraints were obtained and used together with these five to constrain our network.

In order to assess the accuracy of the computed g-dot constraints, a comparison between these and those obtained from previous adjustment (PAGIATAKIS & SALIB, 2003) is performed, results of which are summarized in TABLE 5.1.

TABLE 5.1 shows that most g-dot constraints obtained in this work from WLSR of absolute gravity observations are equivalent to those obtained after the adjustment of the CGSN (PAGIATAKIS & SALIB, 2003) with only Churchill showing significant difference. Both computed g-dots at Nanoose and Ucluelet

show positive trends. These stations were not included in the original adjustment of the CGSN but looking at the unconstrained map (IBID, 2003), regions around Vancouver Island also show subsidence (positive g-dot). Of course this was obtained as a result of extrapolation beyond available information which could be overly optimistic. TABLE 5.1 also shows that, in general, we obtain (Column 4) g-dots constraints with lower standard deviations than those obtained during the previous adjustment of the CGSN (Column 2). This means that measurements provide a better fit after the effect of hydrology is suppressed. Note that computed g-dots constraints will be assigned to all stations within the excentre network, which explains why our network will be constrained at 54 stations from these 10 absolute gravity sites.

TABLE 5.1: Comparison between g-dots obtained from the previous adjustment (PAGIATAKIS & SALIB, 2003) that is, g-dot constraints (Column 2) and g-dots obtained after the adjustment (Column 3) and g-dot constraint obtained in this work from corrected absolute gravity measurements (Column 4).

Station	$\dot{g}$ **constraints used in adj. of CGSN (µGal/a)**	$\dot{g}$ **after adj. of CGSN (µGal/a)**	**New Constraints (µGal/a)**
Calgary	n/a	-1.06 (±0.24)	-1.09 (±0.26)
Churchill	-2.00 (±0.11)	-1.72 (±0.08)	-2.47 (±0.15)
Kuujjuarapik	-2.35 (±0.28)	-2.35 (±0.15)	-2.49 (±0.25)
Nanoose	-	-	+0.46 (±0.12)
Penticton	+0.00 (±0.35)	+0.02 (±0.18)	+0.01 (±0.31)
Schefferville	-1.38 (±0.32)	-1.32 (±0.14)	-1.26 (±0.25)
Ucluelet	-	-	+0.29 (±0.09)
Victoria	n/a	-0.70 (±0.28)	+0.46 (±0.05)
Winnipeg	-1.01 (±0.32)	+0.12 (±0.29)	-0.49 (±0.25)
Yellowknife	-1.51 (±0.32)	-1.69 (±0.17)	-1.85 (±0.23)

5.3 THE VECTOR OF OBSERVATIONS

According to our mathematical model, observations consist of relative gravity measurements between stations on the network (cf. EQUATION (2.21)). Each measurement was obtained with a specific instrument at a particular time therefore information about time of observations and characteristics of instruments are important components to the adjustment. Each row of the vector of observations includes the project number followed by the station number, date and time of the first reading; the station number, date and time of the second reading; the instrument number; the gravity readings; and the letter code of the instrument scale factor. As an illustration, three lines of the vector of observations are shown below

1959002 95361959 18-AUG-1959 1920 95431959 18-AUG-1959 2045 W0431 295.4167 582.7353 A

1966605 95861949 25-NOV-1966 1702 95871949 25-NOV-1966 2136 G0093 4115.4541 4111.8456 A

1990620 90811986 06-JUN-1990 1720 98011988 06-JUN-1990 1836 D0027 166.1580 139.4132 D

The vector of observations is formed by augmenting the vector of observations used in the previous adjustment (PAGIATAKIS & SALIB, 2003) with new measurements. All information necessary to accomplish this is directly obtained from the tie file with the exception of gravity readings (in mGal). Gravity readings are mGal equivalences of dial readings (provided in the tie file) at each station. Constants needed to convert dial readings to gravity readings include higher reading (HRDG) and lower reading (LRDG). They are dial readings, respectively, rounded up and down to the nearest hundred, which are obtained from conversion tables and conveniently provided in the tie file. This conversion was done used the following formulae:

$$R = L + (H - L) * \left(\frac{D}{100} - \text{int}\left(\frac{D}{100} \right) \right) \tag{5.2}$$

where, L is the lower reading, H is the higher reading, D is the dial reading and R is the required gravity readings in mGal. For each measurement, R is calculated independently for each station. Every instrument (except LaCoste-Romberg D) has conversion tables that increment by 100. LaCoste-Romberg D instruments have tables that increment by 10 and therefore '100' in the above formula is replaced by '10' for ties observed with such instruments. These formula and specifications were provided by NRCan (MARC VÉRONNEAU, PERSONAL COMMUNICATION, 2015).

The standard deviation of relative gravity measurements, was not initially provided in the tie file. This very important vector is what controls the weight of each observation in the adjustment that is, it forms the diagonal elements of the variance-covariance matrix of the observations vector. Procedures used to assign realistic weights to observation are described in SECTION 5.5. The final vector of observations consists of 10101 lines representing all relative gravity measurements across all four selected regions of North America (Alaska, Canada, Greenland and continental USA).

5.4 THE VECTOR OF INITIAL APPROXIMATIONS TO UNKNOWN PARAMETERS

A vector of initial approximations to unknown parameters (x^0) is required to compute g-dots via the method of generalized Least-Squares adjustment. This vector is formed by lumping individual vectors of unknown parameters into a single vector that is, lumping the vectors of gravity values, g-dots, instrument scales and instrument drifts in a hypervector (cf. EQUATION (2.20)).

The station file retrieved from the NGDB contains gravity values obtained from the International Gravity Standardization Network of 1971 (IGSN71). These values are used as initial approximations to gravity at the reference epoch ($g_i^{t_0}$) for all stations except constraint stations. Of course the year 2000, not 1971, was the reference epoch. Nevertheless these values are appropriate as they only represent initial approximations

used to estimate g-dots due to a slow GIA. Gravity values obtained from WLSR of absolute gravity observations are used as initial approximations to gravity for the constraint stations.

G-dot values obtained from WLSR of absolute gravity observations (cf. Table 5.1) at each constraint site are used as initial approximations to g-dot for each station at that site. Augmented values to the vector of initial approximation to g-dots used in the previous adjustment (PAGIATAKIS & SALIB, 2003) were set at 0 µGal/a. In order to compensate for these arbitrary values, their standard deviations are chosen such that they are well above the largest standard deviation of constraint stations (see SECTION 5.6). PAGIATAKIS & SALIB (2003) showed that initial values of zero are appropriate because the problem converges after 1 iteration meaning that the solution is robust.

The tie file retrieved from Natural Resources Canada (NRCan) contains scales for all instruments on the network. These are used to augment the vector of initial approximations to instrument scales used in the previous adjustment (PAGIATAKIS & SALIB, 2003). On the other hand, augmented values to the vector of initial approximations to instrument drifts used in the previous adjustment (IBID, 2003) are all set at 0.2628 mGal/a (0.00003 mGal/h), a number equivalent to the average of all initial approximations to instrument drifts used in the previous adjustment (IBID, 2003)

The vector of initial approximate to unknown parameters is provided to GRAVNET via the SPC file. Initial values to gravity values and g-dots are provided in the first block (station block) of the SPC file, while initial values to drifts and scales are provided in the second block (instrument block). See APPENDIX A for more details on these blocks. Examples of three lines of the station block are as follows:

TRIAL GVALUE 98021986 979608.5250 ; G-DOT= 0.00000 0.00100 ; BOULDER

TRIAL GVALUE 95231963 981072.8131 ; G-DOT= 0.00000 0.00100 ; SEPT-ILES

TRIAL GVALUE 95211963 981317.4929 ; G-DOT=-0.00126 0.00025 ; SCHEFFERVILLE

Each line of this block begins with the phrase “TRIAL GVALUE” followed by the station number, the initial approximation to gravity (mGal) at reference epoch, the initial approximation to g-dot (mGal/a) and its standard deviation ending with the name of the station. Note that the standard deviations of the initial approximations to gravity values are provided through the NX-1 file (weight matrix). Station names were obtained from the station file.

On the other hand, below are 3 examples of lines from the instrument block of the SPC file:

TRIAL SCALE G0256.C .1978108 0.999974 0.00013 0.00093

TRIAL SCALE G0256.E .1988502 1.000031 0.00027 0.00093

TRIAL SCALE G0256.F .1990804 1.000639 0.00004 0.00100

Each line of the instrument block begins with the phrase "TRIAL SCALE" followed by the instrument code, initial approximation to instrument scale, ending with the initial approximation to instrument drift (mGal/h) and its standard deviation (mGal/h). Note again that the standard deviations of the initial approximations to the instrument scales are provided through the NX-1 file. The instrument code is formed by concatenating the instrument number, and letter code for instrument scale factor and project number are all obtained from the tie file. For the purpose of this work, a gravimeter was considered a different instrument when it was calibrated, serviced, repaired, upgraded or used in a different project, fact that explains the relatively high number of gravimeters used in the adjustment (740 instruments). The instrument code therefore provides a unique identifier for instruments of the same scale factor and drift.

Our network consists of 1030 gravity stations including stations in Alaska, Canada, Greenland and continental USA, and 740 instruments. Recall from CHAPTER 2 that the vector of observations and the vector of initial parameters can be lumped together in a hypervector (cf. EQUATION 2.22) which leads to a generalized Least-Squares adjustment.

5.5 THE COVARIANCE MATRIX OF OBSERVATIONS

Like in every Least-Squares adjustment problem, assigning realistic weights to our measurements is a major challenge and requires lots of time and effort. The weight matrix (P_l) is generally defined as the inverse of the variance-covariance matrix of the observations (C_l), henceforth known as the covariance matrix of the observations. A covariance matrix is a matrix whose principal diagonal consists of the variances of observations while off diagonal elements are covariances between pairs of observations. The covariance matrix of the observations is formed by augmenting the covariance matrix of the observations used in the previous adjustment with new values (PAGIATAKIS & SALIB, 2003). The major challenge in this work is the assignment of variances to new measurements that is, filling the principal diagonal elements. Off diagonal elements (covariances) are all set to 0 (zero) since the measurements are considered statistically independent. PAGIATAKIS & SALIB (2003) assigned variances to Canada-Canada ties based on a meticulous analysis of field notes and personal communication with observers. Information obtained from field notes includes instruments, atmospheric conditions (temperature and wind), mode of transportation, observational procedures, observers, times and lengths of observations etc. Personal communication with gravimeter operators who obtained most of the measurements as well as technicians who serviced and maintained instruments proved very valuable in assigning reliable variances. Readers are referred to PAGIATAKIS & SALIB (2003) for a deeper understanding of procedures used to assign variances. This

intensive process proved valuable as post adjustment analysis of the final solution shows that realistic weights were assigned to the measurements (IBID, 2003).

In this research, we use procedures similar to those undertaken by PAGIATAKIS & SALIB (2003). In their work, all relative gravity measurements obtained with the same instrument (identified by a unique instrument code) were assigned the same initial standard deviation. Depending on other factors, such as wind, mode of transportation, etc., this error was increased proportionately. They considered two ties to be measured with the same instrument if they were measured with the same gravimeter, within the same project and with the same calibration. Once an instrument was calibrated and/or used in a different project, it was immediately considered a new (or different) instrument. They devised instrument codes to distinguish individual instruments. As mentioned in SECTION 5.4, the instrument code consists of a combination of these 3 important characteristics namely, instrument identifier, project number and letter code for instrument scale factor (determined from calibration).

In order to assign reliable standard deviation, each instrument (instrument code) is assigned a factor, representing the standard deviation of all measurements obtained within an hour. This factor is doubled for measurement obtained within 12 to 24 hours. Linear variation is assumed for ties observed within 1 to 12 hours. This rule of thumb was used by PAGIATAKIS & SALIB (2003) and hence adopted here. This is an empirical equation that was derived based on the average drift of the instruments used. Ties observed in over 24 hours are assigned a standard deviation of 0.500 mGal. These "overnight" ties usually necessitated flying the instrument from one station to another, probably causing perturbations within the instrument, hence the large standard deviation. This rule of thumb can be summarized in the following piecewise function

$$\sigma = \begin{Bmatrix} k & for & \Delta t < 1 \\ \left[\frac{1}{11}\Delta t + \frac{10}{11}\right] * k & for & 1 < \Delta t < 12 \\ 2 * k & for & 12 < \Delta t < 24 \\ 500 & for & \Delta t > 24 \end{Bmatrix}, \tag{5.3}$$

where Δt represents time of observation in hours, which is the time interval between reading 1 and reading 2 and k is a factor (in mGal) discussed below.

Factors are obtained by analyzing the vector of observations used in the previous adjustment (PAGIATAKIS & SALIB, 2003). A measurement obtained with the same instrument (same instrument code) used on a Canada-Canada tie in the previous adjustment is assigned the same factor as the later. In fact, factors of all

instruments used in the previous adjustment are provided in APPENDIX C. The standard deviations of 1259 (of 6143) new ties are assigned this way.

The Worden gravimeters are probably the least precise instruments used in the network (as observed from constant calibration) since observations begun in the 1950s. For this reason, we assign the factor of 0.200 mGal to all ties observed with these instruments. Again, standard deviations for 47 (of 6143) new ties were assigned this way.

At this point, a total of 1306 (of 6143) new ties are assigned realistic standard deviations based on the factors and Equation (5.3) above. All remaining new ties (4837) are assigned factors based on the type of instrument used: C (Canadian) and L (Lacoste) instruments are assigned a factor of 0.021 mGal; S (Scintrex) and X instruments are assigned a factor of 0.028 mGal and D (LaCoste Romberg D-meters) instruments are assigned a factor of 0.019 mGal. G (LaCoste Romberg G-meters) instruments on the other hand are assigned a factor of 0.060 mGal for ties observed in 1950 and 0.040 mGal for ties observed in 1980 - linear variation is assumed between and beyond the two extremes. These factors are assigned in accordance to the rule of thumb used in the previous adjustment (*ibid, 2003*).

Due to insufficient time and resources, additional information which would be used to obtain even more realistic standard deviations e.g. field notes, personal communication with operators, etc. could not be obtained. (See APPENDIX C for details on minimum standard deviation assigned to ties based on the gravimeter used).

5.6 THE COVARIANCE MATRIX OF INITIAL APPROXIMATIONS TO UNKNOWN PARAMETERS

The P_{x^0} matrix is defined as the inverse of the variance-covariance matrix of the initial approximations to unknown parameters (C_{x^0}). This weight matrix is important in the adjustment process and is formed by assigning values to the variances and covariances of the initial approximations to parameters. Compared to the C_l matrix, this process is fairly easy and mostly based on observational procedures and experience of the investigator.

The standard deviation of initial approximations to gravity at reference epoch for each new station is set at 0.0435 mGal, a number equivalent to the average of all standard deviations of initial approximations to gravity used in the previous adjustment (PAGIATAKIS & SALIB, 2003). For non-constrained stations present in the previous adjustment (PAGIATAKIS & SALIB, 2003), we use exactly the same initial approximations

as used in that adjustment. Values obtained from WLSR of the absolute gravity observations are used as standard deviations of the initial approximations to gravity values for the constrained stations.

The standard deviations of the initial approximations to g-dots for all new stations (except constraints) are set at 0.001 mGal/a. As mentioned earlier, 0.001 mGal/a is a number well above the largest standard deviation of any constrained station (±0.00035 mGal/a at Penticton), which allows non-constrained stations to change more during the adjustment. The g-dot values obtained from WLSR of absolute gravity observation (cf., TABLE 5.1) are used as standard deviations of the initial approximations to g-dots for constrained stations. Notice that the network constraints are accomplished by controlling the weights of initial g-dots at the constrained stations. These stations have much lower standard deviations, in comparison to all other stations, making their g-dots "resist" significant correction during the adjustment.

The standard deviations of initial approximations to the instrument drifts for all new instruments are set at 8.76 mGal/a (0.001 mGal/h). This number represents the average of all standard deviations of initial approximations to instrument drifts used in the previous adjustment (PAGIATAKIS & SALIB, 2003) and is large enough to allow for the approximate drift values of the new instruments to adjust more (relative to older ones) during the adjustment. New instruments are those instruments that emerged from the new ties having instrument codes different from those of instruments (old instruments) in the SPC file used in the previous adjustment (IBID, 2003). For old instruments, we use the exact same initial approximations as used in the previous adjustment (IBID, 2003).

Instrument scales obtained from the tie file are considered unreliable as they were simply pulled out of the instrument manual but should have been recomputed after each calibration. For this reason, standard deviations of initial approximations to instrument scales are set to 0.000306, a value equivalent to the average of all standard deviations of initial approximations to instruments scales used in the previous adjustment (PAGIATAKIS & SALIB, 2003). For instruments present in the previous adjustment (IBID, 2003), we use the same initial approximations used in that adjustment.

We assume no correlation between these values and thus, all covariances are set to 0. The standard deviations of g-dot values and those of instrument drifts are provided to GRAVNET via the SPC file, while the variances of gravity values and those of instrument scales are provided via the NX-1 file.

Again, as mentioned in CHAPTER 2, the covariance matrix of observations and the covariance matrix of initial parameters can be lumped together in a hypermatrix (cf. EQUATION 24) for generalized Least-squares adjustment. The scale factor for this matrix, which is the a-priori variance factor, is considered known and is set to 1. This information is provided to GRAVNET via the SPEC file through which we also specify that all statistical tests are carried out at the 95% confidence level.

5.7 INPUTGRAVNET

The g-dot values are computed by casting all measurements, initial estimates to unknown parameters, and their standard deviations into a generalized Least-squares adjustment scheme via GRAVNET. These values are provided to GRAVNET with the help of three input files SPC, TIE and NX-1. The SPEC file controls the specifications, such as the scale factor for standard deviations, maximum number of iterations, significance level for statistical testing, etc. for each adjustment.

As seen in this chapter, input files used by PAGIATAKIS & SALIB (2003) to create the g-dot map of Canada were obtained and augmented in this study using corrected measurements from the National Gravity Data Base (NGDB) to include Alaska, Greenland and continental USA stations as well as ties to/between them. Some segments of these files, e.g., the segment containing the vector of the initial approximations to g-dots, were modified to include entirely new values while others, e.g., the segment containing the vector of observations, were left unaltered and simply augmented. In order to accomplish this, we wrote a piece of software called INPUTGRAVNET, which automates the process thereby becoming a valuable addition to GRAVNET. Recall that the routine for cleaning up relative gravity measurements was written in the first part of INPUTGRAVNET (cf., SUB-SECTION 3.3.1) while the routine for counting the number of ties within and between regions was written in the second part of the software (cf. SUB-SECTION 3.4.1). The last routine modifies and/or augments input files using data from any source (e.g., NGDB) in a specific format of the set parameters. INPUTGRAVNET is therefore a software capable of eliminating gross errors from a set of measurements and using it to create input files required by GRAVNET. This software is in fact one of the major contributions of this research. APPENDIX A provides more information on this software.

5.8 SUMMARY

The method of WLSR was used to estimate g-dot constraints from absolute gravity measurements at selected sites. These estimates will be used to constrain the network during the adjustment process in Chapter 6. Furthermore, a description of the formation of vectors/matrices used in the final adjustment was provided. With the exception of a few parameters, these vectors/matrices were populated using data obtained from the NGDB. We concluded this chapter by providing a brief description of the software used to create input files required by GRAVNET.

In the next chapter, the matrices/vectors formulated in this chapter are used by GRAVNET via its input files to adjust our gravity network. Results from this adjustment are presented, analyzed and used to produce the g-dot map of North America.

Chapter 6

Adjustment, Results and Discussion

6.1 INTRODUCTION

Solid Earth (body) tides, ocean tide loading and hydrology constituted the most significant effects in our measurements. In CHAPTER 4 we used various models and software to remove these effects from absolute and relative gravity measurements. Thorough analysis of the corrected measurements, especially of absolute gravity measurements, showed that most measurements, if not all, were effectively corrected for systematic and gross errors and any remaining errors were considered random to be assessed thoroughly in post-adjustment using statistical tests

The objective of this chapter, which describes the main contribution in this research, is to compute g-dot values across the continent from corrected measurements using the method of least-squares adjustment. Vectors and matrices obtained in the previous chapter are used in software GRAVNET. A complete and thorough discussion of the results is presented at the end of this chapter.

6.2 ADJUSTMENT & RESULTS

Earlier in this work, measurements were corrected for gross errors as well as systematic errors. Absolute gravity measurements were used to compute g-dot constraints and the covariance matrix of observations was formed using procedures similar to those in the previous adjustment (PAGIATAKIS & SALIB, 2003). A total of 1030 gravity stations, 740 gravimeter scales and 10101 relative gravity measurements distributed across Alaska, Canada, Greenland and continental USA are included in this adjustment. 54 stations are constrained using computed g-dot values (cf. Table 5.1) from 10 absolute sites. After pre-processing, all measurements along with their associated covariance matrix are cast into a generalized least squares adjustment scheme. Final solutions include g-dot values ranging from -2.8 to 2.8 μGal/a (see TABLE 6.1 & FIGURE 6.1). Only about 6% (634 out of 10101) of ties are flagged as residual outliers (in the out-of-context sense). It is worth noting that none of these were flagged as in-context outliers. An in-context test is conducted on a measurement being a member of the observation vector as opposed to an out-of-context test in which the measurement under scrutiny is taken out of the observation vector and its compatibility with the statistics of the remainder of the observation vector is examined (KRAKIWSKY ET AL., 1999). In geodesy

we often avoid using "out-of-context" testing as it is very stringent and seems to flag even good measurements (IBID, 1999).

These results, albeit good in quality, necessitate further investigation in an attempt to improve g-dot solutions and obtain a smoother g-dot map. A low residual outlier count is a good indicator that realistic weights were assigned to the measurements. We therefore make an effort to eliminate residual outliers by relating them to a particular instrument, project, base class or year (APPENDIX D). No clear correlation is observed between these characteristics and residual outliers. Consequently no further action is taken to reduce the number of outliers. Though tedious and time consuming, these tests prove to be very beneficial in verifying the quality of the solution. It is important to note that not a single observation is eliminated from the final adjustment.

The final g-dot solution is statistically evaluated at significance level $\alpha = 0.05$ and the X^2 goodness-of-fit test shows that the standardized residuals are derived from a population of normal distribution with mean 0.035 µGal and variance 0.979 µGal^2. Because of the large degrees of freedom, the ratio $\hat{\sigma}_0^2 / \sigma_0^2$ (reduced X^2) was estimated at 0.888, which is statistically less than unity that is, the X^2 test on the variance factor fails at $\alpha = 0.05$. Notwithstanding, this latter test may indicate that only random errors are present in the measurements; all other errors, gross and systematic have been successfully eliminated. It may also indicate the effective elimination of the majority of the outliers based on conclusive observational evidence. The a-posteriori variance factor is statistically smaller than the a-priori, which may indicate the fact that the a-priori variance factor is unknown and that the covariance matrix of observations suffers from a scale defect. This possibility of a scale defect could not really be eliminated prior to the adjustment. If the a-priori variance factor is really unknown then the variances of the final results will have to be scaled by the a-posteriori variance factor that is, the standard deviations given in TABLE 6.1 will have to be scaled by the square root of the a-posteriori variance factor (0.94) making them smaller by 6 percent. As expected, these scaled values will not be significant since Least-squares adjustment is usually optimistic in determining the covariance matrix.

Final g-dot together with formal g-dot error estimates for all sites are displayed in TABLE 6.1. As mentioned earlier, a total of 1030 stations were used in the final adjustment that includes 343 secondary stations whose sole purpose was to fortify the network in areas west of Hudson Bay, but whose final solutions are not used to produce the g-dot map; hence omitted from TABLE 6.1. Each remaining station is part of an excentre network or site (187 in total), the g-dot values of which (Column 8 of TABLE 6.1) are computed by statistical analysis of stations at that site. This computation is accomplished by calculating the mean g-dot, standard deviation and confidence interval using g-dot solutions of all stations at that site that is, all stations on the

TABLE 6.1: Results of Final Adjustment Showing the Geographic Location of the Sites, Number of ties to them, and the Final g-dot and Gravity Solutions Along With Their Formal Errors in µGal/a.

No.	Site Name	N. Latitude	W. Longitude	Sites Tied to	Ties	Years of Obs	g-dot (µGal/a)	Gravity (mGal)
1	Adak	51°52'48"	176°38'48"	1	2	1965-1965	0.12 ± 0.98	981427.6033 ± 0.0420
2	Alamogordo	32°51'00"	106°00'00"	3	24	1967-1967	-0.04 ± 0.59	979116.3262 ± 0.0287
3	Albany	31°36'00"	84°04'59"	2	8	1965-1965	0.09 ± 0.84	979438.6153 ± 0.0319
4	Albuquerque	35°02'59"	106°35'59"	6	78	1966-1967	-0.18 ± 0.59	979194.0223 ± 0.0276
5	Alert	82°31'11"	62°16'59"	5	252	1965-2002	-0.12 ± 0.43	983127.6421 ± 0.0160
6	Amarillo	35°13'47"	101°42'00"	8	78	1961-1966	-0.14 ± 0.47	979408.8824 ± 0.0277
7	Anchorage	61°10'05"	149°58'29"	5	176	1963-1966	-0.70 ± 0.46	981905.9624 ± 0.0282
8	Atlanta	33°38'59"	84°25'23"	3	104	1966-1967	0.01 ± 0.58	979506.3097 ± 0.0281
9	Austin	30°12'15"	97°40'00"	7	105	1961-1973	-0.24 ± 0.40	979274.7198 ± 0.0294
10	Baker Lake	64°19'05"	96°01'36"	15	87	1964-2000	-1.70 ± 0.28	982187.9459 ± 0.0105
11	Bangor	44°47'59"	68°49'00"	4	87	1961-1966	0.01 ± 0.56	980576.4312 ± 0.0289
12	Barter Island	70°08'06"	143°36'47"	5	29	1962-1971	1.86 ± 0.58	982581.5867 ± 0.0263
13	Beaufort	32°28'59"	80°43'00"	2	15	1963-1963	0.11 ± 0.79	979524.3641 ± 0.0299
14	Big Trout Lake	53°48'51"	89°52'41"	1	4	1963-1963	-0.54 ± 0.75	981341.9873 ± 0.0197
15	Billings	45°48'29"	108°31'59"	9	173	1961-1969	0.06 ± 0.56	980357.3513 ± 0.0255
16	Bismarck	46°46'00"	100°45'00"	5	64	1966-1966	0.07 ± 0.80	980613.0149 ± 0.0275
17	Boise	43°34'00"	116°13'23"	4	38	1966-1966	-0.07 ± 0.58	980193.6273 ± 0.0280
18	Boston	42°27'52"	71°17'04"	10	258	1961-1972	0.09 ± 0.47	980381.9682 ± 0.0280
19	Boulder	40°04'59"	105°16'05"	1	16	1986-1986	0.00 ± 0.69	979608.5508 ± 0.0322
20	Browning	48°32'59"	113°01'00"	1	1	1961-1961	0.36 ± 0.92	980541.6921 ± 0.0387
21	Brownsville	25°54'29"	97°25'36"	1	2	1962-1962	0.37 ± 0.89	979036.2915 ± 0.0372
22	Brunswick	31°08'59"	81°22'59"	3	48	1963-1965	0.06 ± 0.57	979434.7471 ± 0.0295
23	Buffalo	42°55'59"	78°43'59"	6	63	1966-1970	-0.04 ± 0.58	980350.6931 ± 0.0261
24	Calgary	51°06'04"	114°01'38"	10	163	1963-1992	-1.01 ± 0.13	980814.3859 ± 0.0055
25	Cambridge Bay	69°06'09"	105°07'25"	18	89	1962-1995	0.12 ± 0.30	982503.3030 ± 0.0061
26	Canyon Creek	60°51'31"	137°03'39"	1	4	1984-1984	0.27 ± 0.97	981758.0368 ± 0.0211
27	Cape Dyer	66°35'48"	61°37'09"	5	52	1964-1980	0.33 ± 0.55	982303.9774 ± 0.0226
28	Cape Parry	70°09'47"	124°42'01"	4	23	1962-1973	0.76 ± 0.54	982607.4279 ± 0.0136
29	Caribou	46°55'40"	67°53'30"	5	56	1961-1965	0.13 ± 0.57	980717.4663 ± 0.0289
30	Casper	42°54'29"	106°28'00"	7	120	1961-1966	-0.11 ± 0.56	979941.3971 ± 0.0280
31	Charleston	32°53'59"	80°01'59"	8	168	1961-1972	0.08 ± 0.58	979552.9832 ± 0.0285
32	Charlotte	35°12'42"	80°56'12"	6	117	1966-1972	0.03 ± 0.58	979713.4316 ± 0.0262
33	Charlottetown	46°16'43"	63°07'59"	4	21	1973-1986	0.46 ± 0.48	980716.6602 ± 0.0192
34	Cheyenne	41°09'18"	104°48'24"	6	190	1961-1967	-0.11 ± 0.40	979686.1669 ± 0.0269
35	Chicago	41°59'35"	87°54'00"	11	187	1962-1972	-0.37 ± 0.60	980273.8874 ± 0.0262
36	Christianshaab	68°49'00"	51°12'00"	3	32	1982-1982	0.14 ± 0.66	982477.6269 ± 0.0211
37	Churchill	58°45'25"	94°03'40"	14	136	1960-1989	-2.47 ± 0.06	981752.7564 ± 0.0029
38	Columbus	40°00'24"	82°52'12"	3	54	1966-1973	-0.07 ± 0.58	980064.2022 ± 0.0284
39	Contact Creek	59°59'57"	127°43'36"	1	5	1978-1990	0.04 ± 0.93	981722.0787 ± 0.0174
40	Coppermine	67°49'41"	115°05'48"	4	8	1962-1966	0.34 ± 0.78	982460.5612 ± 0.0322
41	Cotulla	28°25'00"	99°19'59"	2	8	1965-1965	-0.57 ± 0.82	979139.4214 ± 0.0304
42	Cut Bank	48°37'00"	112°22'30"	2	2	1961-1961	0.14 ± 0.88	980593.7930 ± 0.0364
43	Dallas	32°51'00"	96°51'18"	12	162	1961-1973	-0.05 ± 0.48	979498.4120 ± 0.0270
44	Dawson	64°02'37"	139°07'36"	6	42	1978-1990	2.76 ± 0.45	982076.8413 ± 0.0102
45	Daytona Beach	29°11'05"	81°02'59"	4	60	1961-1965	-0.29 ± 0.56	979262.5192 ± 0.0286

No.	Site Name	N. Latitude	W. Longitude	Sites Tied to	Ties	Years of Obs	g-dot (μGal/a)	Gravity (mGal)
46	Denver	39°43'01"	104°43'31"	21	830	1961-1969	-0.23 ± 0.33	979604.2425 ± 0.0276
47	Detroit	42°13'00"	83°20'59"	5	81	1966-1970	0.10 ± 0.58	980304.4198 ± 0.0264
48	Duluth	46°50'19"	92°11'46"	2	19	1966-1970	0.27 ± 0.82	980695.7880 ± 0.0275
49	Edmonton	53°34'14"	113°31'19"	11	115	1960-1992	-0.81 ± 0.16	981158.5618 ± 0.0040
50	Egedesminde	68°42'00"	52°52'00"	3	32	1982-1982	0.06 ± 0.94	982478.6734 ± 0.0215
51	El Paso	31°48'11"	106°23'48"	6	90	1962-1967	-0.12 ± 0.59	979066.8259 ± 0.0289
52	Eureka	79°59'30"	85°49'10"	5	47	1965-1991	-0.41 ± 0.33	982998.1716 ± 0.0080
53	Fairbanks	64°39'18"	147°04'48"	7	746	1960-1969	-0.40 ± 0.39	982203.5033 ± 0.0277
54	Fairfield	38°15'47"	121°55'41"	2	33	1961-1967	-0.02 ± 0.61	979975.4142 ± 0.0282
55	Fargo	46°54'53"	96°48'53"	2	8	1964-1964	0.33 ± 0.81	980712.6225 ± 0.0302
56	Florence	34°11'23"	79°43'54"	3	59	1961-1965	0.02 ± 0.56	979670.3383 ± 0.0289
57	Fort Mcmurray	56°39'20"	111°13'55"	3	23	1959-2001	0.09 ± 0.35	981515.4185 ± 0.0081
58	Fort Nelson	58°50'22"	122°34'46"	10	70	1977-2001	0.25 ± 0.36	981678.9506 ± 0.0121
59	Fort St. John	56°14'43"	120°44'14"	4	18	1967-1990	-0.38 ± 0.33	981390.4854 ± 0.0072
60	Frederikshaab	61°58'59"	49°40'00"	3	32	1982-1982	0.20 ± 0.66	982052.5919 ± 0.0215
61	Fremont	41°25'00"	96°30'00"	2	12	1964-1965	0.17 ± 0.85	980165.2308 ± 0.0328
62	Godthaab	64°10'18"	51°43'30"	5	142	1972-1982	0.49 ± 0.65	982191.9414 ± 0.0173
63	Goose Bay	53°20'35"	60°23'58"	6	26	1965-1988	-0.73 ± 0.39	981302.9070 ± 0.0199
64	Grand Forks	47°57'00"	97°10'59"	4	55	1966-1970	0.12 ± 0.59	980791.9370 ± 0.0261
65	Grand Junction	39°07'00"	108°31'00"	4	37	1966-1967	0.03 ± 0.58	979606.5757 ± 0.0277
66	Grande Prairie	55°10'47"	118°52'37"	1	2	1978-1978	0.08 ± 0.68	981300.9891 ± 0.0117
67	Great Falls	47°30'29"	111°11'30"	12	595	1961-1969	0.08 ± 0.30	980514.4655 ± 0.0268
68	Grise Fiord	76°25'00"	82°53'48"	2	35	1978-1978	0.31 ± 0.64	982900.1174 ± 0.0235
69	Halifax	44°53'10"	63°30'56"	4	73	1966-1994	0.08 ± 0.26	980565.0018 ± 0.0055
70	Hall Beach	68°46'19"	81°13'57"	4	18	1962-1986	-0.33 ± 0.38	982489.0595 ± 0.0084
71	Hay River	60°50'30"	115°45'58"	7	55	1959-2001	0.34 ± 0.37	981895.6791 ± 0.0084
72	Holsteinsborg	66°55'59"	53°40'59"	3	32	1982-1982	0.09 ± 0.94	982411.3989 ± 0.0218
73	Houston	29°38'59"	95°16'41"	13	438	1961-1972	-0.10 ± 0.27	979278.6869 ± 0.0266
74	Inuvik	68°21'28"	133°42'58"	7	54	1962-1986	-0.66 ± 0.30	982497.6964 ± 0.0087
75	Iqaluit	63°44'58"	68°32'08"	8	91	1966-1992	-0.40 ± 0.25	982151.6754 ± 0.0025
76	Jackfish Creek	58°34'45"	122°39'55"	1	5	1977-1989	0.35 ± 0.93	981643.9463 ± 0.0260
77	Jacksonville	30°25'30"	81°38'30"	7	108	1961-1991	-0.03 ± 0.63	979370.9211 ± 0.0306
78	Jakobshavn	69°13'59"	51°06'00"	4	62	1982-1982	0.03 ± 0.66	982488.2384 ± 0.0205
79	Julianehaab	60°43'00"	46°02'59"	3	16	1982-1982	-0.00 ± 0.66	981925.3935 ± 0.0227
80	Kamloops	50°40'42"	120°20'04"	6	18	1967-1990	0.28 ± 0.41	980936.4874 ± 0.0226
81	Kansas City	39°07'00"	94°35'30"	3	68	1966-1966	-0.01 ± 0.59	979985.4507 ± 0.0285
82	Key West	24°34'45"	81°41'23"	2	12	1965-1965	0.04 ± 0.60	978957.3641 ± 0.0310
83	Knoxville	35°49'00"	83°58'59"	4	112	1966-1967	0.04 ± 0.41	979688.1578 ± 0.0275
84	Kuujjuaq	58°05'55"	68°25'18"	4	12	1973-1990	-1.25 ± 0.35	981715.2674 ± 0.0086
85	Kuujjuarapik	55°16'56"	77°45'26"	5	46	1971-1986	-2.58 ± 0.14	981460.1310 ± 0.0105
86	La Ronge	55°06'11"	105°17'53"	5	35	1960-2001	0.77 ± 0.37	981380.8789 ± 0.0121
87	Laredo	27°32'12"	99°27'24"	4	12	1961-1965	-0.75 ± 0.82	979064.6634 ± 0.0304
88	Las Vegas	36°04'59"	115°10'00"	4	71	1966-1967	-0.03 ± 0.58	979592.8134 ± 0.0278
89	Little Rock	34°43'59"	92°13'59"	3	72	1966-1967	-0.10 ± 0.58	979709.4066 ± 0.0276
90	Los Angeles	34°04'12"	118°26'30"	7	146	1962-1967	0.01 ± 0.41	979583.1057 ± 0.0283
91	Louisville	38°10'59"	85°43'59"	4	40	1966-1973	0.23 ± 0.58	979943.6515 ± 0.0283
92	Lubbock	33°39'18"	101°48'53"	2	16	1964-1964	-0.37 ± 0.79	979308.3796 ± 0.0290

No.	Site Name	N. Latitude	W. Longitude	Sites Tied to	Ties	Years of Obs	g-dot (μGal/a)	Gravity (mGal)
93	Madison	43°04'36"	89°24'00"	11	292	1961-1966	0.04 ± 0.33	980354.1987 ± 0.0312
94	Medford	42°22'11"	122°52'12"	3	37	1966-1966	0.38 ± 0.58	980221.8645 ± 0.0280
95	Memphis	35°02'59"	89°58'59"	6	60	1966-1973	-0.01 ± 0.83	979707.5028 ± 0.0277
96	Miami	25°47'48"	80°16'59"	10	247	1961-1991	0.01 ± 0.38	979039.6054 ± 0.0320
97	Middletown	41°16'00"	72°53'12"	3	68	1961-1967	-0.07 ± 0.78	980297.8514 ± 0.0290
98	Minneapolis	44°53'12"	93°13'11"	11	124	1962-1966	0.17 ± 0.57	980580.8939 ± 0.0276
99	Minot	48°16'00"	101°16'59"	3	32	1966-1966	-0.31 ± 0.58	980761.9115 ± 0.0281
100	Moncton	46°06'17"	64°40'54"	4	22	1968-1973	1.14 ± 0.48	980708.1188 ± 0.0093
101	Montreal	45°27'27"	73°44'53"	6	34	1963-2001	-1.29 ± 0.22	980629.1871 ± 0.0050
102	Moosonee	51°17'04"	80°37'18"	2	12	1976-1984	-1.62 ± 0.45	981164.6155 ± 0.0088
103	Mould Bay	76°14'28"	119°20'35"	4	20	1971-1974	0.01 ± 0.48	982922.3892 ± 0.0110
104	Nakina	50°13'04"	86°42'30"	2	14	1963-1996	-0.63 ± 0.57	980977.8594 ± 0.0072
105	Nanisivik	73°02'28"	84°33'49"	1	8	1991-1991	-0.42 ± 0.47	982674.8019 ± 0.0126
106	Nanoose	49°16'05"	124°08'47"	1	16	1990-1990	0.46 ± 0.08	980989.7802 ± 0.0095
107	Nanoose Bay	49°16'00"	124°08'17"	2	91	1981-1986	0.45 ± 0.08	980991.4282 ± 0.0093
108	Narssaq	60°55'00"	46°02'59"	3	32	1982-1982	-0.03 ± 0.66	981957.9968 ± 0.0218
109	Narssarssuaq	61°10'00"	45°23'59"	2	34	1982-1982	-0.06 ± 0.94	981929.2864 ± 0.0236
110	New Orleans	29°59'35"	90°15'42"	3	55	1966-1967	-0.25 ± 0.58	979314.9588 ± 0.0278
111	New York City	40°38'35"	73°47'12"	6	86	1966-1966	-0.00 ± 0.58	980212.5781 ± 0.0274
112	Nord	81°25'48"	17°30'00"	1	1	2002-2002	0.03 ± 1.00	983068.7751 ± 0.0340
113	Norman Wells	65°16'44"	126°47'17"	4	24	1959-1992	-0.07 ± 0.53	982228.3121 ± 0.0071
114	Ogden	41°07'48"	111°58'18"	2	40	1966-1966	-0.02 ± 0.59	979786.0740 ± 0.0290
115	Ontario	34°04'00"	117°34'00"	4	9	1962-1962	-0.37 ± 0.60	979521.4157 ± 0.0344
116	Orlando	28°26'59"	81°19'59"	14	283	1961-1991	-0.19 ± 0.36	979185.8665 ± 0.0286
117	Ottawa	45°23'39"	75°42'48"	13	2176	1964-2001	-0.72 ± 0.13	980606.8066 ± 0.0049
118	Palisades	41°00'14"	73°54'18"	1	8	1991-1991	-0.07 ± 0.98	980240.9707 ± 0.0228
119	Pasadena	34°10'00"	118°10'00"	3	6	1962-1962	-0.07 ± 0.61	979563.8636 ± 0.0353
120	Penticton	49°30'11"	119°35'35"	2	7	1968-1978	-0.03 ± 0.22	980818.3742 ± 0.0058
121	Phoenix	33°25'59"	112°01'00"	5	80	1966-1967	-0.07 ± 0.48	979476.8327 ± 0.0278
122	Pinawa	50°15'31"	95°51'52"	1	6	1988-1988	-0.74 ± 0.84	980997.7171 ± 0.0044
123	Pink Mountain	57°04'54"	122°35'10"	1	6	1978-1989	0.19 ± 0.92	981380.5627 ± 0.0209
124	Pittsburgh	40°29'40"	80°12'36"	4	36	1966-1966	-0.10 ± 0.58	980084.4525 ± 0.0281
125	Point Barrow	71°19'36"	156°40'36"	3	222	1961-1971	-0.38 ± 0.40	982685.1465 ± 0.0271
126	Pompano Beach	26°13'59"	80°05'59"	3	44	1963-1965	0.04 ± 0.57	979071.5950 ± 0.0289
127	Portland	43°38'48"	70°18'24"	7	122	1961-1966	0.10 ± 0.47	980496.8744 ± 0.0289
128	Prince George	53°54'45"	122°44'30"	4	47	1963-1994	-0.35 ± 0.31	981194.1007 ± 0.0159
129	Prince Rupert	54°19'55"	130°17'01"	3	20	1963-1993	0.79 ± 0.54	981429.9671 ± 0.0253
130	Princeton	40°01'36"	74°35'48"	6	110	1961-1968	0.05 ± 0.56	980198.3474 ± 0.0295
131	Quebec	46°46'52"	71°16'25"	3	16	1965-1982	0.45 ± 0.35	980713.9873 ± 0.0090
132	Raleigh	35°52'11"	78°46'59"	5	122	1961-1991	-0.04 ± 0.58	979787.3755 ± 0.0276
133	Rapid City	44°02'59"	103°04'00"	4	40	1966-1966	0.02 ± 0.58	980237.0605 ± 0.0277
134	Red Lake	51°01'07"	93°49'13"	2	20	1968-1992	-0.59 ± 0.38	981053.4992 ± 0.0230
135	Regina	50°25'37"	104°36'16"	6	50	1975-2001	0.43 ± 0.39	980940.4124 ± 0.0088
136	Reno	39°30'00"	119°46'00"	4	53	1966-1966	-0.05 ± 0.59	979675.2159 ± 0.0278
137	Resolute	74°43'05"	94°59'07"	5	32	1971-1982	-2.77 ± 0.35	982848.5020 ± 0.0048
138	Richmond	37°33'29"	77°23'53"	3	51	1961-1965	0.27 ± 0.57	979938.6478 ± 0.0293
139	Roberval	48°31'29"	72°16'04"	1	2	1964-1964	-0.85 ± 0.42	980828.2554 ± 0.0077

No.	Site Name	N. Latitude	W. Longitude	Sites Tied to	Ties	Years of Obs	g-dot (μGal/a)	Gravity (mGal)
140	Salt Lake City	40°46'59"	111°58'00"	6	118	1966-1966	-0.12 ± 0.58	979801.6034 ± 0.0275
141	San Antonio	29°22'55"	98°34'25"	8	251	1961-1967	-0.27 ± 0.33	979194.1127 ± 0.0274
142	San Francisco	37°37'00"	122°22'47"	12	210	1961-1967	0.03 ± 0.49	979973.8018 ± 0.0356
143	Saskatoon	52°07'48"	106°39'37"	3	17	1979-2001	-0.64 ± 0.34	981123.3943 ± 0.0077
144	Sault Ste Marie	46°31'04"	84°16'47"	2	20	1969-1980	-0.12 ± 0.22	980661.1267 ± 0.0075
145	Savannah	32°01'41"	81°07'59"	5	54	1961-1965	-0.11 ± 0.57	979483.0869 ± 0.0289
146	Schefferville	54°48'07"	66°48'30"	4	24	1961-1973	-1.18 ± 0.17	981316.7444 ± 0.0037
147	Seattle	47°26'30"	122°17'59"	7	180	1962-1966	0.18 ± 0.37	980760.7543 ± 0.0274
148	Sept-Iles	50°13'05"	66°15'49"	2	11	1963-1981	-0.18 ± 0.37	981072.8138 ± 0.0092
149	Sheridan	44°46'29"	106°58'00"	6	279	1961-1967	0.04 ± 0.56	980212.1061 ± 0.0269
150	Sikanni Chief	57°14'14"	122°41'29"	2	6	1978-1981	0.27 ± 0.95	981424.0059 ± 0.0232
151	Sioux City	42°23'59"	96°22'59"	4	40	1966-1966	0.04 ± 0.58	980292.9679 ± 0.0279
152	Sioux Falls	43°34'47"	96°44'35"	4	56	1966-1966	-0.02 ± 0.59	980347.4756 ± 0.0279
153	Sondre Stromfjord	67°00'00"	50°42'29"	7	151	1964-1982	0.24 ± 0.61	982369.9679 ± 0.0231
154	Spencer Creek	60°07'27"	130°16'30"	1	9	1990-1990	0.30 ± 0.99	981626.4552 ± 0.0165
155	Spokane	47°37'00"	117°31'59"	3	72	1966-1966	0.23 ± 0.47	980633.0056 ± 0.0276
156	St Augustine	29°56'59"	81°19'59"	3	48	1963-1965	-0.13 ± 0.57	979327.2283 ± 0.0286
157	St Louis	38°45'00"	90°22'00"	4	87	1965-1966	0.19 ± 0.42	979989.4580 ± 0.0285
158	St. John's	47°36'46"	52°44'39"	3	36	1976-1985	-1.04 ± 0.22	980807.8806 ± 0.0063
159	Stephenville	48°32'46"	58°33'52"	2	10	1977-1997	0.22 ± 0.61	980917.4340 ± 0.0110
160	Stuart	41°30'00"	94°30'00"	1	2	1965-1965	0.07 ± 0.92	980193.9360 ± 0.0376
161	Sukkertoppen	65°24'00"	52°55'00"	3	32	1982-1982	-0.16 ± 0.66	982293.2527 ± 0.0212
162	Syracuse	43°04'23"	76°15'29"	4	102	1966-1970	0.17 ± 0.58	980382.6791 ± 0.0263
163	Tabor Mountain	53°56'42"	122°27'16"	1	8	1977-1977	0.27 ± 0.94	981163.2559 ± 0.0267
164	Tampa	27°58'30"	82°31'23"	2	2	1961-1961	-0.11 ± 0.85	979189.6056 ± 0.0349
165	Taylor Hwy	64°05'08"	140°59'51"	1	7	1978-1990	1.37 ± 0.92	981889.7581 ± 0.0214
166	Thompson	55°44'24"	97°49'47"	2	2	1965-1965	-1.36 ± 0.73	981469.8662 ± 0.0169
167	Thule	76°32'12"	68°45'17"	6	101	1965-1994	-0.60 ± 0.62	982914.1644 ± 0.0262
168	Thunder Bay	48°22'21"	89°18'45"	6	46	1980-2001	-0.72 ± 0.35	980802.7487 ± 0.0071
169	Timmins	48°28'38"	81°12'24"	9	60	1963-2001	-0.52 ± 0.36	980817.8841 ± 0.0077
170	Toronto	43°41'30"	79°37'54"	11	320	1960-2009	0.20 ± 0.41	980415.0810 ± 0.0281
171	Ucluelet	48°55'17"	125°32'21"	1	28	1976-1990	0.02 ± 0.06	980962.3916 ± 0.0063
172	Upernavik	72°46'59"	56°10'00"	2	30	1982-1982	0.11 ± 0.67	982738.5877 ± 0.0286
173	Uranium City	59°33'46"	108°35'49"	8	50	1960-2001	-1.65 ± 0.29	981774.0216 ± 0.0105
174	Val D'or	48°06'31"	77°46'32"	5	57	1963-2001	-0.76 ± 0.47	980794.5761 ± 0.0271
175	Vancouver	49°11'44"	123°10'53"	7	40	1961-1980	0.45 ± 0.19	980915.6304 ± 0.0032
176	Vero Beach	27°38'59"	80°25'00"	3	44	1963-1965	-0.13 ± 0.58	979159.0516 ± 0.0300
177	Victoria	48°38'58"	123°26'59"	9	77	1960-1988	0.46 ± 0.03	980932.6242 ± 0.0043
178	Washington	38°50'33"	77°00'51"	16	384	1961-1991	0.05 ± 0.33	980095.4328 ± 0.0300
179	Washington Dc	39°15'00"	77°10'00"	1	9	1972-1972	-0.47 ± 0.91	980102.4316 ± 0.0326
180	Watson Lake	60°06'48"	128°49'17"	8	64	1978-1993	0.70 ± 0.46	981699.9054 ± 0.0051
181	West Palm Beach	26°41'12"	80°05'30"	5	55	1961-1965	-0.01 ± 0.57	979118.7160 ± 0.0289
182	Whitehorse	60°42'34"	135°04'05"	7	55	1978-1993	-0.19 ± 0.27	981733.7609 ± 0.0049
183	Wichita	37°38'30"	97°25'29"	3	52	1966-1966	0.10 ± 0.58	979826.2548 ± 0.0280
184	Windsor	42°15'57"	82°57'37"	5	58	1968-1995	0.19 ± 0.46	980310.2932 ± 0.0064
185	Winisk	55°13'45"	85°07'32"	1	2	1976-1976	-1.38 ± 0.64	981487.6828 ± 0.0443
186	Winnipeg	49°53'46"	97°13'18"	17	132	1960-2001	-0.38 ± 0.14	980977.6243 ± 0.0006

No.	Site Name	N. Latitude	W. Longitude	Sites Tied to	Ties	Years of Obs	g-dot (uGal/a)	Gravity (mgal)
187	Yellowknife	62°27'16"	114°22'31"	28	188	1959-1996	-1.86 ± 0.11	982027.5039 ± 0.0057

excentre network. The average of all g-dots within the confidence interval represents the g-dot at that site. On the other hand, gravity values (Column 9) and site locations (Column 3 and 4) shown in TABLE 6.1 are simply those attributed to the primary station on the excentre network.

6.3 DISCUSSION

Our final solution is illustrated in FIGURE 6.1 as the first of its kind g-dot map of North America and depict clearly the zero line of the Glacial Isostatic Adjustment (yellow region). FIGURE 6.1 shows a pattern very similar to that of the g-dot map of Canada (PAGIATAKIS & SALIB, 2003) in areas within inland Canada. In the South, the zero line follows the St. Lawrence River and Great Lakes but then deviates to the North following the Canadian Shield margin. MITROVICA ET AL., (1994) and WU (2002) also show a zero line following the St. Lawrence River and Great Lakes, but then deviating west of the Canadian Shield margin. SELLA ET AL., (2007) also showed a very similar zero line (cf. FIGURE 2.1) with uplift north of the line and subsidence to the south. As expected, GIA is evident in north USA as the ice is thought to have covered these areas (FIGURE 1.1). However, the rest of the US was never covered in ice, notice the yellow coloration covering almost entirely the landmass, with just few spots of weak g-dot signals. We believe that these are statistically equivalent to zero as they are within the error margin.

In the East, the zero line follows roughly the Canadian East Coast along Labrador Sea and is consistent with the zero lines shown by MITROVICA ET AL., (1994) and WU (2002). Rebound rates reduce slowly eastward and towards Greenland, through Davis Strait and continues until it hits the zero mark in Greenland where zero g-dot is virtually constant throughout the landmass. Note that gravity stations were only available in the north and west part of Greenland. Consequently, for regions within the east half of Greenland and toward the ocean, our map is merely an extrapolation based on the inland stations and perhaps an artefact of the gridding algorithm used (Kriging). We also want to bring to the reader's attention the fact that the ice that covered Greenland during the LGM (Greenland sheet) is still present today, albeit reduced in thickness hence, we do not expect to observe any significant GIA signals in the region since any small signal due to pure crustal uplift is counteracted by the gravitational effect of the ice mass reduction, considering that the level of the ice is higher than the gravity station situated on the bedrock.

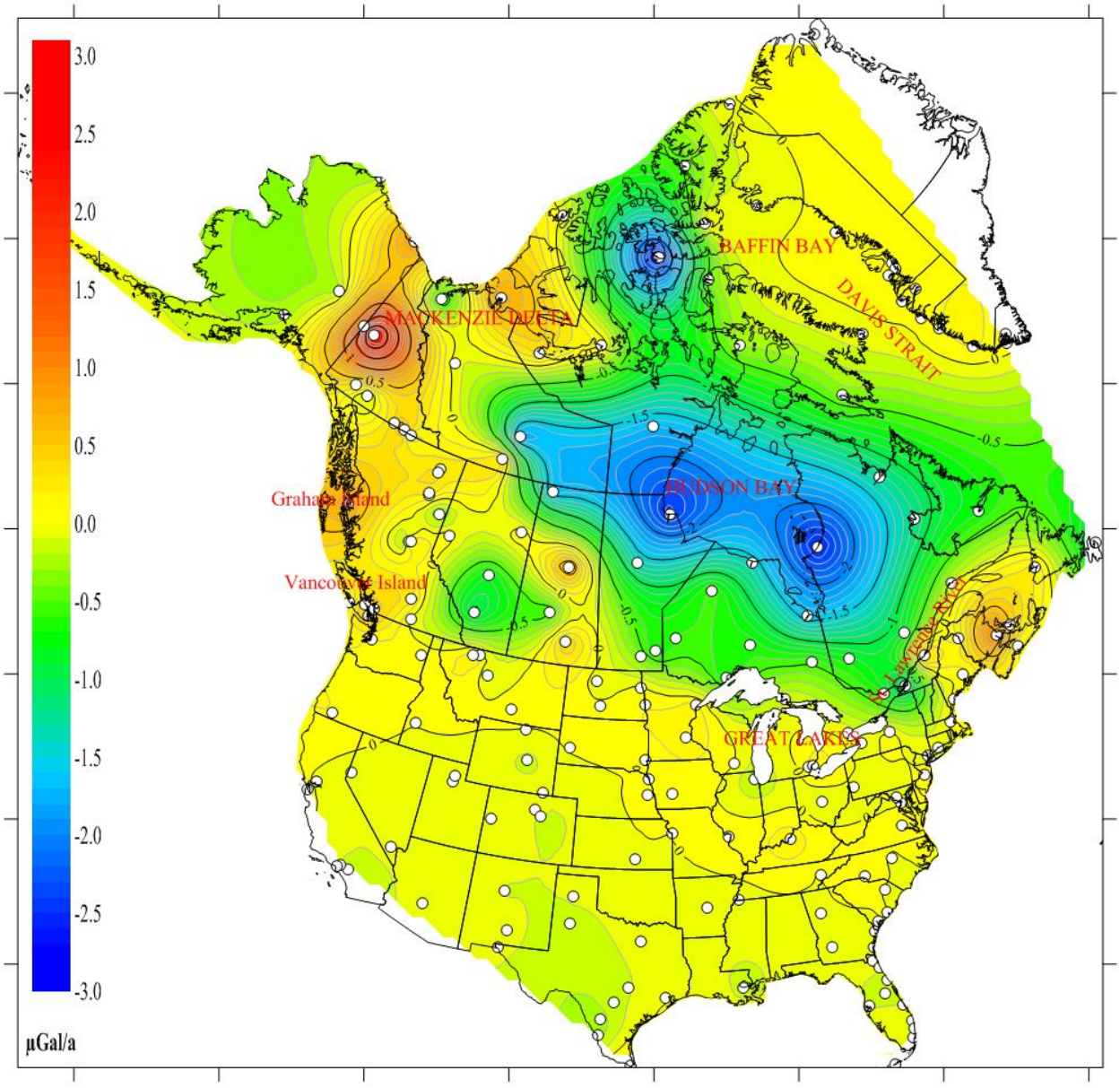

FIGURE 6.1: the g-dot map of North America. Contour interval 0.1 µGal/a [Base map: NATURAL EARTH, 2013]. White circles indicate the location of primary and excentre stations.

Our map agrees with NIELSEN ET AL., (2014) who showed that Greenland experiences a GIA gravity signal of less than 1 µGal/year. Also, in the previous adjustment of the CGSN, PAGIATAKIS & SALIB (2003) predicted lower g-dot values in Greenland compared to those in Canada as ice in Greenland was not as thick and is still present today. Naturally, rebound rates will be slower in this region. Our map also shows subsidence along Davis Strait/Baffin Bay area that agrees in sign with the radial deformation rates of MITROVICA ET AL., (1994).

In general, the West coast of the United States and Canada are believed to experience other geological processes, such as subduction, erosion, recent melting of mountain glaciers, thermal and other tectonic events (e.g., GOUGH, 1986), which may also be important contributors to the g-dot in the area. The Pacific coast of Canada is one of the few areas in the world where four tectonic plates meet and interact (KOOHZARE ET AL., 2008). Time rate of change of gravity caused by these processes is evident in our work as we noticed subsidence in regions around Graham Island. Note that this is not an artefact of the gridding algorithm as Sandspit station found on the island has ties to, amongst others, Prince Rupert and Terrace station on mainland Canada. Also, GPS observations from stations along the west coast of Canada, including Sandspit, have been used to investigate the consistent periodic displacement taking place in the region (NYKOLAISHEN ET AL., 2015). These signals therefore interfere with GIA signals making it difficult to accurately predict the later. Nonetheless, the orange colouration (slight subsidence) observed in this region continues down along the west coast to Vancouver Island which contains two constraint stations, Ucluelet and Nanoose, both of positive g-dots. We would expect this trend to continue south into the US, which is however not the case here. We believe that tectonic signals are not detected in the west coast of the United States simply because of the sparse nature of stations and low observation count. Calgary experiences a strong negative g-dot (-1.06 ± 0.24 µGal/a) that extends slightly to the North and to the West. This is consistent with PAGIATAKIS & SALIB (2003), only now, to a smaller extend. The Calgary station is considered to be stable and subject to regular observations. We believe that the signal is real but its origin may be due to oil extraction.

Unlike SATO ET AL., (2012), who obtained a mean g-dot of -4.5 ± 0.76 µGal/a (very significant uplift) in South East Alaska, our g-dot map reveals subsidence in the area, notice the red colouration. Recall that they (IBID, 2012) estimated g-dot value from only 3 years of measurements obtained at 6 gravity stations. Due of the slow nature of GIA, is would be impossible to observe very accurately the time rate of change of gravity within this short time period. We therefore conclude that results obtained in this work are accurate and unbiased. On the other hand, West Alaska shows slight uplift. Note that there are almost no stations on the west half of the state of Alaska, and we therefore conclude that this signal is not real but perhaps an artefact of the gridding algorithm used.

A careful examination of the entire map reveals that the g-dot pattern is not homogeneous, but rather shows ‘‘domes’’ with strong negative g-dot values. The presence of these ‘‘domes’’ may suggest variable ice sheet thickness in the interior. As expected, regions west and south east of Hudson Bay show the largest rebound rate that is, highly negative g-dot values (shown in blue). This region is enclosed within a region experiencing slower rebound (less negative g-dot) depicted by the light blue then greenish colouration,

asserting glaciologists' (e.g. GORDON, 1983; GOSNELL, 2007; SELLA ET AL., 2007) believe that, during the ice age, ice was thickest around Hudson Bay.

Notice that our g-dot map contains a few spikes in northwest Canada. GIA is a long wavelength phenomenon therefore, such spikes may be due to other local tectonic/geological phenomena, or caused by poor quality measurements in the area. Due to lack of additional information, nothing was done to remedy this situation.

6.4 ANALYSIS

In this work, we produced the g-dot map of North America (FIGURE 6.1) using g-dot values obtained from the Least-Squares adjustment of a network consisting of gravity stations connected together by gravity ties. The standard deviations (cf. TABLE 6.1) of these g-dot values describe how well they were estimated and are different for each station, meaning that some g-dots are estimated to a higher precision than others. We attempt to evaluate the error in our map by analyzing the spatial distribution of standard deviations of g-dots across the land mass (FIGURE 6.2).

FIGURE 6.2 shows that the error in the g-dot map of North America ranges from 0.03 µGal/a in Victoria to 1 µGal/a in the North with an average about 0.52 µGal/a depicting a high accuracy in the g-dot map of North America (FIGURE 6.1). Recall that for an unknown a-priori variance factor, the estimated standard deviations of g-dots would be obtained by scaling the current standard deviations (cf., TABLE 6.1) by the square root of the a-posteriori variance factor forcing this average error to reduce to 0.49 µGal/a. Also, the large variation in the errors of g-dot values come from the fact that WLSR of absolute gravity measurements is used to obtain precise g-dots with low standard deviations at constrained stations. During the adjustment, these standard deviations are used as initial approximations to standard deviations of g-dots for the constrained stations, while 1 µGal/a is used for all other stations (cf., SECTION 5.6). As expected, the standard deviations of g-dots at each station did not change much during the adjustment maintaining the large discrepancy initially present. Notice how only constrained stations have standard deviations as low as 0.03 µGal/a. Generally, the error in the g-dot map is randomly distributed across the continent with the USA and Greenland showing slightly larger errors. The larger errors in these regions can be explained by the fact that the standard deviations of the ties in these regions could not be estimated to a high degree of certainty as those of Canadian stations due to lack of additional information, such as field books, calibration notes, personal communication with instrument operators etc.

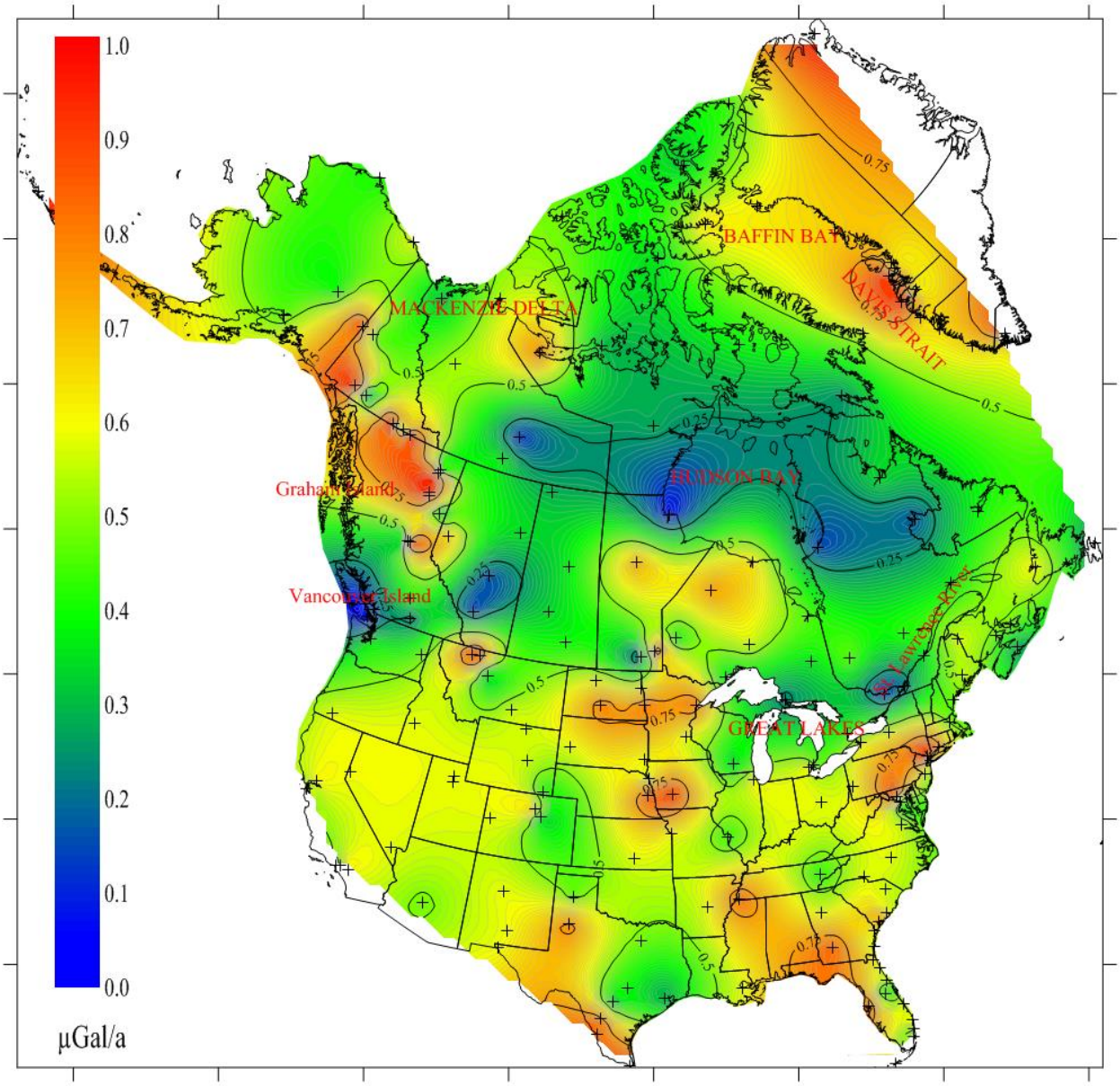

FIGURE 6.2: Error in g-dot map of North America. Contour interval 0.01 µGal/a [Base map: NATURAL EARTH, 2013]. Crosses indicate the location of primary and excentre stations.

In order to assess the accuracy of our g-dot values, a comparison with those obtained by PAGIATAKIS & SALIB (2003) in the previous adjustment is performed. This comparison is achieved by producing a map of the differences in g-dot between values obtained here (TABLE 6.1) and those obtained in the previous adjustment (IBID, 2003). FIGURE 6.3 represents this map of differences in g-dot and shows how well both maps fit each other in regions around Canada.

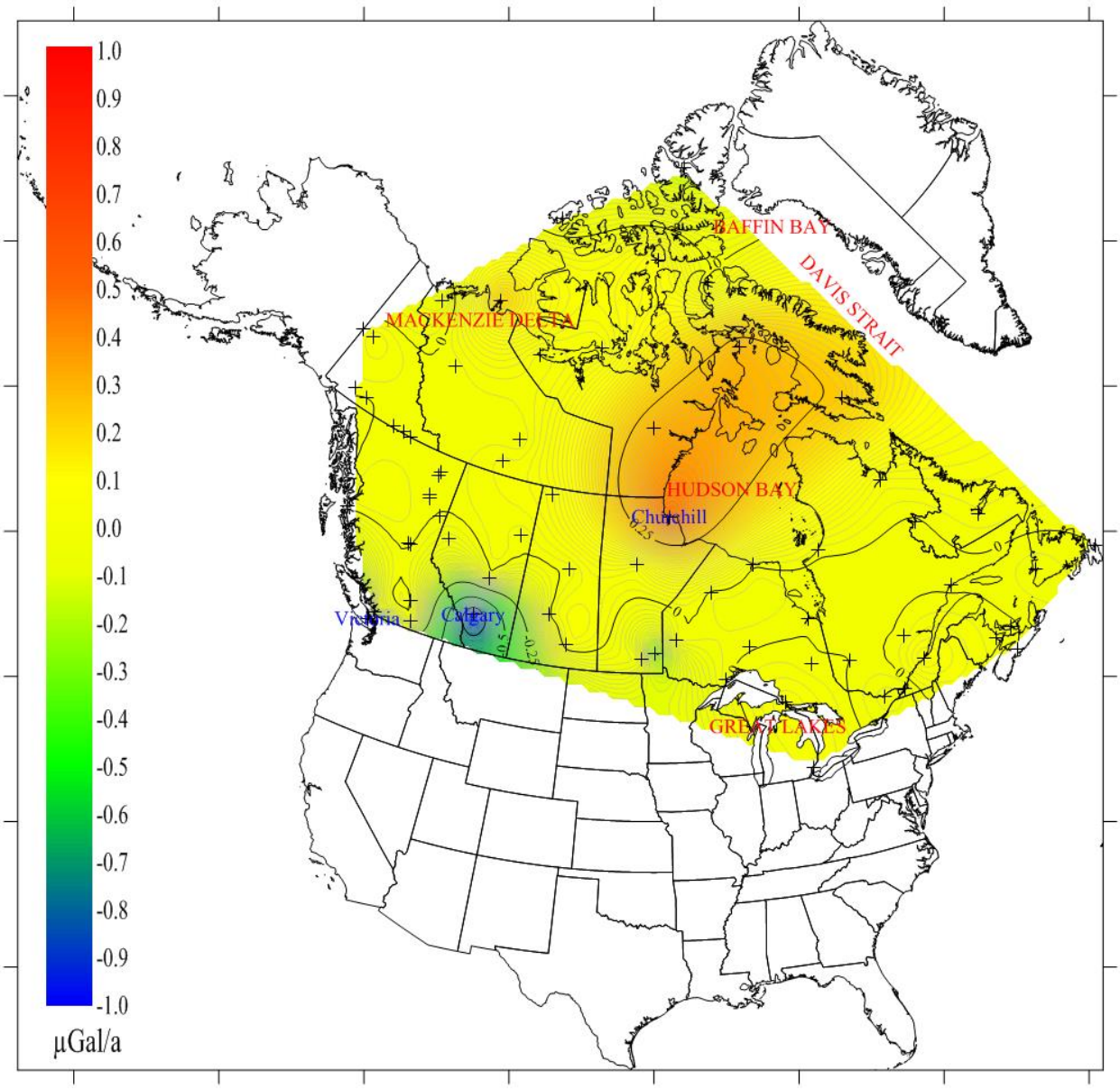

FIGURE 6.3: Map of change in g-dot between previous (PAGIATAKIS & SALIB, 2003) and current adjustment. Contour interval 0.01 µGal/a [Base map: NATURAL EARTH, 2013]. Crosses indicate the location of primary and excentre stations.

FIGURE 6.3 shows an almost perfect fit between the g-dot maps of North America and of Canada in regions around Canada. This good fit is depicted by the small differences in g-dots in most areas of Canada with almost all stations showing negligible differences. In fact, the differences in g-dot range from -0.9 to 0.5 µGal/a (FIGURE 6.1) with a mean of 0.0 µGal/a. Three stations, Calgary, Victoria and Churchill however show a large discrepancy. Notice that these are all constrained stations for which g-dot values were obtained from WLSP of corrected absolute gravity measurements. In the previous adjustment (PAGIATAKIS & SALIB,

2003), g-dot values for Calgary and Victoria stations were only obtained following the adjustment that is, these two stations were not used to constrain the network. Churchill however was used as constraint in both adjustments. The large discrepancy in this station was already noticeable following WLSR, where we obtained a constraint of -2.4 µGal/a while PAGIATAKIS & SALIB (2003) estimated it at -1.7 and -2.0 µGal/a. Recall that, in the previous adjustment (IBID, 2003), systematic effects from hydrology were not eliminated from absolute gravity measurements. This significant effect is therefore at the centre of the large discrepancy between the two values, making results obtained here more accurate.

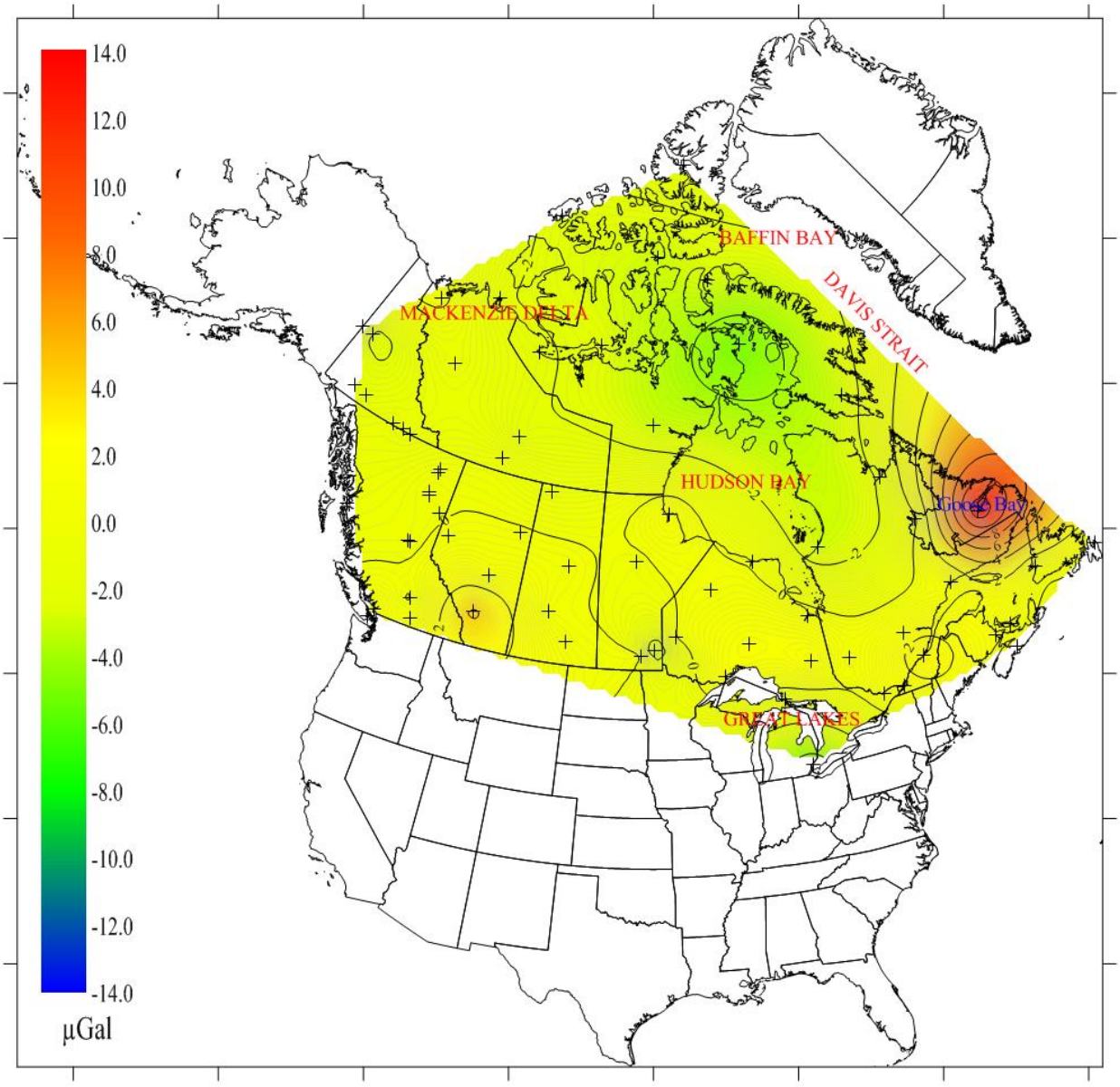

FIGURE 6.4: Map of change in gravity values between previous (PAGIATAKIS & SALIB, 2003) and current adjustment. Contour interval 1 µGal [Base map: NATURAL EARTH, 2013]. Crosses indicate the location of primary and excentre stations.

Similarly, the accuracies of the gravity values obtained here are assessed by comparing them to those obtained in the previous adjustment (PAGIATAKIS & SALIB, 2003).

Results of this comparison shows that the differences in gravity values at the reference epoch range roughly between -4.0 and 4.0 µGal with an average of -0.2 µGal across all Canadian stations (FIGUREs 6.4). Goose Bay station however, shows a very large difference (13.4 µGal); notice the red area around northeast Canada. It is the only station that depicts such a large difference and we conclude that this discrepancy must have been the result of one or more poor observation in the area. Overall, these insignificant differences demonstrate how well gravity values obtained from both adjustments agree.

The differences in instrument drifts and instrument scales between our results and those of PAGIATAKIS & SALIB (2003) were also evaluated. Recall that PAGIATAKIS & SALIB (2003) used only 492 instruments in their adjustment therefore, only solutions from these instruments were compared, results of which are presented in form of histograms in FIGUREs 6.5 and 6.6.

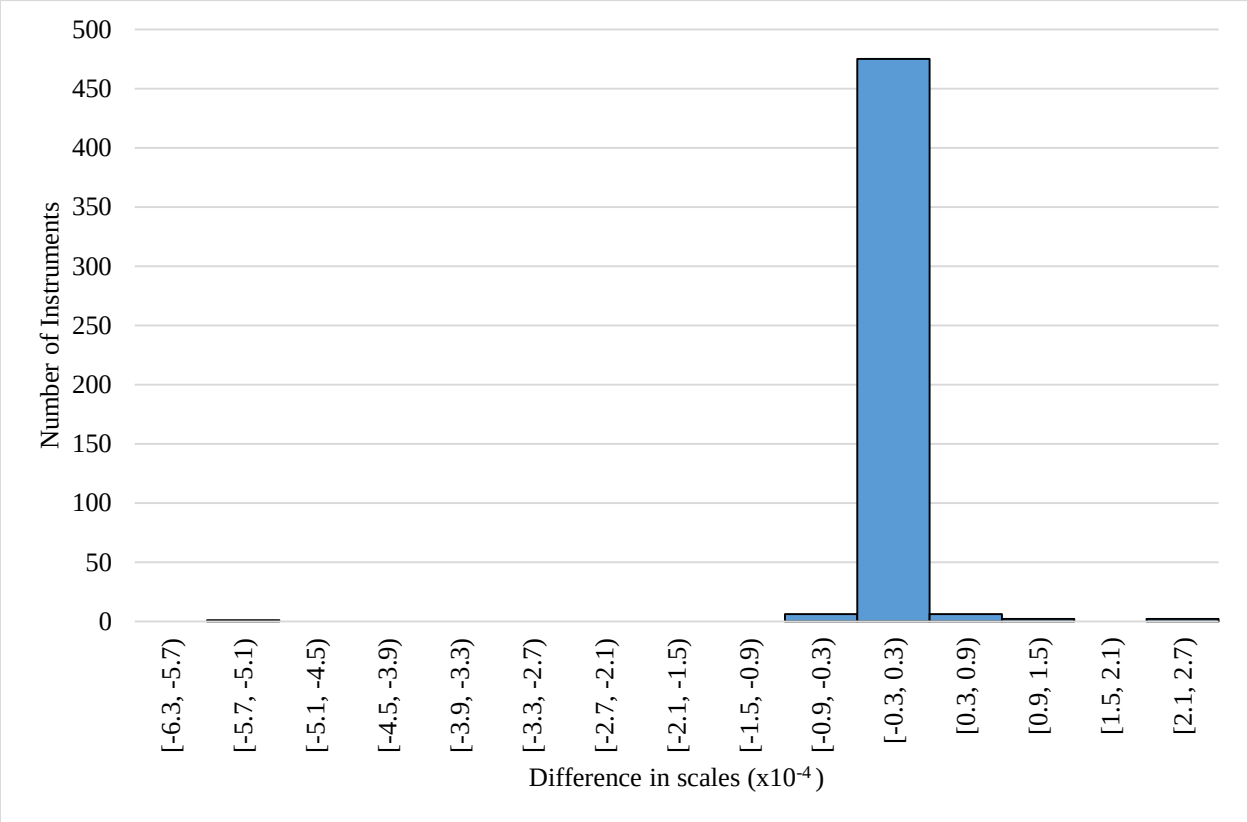

FIGURE 6.5: Histogram depicting the distribution of differences in instrument scales between our final solution and the solution obtained by PAGIATAKIS & SALIB (2003).

Further investigation of both adjustments shows that the scale of a typical instrument is obtained to within $\pm 1.2 \times 10^{-4}$, meaning that, according to the adjustment, it is impossible to estimate the scale of an instrument

to a resolution better than $\pm 1.2 \times 10^{-4}$. FIGURE 6.5 shows that the differences in instrument scales for almost all instruments range between -3×10^{-5} and 3×10^{-5} with a mean of 1.3×10^{-6}. Now notice how both the mean and the range of differences in instrument scales are at least one order of magnitude smaller than the resolution of instrument scales. These differences are therefore insignificant and we conclude that instrument scales obtained in this adjustment are statistically equivalent to those obtained from the previous adjustment (PAGIATAKIS & SALIB, 2003).

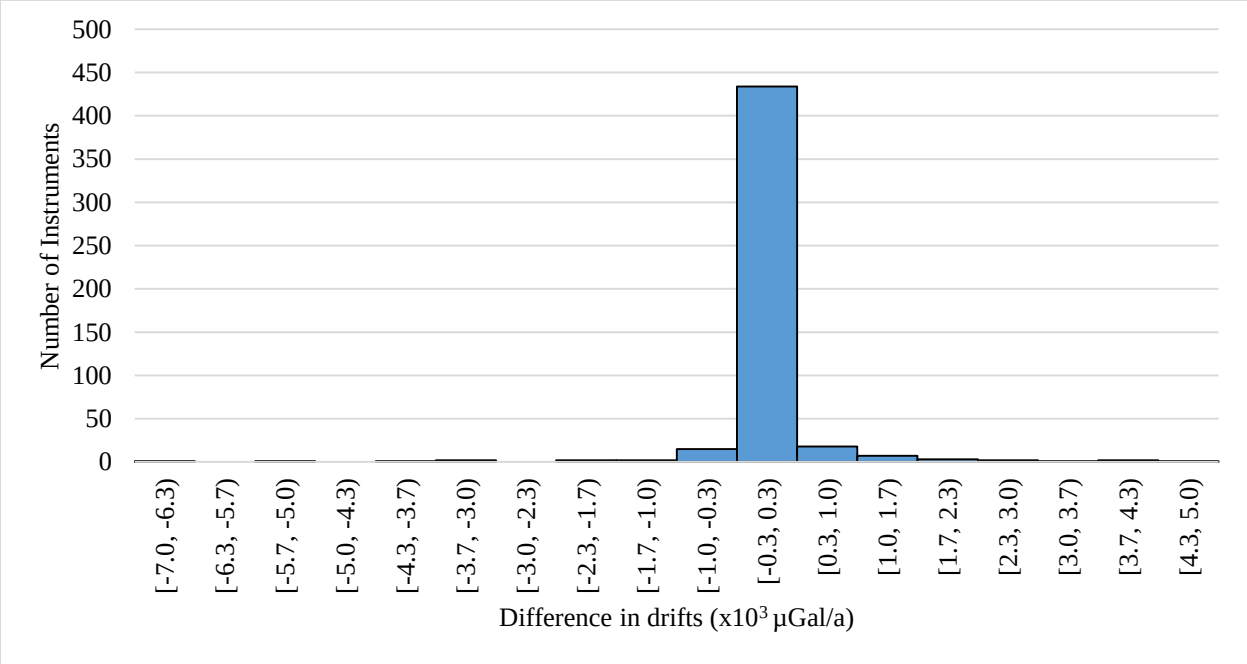

FIGURE 6.6: Histogram depicting the distribution of differences in instrument drifts between our final solution and the solution obtained by PAGIATAKIS & SALIB, (2003).

Similarly, FIGURE 6.6 shows that the differences in instrument drifts for almost all instruments range between -300 µGal/a and 300 µGal/a with a mean of 26 µGal/a. Again notice how this mean differences in instrument drift is two orders of magnitude smaller than the resolution of instrument drifts estimated at 6000 µGal/a. These differences are therefore insignificant and we conclude that instrument drifts obtained in this adjustment are statistically equivalent to those obtained from the previous adjustment (PAGIATAKIS & SALIB, 2003).

To further ascertain our solution, we compare our map to a crustal deformation map of Canada. KOOHZARE ET AL., (2008) compiled a map of vertical crustal movements (VCM) using levelling data and tide gauge records collected across Canada and Northern USA. They divided the study area into sections and used the method of smooth piecewise algebraic approximation to fit the pieces to tide gauge trends and height difference differences (IBID, 2008). The VCM model obtained based on this study is shown in FIGURE 6.7

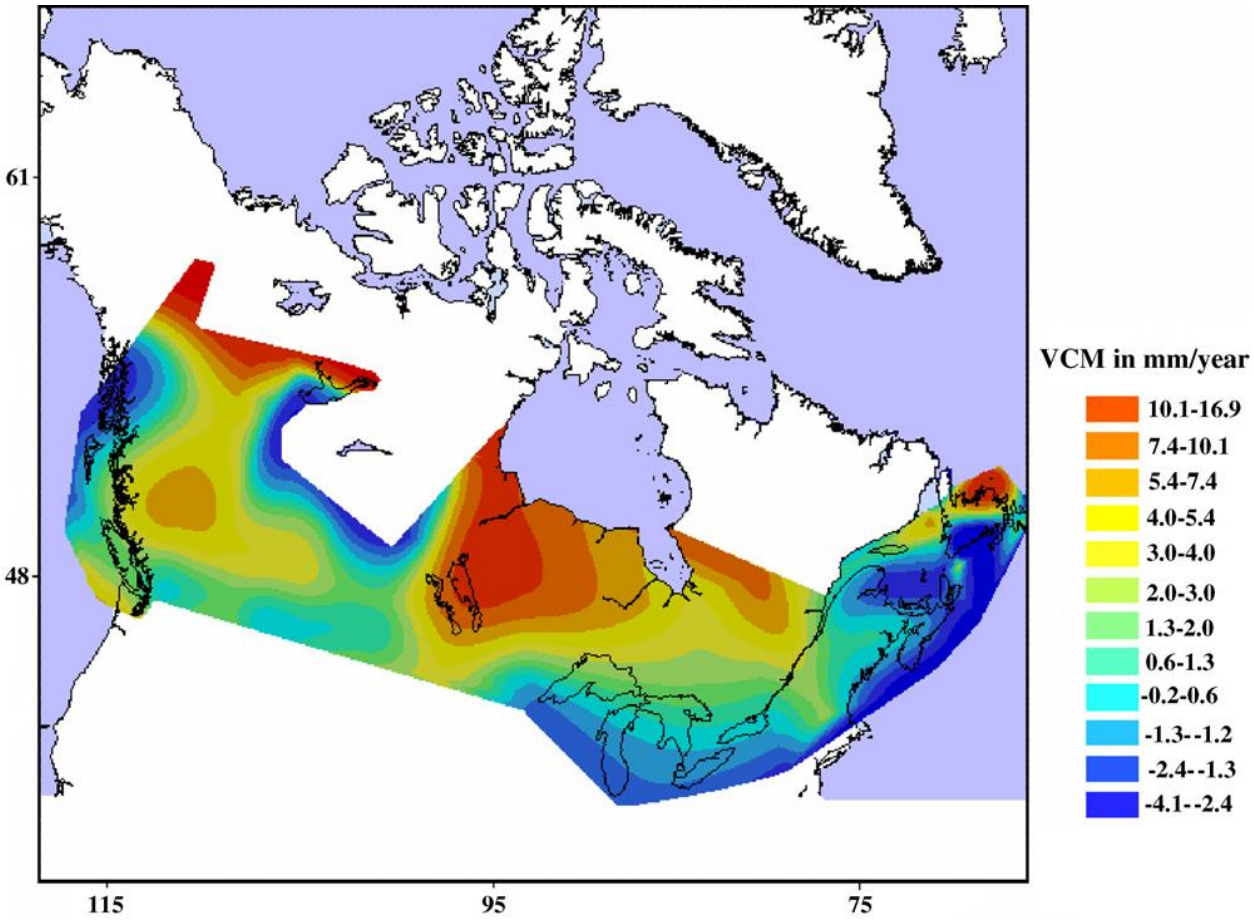

Figure 6.7: A color map of vertical crustal movements in Canada (KOOHZARE ET AL., 2008)

FIGURE 6.7 shows that areas southeast and southwest of Hudson Bay experience the highest positive crustal movement, notice the red coloration. This pattern agrees perfectly with our map suggesting highest crustal uplift rates around Hudson Bay. The magnitude of this uplift reduces slowly westward until it reaches the zero mark after which subsidence is observed and slowly increases until the Pacific coast where it is at its highest. Again, this pattern is in agreement with our map which shows positive g-dot along the west coast suggesting subsidence. In addition, their zero line is consistent with ours, appearing from the island of Newfoundland and Gulf of St. Lawrence, following the Atlantic coast line to the south, heading westward through the Great Lakes then the large lakes and finally deviating to the north following the pacific coast line. It is worth mentioning that gravity does not necessarily vary linearly with height variation as it is also affected by mass change/redistribution. Therefore, unlike our map, this VCM model shows no crustal movement around Calgary suggesting that the signal we show is really not caused by crustal movement but by mass changes due to oil extraction.

Gravity variation in North America has also been studied using measurements from GRACE satellite mission e.g. RANGELOVA ET AL., (2008). RANGELOVA ET AL., (2007) used observations from GRACE satellite to study mass variation in North America and concluded that GIA is the dominant signal in GRACE data. The particular study (IBID, 2007) also produced a crustal deformation map of North America (FIGURE 6.8) which when compared to ours showed the same general pattern.

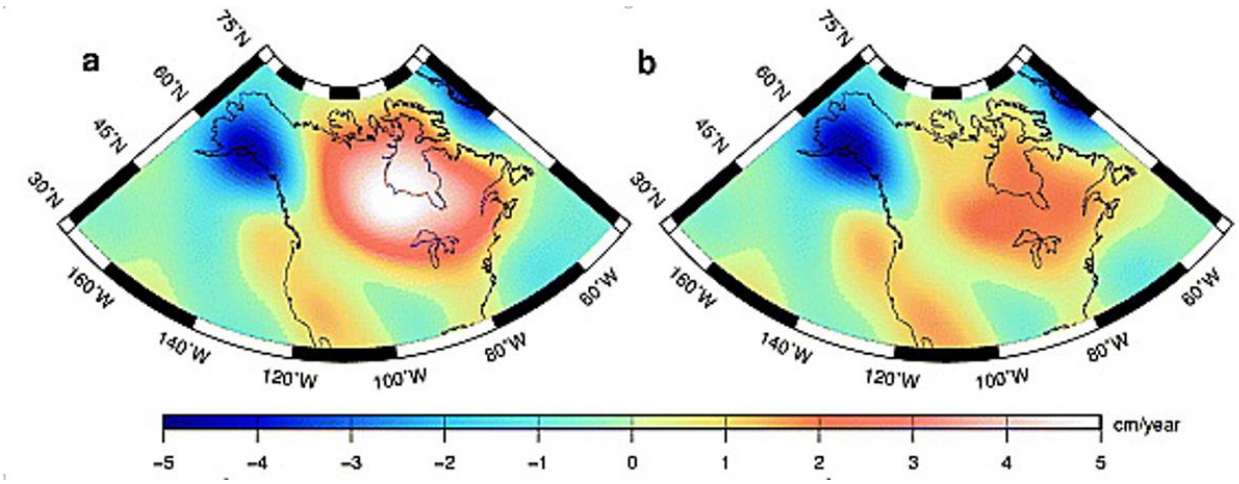

Figure 6.8: (a) Trend in mass variations estimated via weighted Least-Squares fitting of the 4-year GRACE time series. The secular postglacial rebound rate is the dominant signal in the GRACE data; (b) long-term mass changes after removing the postglacial rebound signal (RANGELOVA ET AL., 2007).

Mass variation in North America as observed from GRACE measurements is shown in FIGURE 6.8 (a) and also in FIGURE 6.8 (b), but only now, GIA signals have been removed. The difference between these two figures shows the general pattern of GIA in North America, which is very similar to the one obtained in this research with the highest rebound rates around Hudson Bay and the highest subsidence rates along the west coast of Canada. Note that GRACE signals are long wavelength. It is therefore impossible to attain the resolution observed from ground measurements.

6.5 SUMMARY

In this chapter, we performed an adjustment of the network using corrected gravity measurements and g-dot constraints described in previous chapters. Results of this adjustment were presented and a complete discussion provided. We ended this chapter with a comparison between these results and those obtained from the adjustment of the CGSN (PAGIATAKIS & SALIB, 2003). In the next chapter, we provide general conclusions of this work and recommendations for possible future works.

Chapter 7

Conclusion and Recommendations

7.1 CONCLUSIONS AND CONTRIBUTIONS

PAGIATAKIS & SALIB (2003) provided significant contribution to IGOS by using historical relative and absolute gravity measurements to determine g-dots at selected sites across Canada. The outcome of our research is a g-dot solution over North America and Greenland obtained from ground based measurements collected across the landmass. The meticulous process involved ensures high qualitaty and most importantly reliable g-dot solution, which provides a great contribution to IGOS. The Integrated Global Observing Strategy (IGOS) unites the major satellite and ground based observing systems for global environmental observations of the atmosphere, oceans and land in a framework that delivers maximum benefit and effectiveness in their final use (IGOS PARTNERS, 1999). IGOS's initiatives implies integration of different geodetic techniques, models, and approaches (Integrated Geosciences) to ensure long-term monitoring of the geodetic observables for a better understanding of the Earth. In addition, the g-dot solution extends the g-dot map of Canada produced by PAGIATAKIS & SALIB (2003) to the rest of the continent. This led to the production of the first of its kind g-dot map of North America. GIA signals are evident in Alaska, east Greenland and in the northern US. Signals shown in other regions are either noise or caused by geophysical processes other than GIA (e.g., tectonic movements) or manmade process (e.g., mining, oil extraction).

Systematic effects on the gravity measurements come from geophysical processes, such as solid Earth tides, ocean tide loading, hydrology and geodynamical processes, such as polar motion, crustal deformation and plate movements. In this research, we provided a scheme through which raw gravity measurements were processed (reduced) by removing systematic and gross errors. These gravity measurements are therefore an important contribution to IGOS as they are information product which can be used in decision making about the environment. Indeed they were used here by GRAVNET to investigate the rate of change of gravity across North America for the purpose of producing the g-dot map of the area. IGOS focuses on providing environmental information for decision making by collecting data (physical, chemical, biological, etc.) around the globe. It must be recognized that such data collection is not an end in itself but only become useful when they are processed and assessed to become information products (IGOS PARTNERS, 1999). There is therefore a need to process raw measurements, in this case, absolute and relative gravity measurements, by eliminating systematic effects and outliers.

Canada's NGDB is an important and reliable source of information for many geophysical and geodynamical investigations. As seen earlier, the Canadian Gravity Standardization Network (CGSN) comprises thousands of stations across the nation linked together by relative gravity measurements (gravity ties) whose primary purpose was to provide gravity reference for exploration geophysics. The Canadian National Gravity Data Base (NGDB) contains absolute and relative gravity measurements meticulously collected over the CGSN and selected USA and Greenland gravity stations over a span of more than 60 years. Although these measurements were not observed uniformly in time, they provide an adequate source of information for several geophysical investigations, such as g-dot determination as was the case in this work.

There will soon be a need to readjust the network and provide updated g-dot solutions. A software package, capable of systematically performing this adjustment was the outcome of this work. PREGRAVNET and POSTGRAVNET, developed in the course of this research, are important additions to GRAVNET as they respectively process measurements and solutions before and after the adjustment. These software constitute a significant contribution of this research. The CGSN is still being observed today, meaning that more gravity measurements of higher precision will soon be available. By the same token, geophysical models, such as Finite Element Solution (FES) and WaterGAP Global Hydrological Model (WGHM) are being refined as more measurements and/or methodologies are becoming available. In addition, if there is a need to provide g-dot solutions for other areas of the globe from historical gravity measurements, this software package will render the process considerably easier as it includes all the required steps of the process. Of course a few challenges, specific to the area of investigation and observational procedures, might arise.

It is also important to keep in mind that there existed no manual for GRAVNET prior to this work. An important contribution of this research was therefore a complete manual (APPENDIX A) of this powerful software. In the past, users were expected to study the software's script in order to obtain a general understanding of its functionality. This manual will therefore ease future use of GRAVNET.

ALI (2006) calculated the effect of gravity changes on geoid height (or geoid undulation) in Canada using GRAVSOFT software. With new g-dots available, this effect can be calculated for the rest of the landmass. In modern Geodesy, it is well known that geoid undulation (N) is not constant but varies by as much as a few millimetres per year. This variation is partly due to the rebound of land masses caused to melting ice sheet (GIA). The time rate of change of geoid undulation due to GIA (N-dot), is therefore more significant in some parts of the world (e.g., the northern hemisphere) than others (e.g., equatorial regions).

The NGDB contains terrestrial observations which, in this work, were used to study the effect of GIA on gravity. In addition, the establishment of the Global Navigation Satellite System (GNSS) comprising GPS, GLONASS, Galileo and BeiDou satellite constellations and the undertaking of gravity missions, such as

Gravity Field and Steady-State Ocean Circulation Explorer (GOCE) and Gravity Recovery and Climate Experiment (GRACE) are major advancement in the field of Space Geodesy. Amongst others, SHAHRISVAND ET AL., (2014) and ZOU ET AL., (2010) used satellite observations (GRACE mission) to study variations in gravity at different points on the globe. In an attempt to obtain a general understanding of the Earth and its geophysical processes, a combination of findings from both terrestrial and space observations is necessary.

7.2 FUTURE WORK

In order to obtain a complete g-dot signature of North America, future work could be geared towards selecting quality historical gravity measurements from stations located in Mexico. This will extend the network to Mexico thereby ensuring that all three major countries on the North American plate are covered. This work is currently underway.

The network was constrained at only ten (10) sites in Canada. Repeated absolute gravity measurements from additional stations in Canada as well as in Greenland, USA and eventually in Mexico are important to ensure reliable solutions from uniformly distributed gravity and g-dot constraints. Recall that many absolute stations existed in Canada, but only a few had the minimum number of useful observational epochs required to perform a reliable Weighted Least-Squares Regression (WLSR). Re-occupations of critical stations by absolute gravimeters is therefore imperative to improve the number and quality of constraints.

Also, a correlation analysis between the time rate of change of gravity (g-dot) and the time rate of change of heights (h-dot) obtained from Continuously Operating Reference Station (CORS) (NOAA, 2017), Canadian Base Network (CBN) (NRCAN, 2003), Canadian Active Control System (CACS) (NRCAN, 2016), benchmarks, and other height networks around North America could have proved useful in evaluating the results of the work presented here. We do not necessarily expect g-dot to vary linearly with heights as mass redistribution also influences g-dot but the ratio g-dot/h-dot which carries some geophysical information could be evaluated.

Furthermore, the time rate of change of geoid undulation, also called N-dot is an important component in today's geoid computation. Interested researchers can use results from this work to produce a N-dot map of North America.

Well-known regional tectonic deformations could be eliminated from the solution using crustal deformation maps and plate tectonic models providing a true GIA signature.

REFERENCES

Alcamo, J., P. Döll, F. Kaspar, and S. Siebert, Global Change and Global Scenarios of Water Use and Availability: An Application of WaterGAP 1.0. Report A9701, Centre for Environmental Systems Research, University of Kassel, Germany, 1997.

Ali, I. F. M., A Globally Consistent and Dynamic Canadian Gravity Reference Frame for a Modern Heighting System and other Applications, Graduate Program in Earth and Space Science, York University, Toronto, Ontario, 2006.

Barletta, V. R., R. Sabadini and A. Bordoni, Isolating the PGR Signal in the GRACE Data: Impact on Mass Balance Estimates in Antarctica and Greenland, *Geophysical Journal International*, 172(1), 18-30, 2008.

Booth, D. B., K. G. Troost, J. J. Clague, and R. B. Waitt, The Cordilleran Ice Sheet, *Developments in Quaternary Sciences*, 1, 17-43, 2003.

Bevis, M., J. Wahr, S. A. Khan, F. B. Madsen, A. Brown, M. Willis, E. Kendrick, P. Knudsen, J. E. Box, T. Dam, D. J. Caccamise II, B. Johns, T. Nylen, R. Abbotth, S. White, J. Miner, R. Forsberg, H. Zhou, J. Wang, T. Wilson, D. Bromwich, and O. Francis, Bedrock Displacements in Greenland Manifest Ice Mass Variations, Climate Cycles and Climate Change, *Proceedings of the National Academy of Sciences*, 109 (30), 11944-1948, 2012.

Chen, J. L., C. R. Wilson, and B. D. Tapley, Satellite Gravity Measurements Confirm Accelerated Melting of Greenland Ice Sheet, *Science*, 313 (5795), 1958-1960, 2006.

Creutzfeldt, B., A. Guntner, H. Wziontek, and B. Merz, Reducing Local Hydrology from High-Precision Gravity Measurements: A Lysimeter-Based Approach, *Geophysical Journal International*, 183, 178–187, 2010.

Doll P., F. Kaspar, and B. Lehner, A Global Hydrological Model for Deriving Water Availability Indicators: Model Tuning and Validation, *Journal of Hydrology*, 270(2003), 105–134, 2003.

Dyke, A. S., J. T. Andrews, P. U. Clark, J.H. England, G. H. Miller, J. Shaw, and J.J. Veillette, The Laurentide and Innuitian Ice Sheets during the Last Glacial Maximum, *Quaternary Science Reviews*, 21, 9–31, 2002.

Ekman, M., and J. Makinen, Recent Postglacial Rebound, Gravity Change and Mantle Flow in Fennoscandia, *Geophysical Journal International*, 126, 229– 234, 1996.

Farrell W.E. (1972)."Deformation of the Earth Under Surface Mass Loads." *Reviews of Geophysics and Space Physics, 10 (3),* 761-797.

Gong, X., X. Zhang, G. Lohmann, W. Wei, X. Zhang, and M. Pfeiffer, Higher Laurentide and Greenland Ice Sheets Strengthen the North Atlantic Ocean Circulation, *Climate Dynamics*, 45(1), 139–150, 2015.

Gordon, Q. R., The Climatic Record in Polar Ice Sheets, *Cambridge University Press*, 217 pp., New York, USA, 1983.

Gosnell, M., Ice: The Nature, The History and The Used of an Astonishing Substance, *The University of Chicago Press*, USA, 2007.

Gough, D. I., Mantle Upflow Tectonics in the Canadian Cordillera, *Journal of Geophysical Research*, 91(B2), 1909– 1919, 1986.

Hasan, S., P. A. Troch, J. Boll, and C. Kroner, Modeling the Hydrological Effect on Local Gravity at Moxa, Germany, *Journal of Hydrometeorology*, 7, 346-354, 2005.

Heiskanen, W.A., and H. Moritz, Physical Geodesy, *W. H. Freeman and Company*, San Francisco, 1967.

Hicks, S. D., Understanding Tides, Centre for Operational Oceanographic Products and Services, National Ocean Service, *National Oceanic and Atmospheric Administration (NOAA)*, 2006.

Hulton, N. R. J., R. S. Purves, R. D. McCulloch, D. E. Sugden, and M. J. Bentley, The Last Glacial Maximum and Deglaciation in Southern South America, *Quaternary Science Reviews*, 21, 233–241, 2002.

IGOS Partners, IGOS – Integrated Global Observing Strategy, United Nations (UN) Earthwatch, Retrieved October 28th, 2016, from URL: http://www.un.org/earthwatch/about/docs/igosstr.htm. Revised October 1999.

Johansson, J. M., J. L. Davis, H.-G. Scherneck, G.A. Milne, M. Vermeer, J.X. Mitrovica, R.A. Bennett, B. Jonsson, G. Elgered, P. Elósegui, H. Koivula, M. Poutanen, B.O. Rönnäng, and I.I. Shapiro, Continuous GPS Measurements of Postglacial Adjustment in Fennoscandia 1. Geodetic Results, *Journal of Geophysical Research*, 107 (B8), 2002.

Khan, S. A., A. Aschwanden, A. A Bjørk, J. Wahr, K. K. Kjeldsen, and K. H. Kjær, Greenland Ice Sheet Mass Balance: A Review, *Reports on Progress in Physics*, 78(4), 2015.

Khan, S. A., I. Sasgen, M. Bevis, T. Dam, J. L. Bamber, J. Wahr, M. Willis, K. H. Kjær, B. Wouters, V. Helm, B. Csatho, K. Fleming, A. A. Bjørk, A. Aschwanden, P. Knudsen, and P. K. Munneke, Geodetic Measurements Reveal Similarities Between Post–Last Glacial Maximum and Present-Day Mass Loss from The Greenland Ice Sheet, *Science Advances*, 2(9), 2016.

Kim, T. H., K. Shibuya, K. Doi, Yuichi Aoyama, and H. Hayakawa, Validation of Global Ocean Tide Models Using the Superconducting Gravimeter Data at Syowa Station, Antarctica, and in situ Tide Gauge and Bottom-Pressure Observations, *Polar Science*, 5(1), 21–39, 2011.

Koohzare, A., P. Vanicek and M. Santos, Pattern of Recent Vertical Crustal Movements in Canada, *Journal of Geodynamics*, 45, 133–145, 2008.

Krakiwsky, E. J., D. J. Szabo, P. Vanícek, and M. R. Craymer, Development and Testing of In-Context Confidence Regions for Geodetic Survey Networks. Final Contract Report for Geodetic Survey Division of Geomatics Canada, by the Department of Geomatics Engineering, The University of Calgary, the Department of Geodesy and Geomatics Engineering, the University of New Brunswick, and the Geodetic Survey Division of Geomatics Canada. Department of Geodesy and Geomatics Engineering Technical Report No. 198, University of New Brunswick, Fredericton, New Brunswick, Canada, 24 pp., 1999.

Kreemer, C, A.J. Haines, W.E. Holt, G. Blewitt, and D. Lavalée, On the Determination of a Global Strain Rate Model, *Earth Planets Space*, 52, 765-770, 2000.

Kroner, C., T. Jahr, M. Naujoks and A. Weise, Hydrological Signals in Gravity – Foe or Friend?, *Dynamic Planet*, 504 – 510, 2007.

Lambert, A., Billiyard, A.P., and S.D. Pagiatakis, (1991). Numerical representation of ocean tides in Canadian waters and its use in the calculation of gravity tides. *Bulletin International des Marées Terrestres,* Vol. 110, p. 8017.

Lambert, A., S. D. Pagiatakis, A. P. Billyard, and H. Dragert, Improved Ocean Tide Loading Corrections for Gravity and Displacement: Canada and Northern United States, *Journal of Geophysical Research*, 103(B12), 30,231-30,244, 1998.

Lampitelli, C., and O. Francis, Hydrological Effects on Gravity and Correlations Between Gravitational Variations and Level of The Alzette River at The Station of Walferdange, Luxembourg, *Journal of Geodynamics*, 49(1), 31–38, 2010.

Le Provost, C., F. Lyard, J. M. Molines, M. L. Genco, and F. Rabilloud, A Hydrodynamic Ocean Tide Model Improved by Assimilating a Satellite Altimeter-Derived Data Set, *Journal of Geophysical Research*, 103 (C3), 5513–5529, 1998.

Leirião, S., X. He, L. Christiansen, O. B. Andersen, and P. Bauer-Gottwein, Calculation of the Temporal Gravity Variation from Spatially Variable Water Storage Change in Soils and Aquifers, *Journal of Hydrology*, 365(3-4), 302–309, 2009.

Lidberg, M., J. M. Johansson, H.-G. Scherneck, and G. A. Milne, Recent Results Based on Continuous GPS Observations of the GIA Process in Fennoscandia from BIFROST, *Journal of Geodynamics*, 50(1), 8-18, 2010.

Lougheed, S. C., and N. Morrill, Quaternary History of Eastern Ontario: Impacts on Physical Landscape and Biota, Department of Biology, Queen's University, Retrieved December 2nd, 2016, from URL: https://opinicon.wordpress.com/physical-environment/quaternary/.

Matson, P. A., T. Dietz, W. Abdalati, A. J. Busalacchi, K. Caldeira, R. W. Corell, R. S. Defries, I. Y. Fung, S. Gaines, G. M. Hornberger, M. C. Lemos, S. C. Moser, R. H. Moss, E. A. Parson, A. R. Ravishankara, R. W. Schmitt, B. L. Turner, W. M. Washington, J. P. Weyant, and D. A. Whelan, Advancing The Science of Climate Change, Division on Earth and Life Studies, National Research Council of The National Academies, The National Academies Press, Washington, D.C., 2010.

Merriam, J., GWAVE, The University of Saskatchewan, 1994.

Mikolaj, M., B. Meurers, and M. Mojzeš, The Reduction of Hydrology-Induced Gravity Variations at Sites with Insufficient Hydrological Instrumentation, *Studia Geophysica et Geodaetica*, 59, 2015.

Mitrovica, J. X., J. L. Davis, and I. I. Shapiro, A Spectral Formalism For Computing Three-Dimensional Deformations Due To Surface Loads. 2. Present-Day Glacial Isostatic Adjustment, *Journal of Geophysical Research*, 99(B4), 7075-7101, 1994.

National Oceanic and Atmospheric Administration (NOAA), Continuously Operating Reference Station (CORS), NOAA, National Geodetic Survey, Retrieved February 18, 2017, from URL: https://www.ngs.noaa.gov/CORS/. Revision: February 16, 2017.

National Oceanic and Atmospheric Administration (NOAA), What are tides?, National Oceanic and Atmospheric Administration, Retrieved March 9th, 2016, from URL: http://oceanservice.noaa.gov/facts/tides.html. Revision: February 06, 2015.

National Oceanic and Atmospheric Administration (NOAA), What is Geodesy? – National Oceanic and Atmospheric Administration, Retrieved January 9th, 2016, from URL: http://oceanservice.noaa.gov/facts/geodesy.html. Revision: February 07, 2015.

Natural Earth, Internal Administrative Boundaries, Natural Earth, Retrieved June 21st, 2016, from URL: http://www.naturalearthdata.com/downloads/10m-cultural-vectors/10m-admin-1-states-provinces/. Revision: October 07, 2013.

Natural Resources Canada (NRCan), Canadian Base Network - Level 1, Natural Resources Canada, Earth Sciences, Geodetic Survey Division, Retrieved February 18, 2017, from URL: http://geogratis.gc.ca/api/en/nrcan-rncan/ess-sst/09fd34ee-22eb-431b-b4a6-99a828199f14.html#distribution. Revision: November 19, 2003.

Natural Resources Canada (NRCan), The Canadian Spatial Reference System (CSRS), Natural Resources Canada, Earth Sciences, Geodetic Survey Division, Retrieved February 18, 2017, from URL: http://www.nrcan.gc.ca/earth-sciences/geomatics/geodetic-reference-systems/9052. Revision: August 30, 2016.

Naujoks, M., C. Kroner, A. Weise, T. Jahr, P. Krause and S. Eisner, Evaluating Local Hydrological Modelling by Temporal Gravity Observations and A Gravimetric Three-Dimensional Model, *Geophysical Journal International*, 182, 233–249, 2010.

Nielsen, E., G. Strykowski, R. Forsberg, and F.B. Madsen, Estimation of PGR Induced Absolute Gravity Changes at Greenland GNET Stations, Earth on the Edge: Science for a Sustainable Planet: *International Association of Geodesy Symposia*, 139, 97-102, 2014.

Noveltis, Legos and CLS Space Oceanography Division, FES2012 was produced by Noveltis, Legos and CLS Space Oceanography Division and distributed by Aviso, with support from CNES (http://www.aviso.altimetry.fr/), 2012.

Nykolaishen, L., H. Dragert, K. Wang, T. S. James, and M. Schmidt, GPS Observations of Crustal Deformation Associated with the 2012 Mw 7.8 Haida Gwaii Earthquake, *Bulletin of the Seismological Society of America*, 105, 2B, 2015.

Oches, E.A., Quaternary History, Earth System: History and Natural Variability, 2, 316-344, 2009.

Pagiatakis, S. D., and Salib P., Historical Relative Gravity Observations and the Time Rate of Change of Gravity Due to Post Glacial Rebound and other Tectonic Movements in Canada, *Journal of Geophysical Research*, 108(B9), 206-218, 2003.

Pagiatakis, S. D., Application of the Least-Squares Spectral Analysis to Superconducting Gravimeter Data Treatment and Analysis, *Eur. Cent. Geodynamic Sysmology*, 17, 103-113, 2000.

Pagiatakis, S. D., H. Yin, and M. A. El-Gelil, Least-Squares Self-Coherency Analysis of Superconducting Gravimeter Records in Search for the Slichter Triplet, *Physics of the Earth and Planetary Interiors*, 160(2), 108-123, 2007.

Pagiatakis, S. D., Ocean Tide Loading, Body Tide and Polar Motion Effects on Very Long Baseline Interferometry, Technical Report No. 92, University of New Brunswick, Fredericton, New Brunswick, 1982.

Pagiatakis S. D., Ocean tide loading on a self-gravitating, compressible, layered, anisotropic, viscoelastic and rotating Earth with solid inner core and fluid outer core, Technical Report No. 139, University of New Brunswick, Fredericton, New Brunswick, 1988.Pagiatakis, S. D., Stochastic Significance of Peaks in the Least-Squares Spectrum, *Journal of Geodesy*, 73(2), 67-78, 1999.

Pagiatakis, S. D., The response of a Realistic Earth to Ocean Tide Loading, *Geophysical Journal International*, 103, 541-560, 1990.

Peltier, W. R., Global Glacial Isostasy and the Surface of the Ice-Age Earth: The ICE-5G (VM2) Model and GRACE, *Annual Review of Earth and Planetary Sciences*, 32, 111-149, 2004.

Peltier, W. R., Ice Age Paleotopography, *Science*, 265, 195–201, 1994.

Pertsev, B. P., Tidal Corrections to Gravity Measurements, *Physics of the Solid Earth*, 43(7), 547-553, 2007.

Petit, G., and B. Luzum, IERS Conventions (2010), Technical Note No. 36, International Earth Rotation and Reference Systems Service, Frankfurt am Main, Germany, 2010.

Rangelova, E., and M. G. Sideris, Contributions of Terrestrial and Grace Data to the Study of the Secular Geoid Changes in North America, *Journal of Geodynamics*, 46, 3–5, 131–143, 2008.

Rangelova, E., W. van der Wal, A. Braun, M. G. Sideris, and P. Wu, Analysis of Gravity Recovery and Climate Experiment Time-Variable Mass Redistribution Signals over North America by Means of Principal Component Analysis, *Journal of Geophysical Research*, 112, F3, 2007.

Sato, T., S. Miura, W. Sun, T. Sugano, J. T. Freymueller, C. F. Larsen, Y. Ohta, H. Fujimoto, D. Inazu, and R. J. Motyka, Gravity and Uplift Rates Observed in Southeast Alaska and their Comparison with GIA Model Predictions, *Journal of Geophysical Research*, 117, B01401, 2012.

Schmid, H. H., and E. Schmid, A Generalised Least Squares Solution for Hybrid Measuring Systems, *Canadian Surveyor*, 19(1), 27– 41, 1965.

Scherneck, H.-G., J.M. Johansson, G. Elgered, J.L. Davis, B. Jonsson, G. Hedling, H. Koivula, M. Ollikainen, M. Poutanen, M. Vermeer, J.X. Mitrovica, and G.A. Milne, BIFROST: Observing The Three-Dimensional Deformation of Fennoscandia Ice Sheets, Sea Level and The Dynamic Earth; Geodynamic Series 29, *American Geophysical Union*, 2002.

Shahrisvand, M., M. Akhoondzadeh, and M. A. Sharifi, Detection of Gravity Changes Before Powerful Earthquakes in GRACE Satellite Observations, *Annals Of Geophysics*, 57(5), 2014.

Shepherd, A., E. R. Ivins, A. Geruo, V. R. Barletta, M. J. Bentley, S. Bettadpur, K. H. Briggs, D. H. Bromwich, R. Forsberg, N. Galin, M. Horwath, S. Jacobs, I. Joughin, M. A. King, J. T. M. Lenaerts, J. Li, S. R. M. Ligtenberg, A. Luckman, S. B. Luthcke, M. McMillan, R. Meister, G. Milne, J. Mouginot, A. Muir, J. P. Nicolas, J. Paden, A. J. Payne, H. Pritchard, E. Rignot, H. Rott, L. S. Sørensen, T. A. Scambos, B. Scheuchl, E. J. O. Schrama, B. Smith, A. V. Sundal, J. H. V. Angelen, W. J. V. Berg, M. R. V. Broeke, D. G. Vaughan, I. Velicogna, J. Wahr, P. L. Whitehouse, D. J. Wingham, D. Yi, D. Young, and H. J. Zwally, A Reconciled Estimate of Ice-Sheet Mass Balance, *Science*, 338(6111), 1183-1189, 2012

Sjoberg, L. E., P. Vanicek, and M. Kwimbere, Estimates of Present Rates of Land and Geoid Uplift in Eastern North America, *Manuscripta Geodaetica*, 15(5), 261-272, 1990.

Sella G. F., S. Stein, T. H. Dixon, M. Craymer, T. S. James, S. Mazzotti, and R. K. Dokka, Observation of Glacial Isostatic Adjustment in “Stable” North America with GPS, *Geophysical Research Letters*, 34(2), L02306, 2007.

Telford, W. M., L. P. Geldart, and R. E. Sheriff, Applied Geophysics, 2th edition, *Cambridge University Press*, New York, USA, 1990.

UN Department of Economic and Social Affairs, Population Division, World Population Prospects: The 2012 Revision. Retrieved July 24th, 2016, from URL: http://www.geohive.com/earth/area_top50.aspx. Revision: 2012.

Vanícek, P., and E. J. Krakiwsky, Geodesy: The Concepts, 2th edition, 697 pp., *Elsevier Science Publishers*, Amsterdam, Netherlands, 1986.

Velicogna I., and J. Wahr, Postglacial Rebound and Earth's Viscosity Structure from GRACE, *Journal of Geophysical Research*, 107(B12), 2376, 2002

Wahr, J. M., Deformation Induced by Polar Motion, *Journal of Geophysical Research*, 90(Bll), 9363-9368, 1985.

Wahr, J. M., H. DaZhong, and A. Trupin, Predictions of Vertical Uplift Caused by Changing Polar Ice Volumes on a Viscoelastic Earth, *Geophysical Research Letters*, 22(8), 977-980, 1995.

Wahr, J. M., and I. Velicogna, What Might GRACE Contribute to Studies of Post Glacial Rebound? *Space Science Reviews*, 108(1-2), 319-330, 2003.

Wells, D. E., and E. J. Krakiwsky, The Method of Least-Squares, Lecture Note 18, Department of Geodesy and Geomatic Engineering, University of New Brunswick, Fredericton, New Brunswick, 1971.

Wells, D. E., P. Vanicek, and S. D. Pagiatakis, Least-Squares Spectral Analysis Revisited, Technical Report No. 84, Department of Geodesy and Geomatic Engineering, University of New Brunswick, Fredericton, New Brunswick, 1985.

Worldatlas, Geography Statistics of United States of America, Worldatlas. Retrieved July 24th, 2016, from URL: http://www.worldatlas.com/webimage/countrys/namerica/us.htm. Revision: July 13, 2016.

Wu, P., Effects of Mantle Flow Law Stress Exponent on Postglacial Induced Surface Motion and Gravity in Laurentia, *Geophysical Journal International*, 148, 676–686, 2002.

Zou, Z., H. Lee, Z. Luo, and L. Xing, Seasonal Gravity Changes Estimated from GRACE Data, *Geodesy and Geodynamics*, 1(1), 57-63, 2010.

APPENDIX A

SOFTWARE PACKAGE

Written by

Franck Kapoko Kamtchang

February 2017

Section 1

Introduction

This is a manual for GRAVNET, software written by Dr. Spiros Pagiatakis to adjust the Canadian Gravity Standardization Network (CGSN). One of the outreaching goals of this research was to put in place a complete software package that could be used, not only to adjust and obtain g-dots over a gravity network but also to treat and preprocess raw data pre-adjustment. By this, we mean creating a software package that will use gravity measurements, in their raw form, correct for blunders or gross errors, evaluate their sufficiency or reliability in obtaining realistic g-dot solution, correct for systematic errors such as tides, tide loading, use them to obtain g-dot solutions, statistically analyze the residual in an attempt to determine questionable observation projects/instruments/years and finally make results available in a format that can easily be plotted by common commercial software packages.

GRAVNET is a Least-Squares adjustment software made up of 6 module that computes the time rate of change of gravity (g-dot) from repeated relative and absolute gravity measurements. PREGRAVNET and POSTGRAVNET, as the names indicate, were created to respectively treat the data before the adjustment and the results after the adjustment. These three software which form the complete package needed to reproduce the g-dot map from new models and/or measurements are described in SECTIONS 2, 3 and 4.

Section 2

PREGRAVNET

7.3 INTRODUCTION

PREGRAVNET consists of 3 modules that is, INPUTGRAVNET, TIDES and OCEAN LOADING.

7.4 MODULE 1 - INPUTGRAVNET

INPUTGRAVNET is a software designed to produce input files needed by GRAVNET that is, TIE, SPC and NX-1 files. The fact that these files are created from raw measurements brought up a few questions: Are these measurements blunder free? Is there sufficient data to reliably estimate g-dots across the region? These questions could only be answered by performing a pre-adjustment analysis of the data.

The first part of INPUTGRAVNET therefore aims at cleaning relative gravity observation by eliminating any possible gross error.

The second part of the software consist of a quality and quantity analysis of the data. It evaluates the number of absolute/relative stations and uniformity in their distribution; base class of stations; number of ties and uniformity in their distribution; range, repetition and spread of absolute gravity measurements; and range, repetition and spread of relative gravity measurements. Results from this analysis provides the user with a general overview of the data.

The last part of INPUTGRAVNET creates GRAVNET input files from measurements free of gross errors. G-dots are computed by casting all measurements, initial estimates to unknown parameters, and their standard deviations into a generalized Least-Square adjustment scheme via GRAVNET. This is done with the help of three input files SPC, TIE and NX-1. A SPEC file controls specifications such as scale factor of standard deviations, maximum number of iterations, significance level for statistical testing etc. for each adjustment. Input files from a previous adjustment can be obtained and augmented using corrected measurements from any source, e.g. the National Gravity Data Base (NGDB). Some parts of these files may require complete modifications while others may simply be augmented. INPUTGRAVNET was written to eases and automates the process thereby becoming a valuable addition to GRAVNET. This routine modifies and/or augments input files using data from any source (e.g. NGDB) in a specific format with set parameters.

INPUTGRAVNET is therefore a software capable of eliminating gross errors from a set of measurements and using it to create input files useful for GRAVNET.

7.5 MODULE 2 - TIDES

The second module consists of one software GWAVE. This is a gravity tide prediction program written in 1994 by J. Merriam at the University of Saskatchewan to remove the gravity tide signal from superconducting gravity meters. This module was therefore used to correct relative gravity measurements for ocean and body tides.

7.6 MODULE 3 – OCEAN LOADING

The third module consists of four software LOADSDP_LOAD, LOCAL, ADD and GENLOAD. LOADSDP_LOAD uses a direct access form of a global load model (e.g. FES2012) to compute amplitudes and phases of constituent tidal waves. LOCAL uses a local load model (if available) to compute amplitudes and phases of constituent tidal waves. These two phasor information are algebraically added by ADD and used by GENLOAD to compute load corrections.

Section 3

GRAVNET

3.1 INTRODUCTION

PAGIATAKIS & SALIB (2003) parameterized time rate of change of gravity (g-dot) into the mathematical model and used generalized Least-Squares adjustment to compute this factor at various stations from relative and absolute gravity measurements. Although originally created to adjust the CGSN, GRAVNET can be used on any network provided similar observations are available. The theory behind these thousands of lines of code is based on the method of Least-Squares adjustment illustrated by WELLS & KRAKIWSKY (1971).

GRAVNET consists of 6 modules, and 4 input files, SPECS.IN, .TIE, .SPC and NX-1.

3.2 INPUT FILES

GRAVNET consists 3 input files that is, **.TIE, **.SPC and NX-1 files and 1 specification file SPECS.IN. Each of these files is required and in a specific format for the program to run. These files and their formats will therefore be described in this sub-section.

3.2.1. SPECS.IN

In order to run the program, SPECS.IN needs to be filled in appropriately. This file contains project specifications including project title, input file names (note that both .TIE and .SPC must have the same names), a-priory variance factor, scale factor for standard deviation, level of significance for statistical testing etc.

3.2.2. **.TIE file

This is the observation file; each line represents a relative gravity measurement plus its metadata. This metadata includes project number, stations code, stations names, time and day each station was observed, instrument used, observation errors etc. written in the format presented in TABLE 1.

Table 1: Format for writing **.TIE file - file of relative gravity measurements.

Column No	Code	FMT	Description
2–8	PROJ	A7	Project number
14–21	BASE1	A8	Station number – Base1
23–25	DAY1	I2.2	Observation day – Base1
26-28	MTH1	A3	Observation month – Base1
30-33	YR1	I4	Observation year – Base1
35–36	HR1	I2	GMT observation hour – Base1
37-38	MIN1	I2	Observation min – Base1
57–64	BASE2	A8	Station number – Base2
66–67	DAY2	I2.2	Observation day – Base2
69-71	MTH2	A3	Observation month – Base2
73-76	YR2	I4	Observation year – Base2
78–79	HR2	I2	GMT observation hour – Base2
80-81	MIN2	I2	Observation min – Base2
100–104	INSTNO	A5	Instrument number
118–137	NAME1	A20	Station name Base1
139–158	NAME2	A20	Station name Base2
160–168	R1	F9.4	Dial1 readings in mGal
170-178	R2	F9.4	Dial2 readings in mGal
182-183	LETTER	A2	Letter code for the instrument scale factor
185-189	PP	F5.3	Estimated gravity difference error (mGal)
219-220	CODE	A2	Tie code

Note that the program assumes each observation has been corrected for significant systematic errors such as tides and ocean tide loading.

3.2.3. **.SPC file

This file contains initial approximations needed for the first iteration. This includes initial approximations to gravity values, g-dots, scales and drifts. It also contains initial approximations to g-dots errors and instrument drifts errors. Note that initial approximations to the gravity errors and instrument scales errors are not included in this file but provided in the NX-1 file (See SUB-SECTION 3.2.4). The SPC file is made up of two sections (or blocks); the first contains station informing (herein referred to as station block) and the second contains instrument information (herein referred to as instrument block).

Each line of the station block begins with the phrase “TRIAL GVALUE” while lines of the second block, instrument block, begin with the phrase “TRIAL SCALE”. The software requires that all lines of the station block first be written followed by all lines of the instrument block. The formats for writing each of these blocks are given in TABLE 2 and TABLE 3.

Table 2: Format for writing station block of **.SPC file – stations information

Column No	Code	FMT	Description
1-12	“TRIAL GVALUE”	A12	Lines of this block must begin with this descriptor
14-21	BASE	I8	Station number
23-33	G	F11.4	Initial gravity (mGal)
35	“;”	A1	Semi column
37-42	“G-DOT=”	A6	Descriptor
44-50	G-DOT	F8.5	Initial g-dot (mGal)
52-58	SIGMA_G-DOT	F7.5	Standard Deviation of initial g-dot(mGal)
60	“;”	A1	Semi column
62-86	BASENM	A25	Station name
88	CODE	A1	A=Alaska; C=Canada; G=Greenland; U=USA

*NOTE: Anything within quotation marks represents text and must be written as is.

Table 3: Format for writing Instrument block of .SPC file – instruments information

Column No	Code	FMT	Description
1-11	“TRIAL SCALE”	A11	Lines of this block must begin with this descriptor
14-29	CODE	A16	Instrument code (Inst+Inst letter+Proj #)
31-38	SCALE	F8.6	Initial scale
40-49	DRIFT	F10.5	Initial drift (mGal/a)
51-59	SIGMA_DRIFT	F9.5	Standard Deviation of initial drift (mGal/a)

*NOTE: Anything within quotation marks represents text and must be written as is.

3.2.4. NX-1 file

The first entry of the NX-1 file is the scale factor of the a-priori variance factor. The next lines make up an upper triangular matrix containing the variances and covariances of initial approximations to gravity and initial scale. The first column represents variances and the remaining columns represent covariances. Variances of initial approximations to gravity are listed first followed by variances of approximations to scale factors.

3.3 SOFTWARE

The entire program (module 1 to 6) is based on the principle of Least-Squares, each module designed on to perform a particular step of the computation. Before we describe what each module does, we will first review the principle on which this routine is based.

3.3.1. Theory

The theory behind the thousands of lines of code is based on the method of Least-Squares adjustment illustrated by WELLS & KRAKIWSKY (1971). PAGIATAKIS & SALIB (2003) used the non-linear combined adjustment with constraints approach to estimate g-dots from the following mathematical model

$$g_i^{t_0} - \dot{g}_i(t-t_0) - g_j^{t_0} + \dot{g}_j(t-t_0) - D_k^t \Delta t_{ij}^t - S_k^t \Delta g_{ij}^t = 0 \qquad (1)$$

where $g_i^{t_0}$ and $g_j^{t_0}$ are the gravity values at point i and j at reference epoch t_0; and $\dot{g}_i$ and $\dot{g}_j$ are time rate of change of gravity at i and j respectively.

The Least-Squares solution to this mathematical model is given by

$$\hat{\bar{x}} = -(A^T(BP^{-1}B^T)^{-1}A)^{-1}A^T(BP^{-1}B^T)^{-1}w + x^0 \qquad (2)$$

and estimated residuals

$$\hat{v} = -P^{-1}B^T(BP^{-1}B^T)^{-1}(A\hat{\bar{x}} + w) \qquad (3)$$

Following procedures from WELLS & KRAKIWSKY (1971) variables are obtained as:

$$A = \begin{bmatrix} -(t-t_0) & (t-t_0) & 1 & -1 & -\Delta t_{ij}^t & -\Delta g_{ij}^t \end{bmatrix} \qquad (4)$$

$$B = \begin{bmatrix} S_k^t \end{bmatrix} \qquad (5)$$

$$W = g_{i_0}^{t_0} - \dot{g}_{i_0}(t-t_0) - g_{j_0}^{t_0} - \dot{g}_{j_0}(t-t_0) - D_{k_0}^t \Delta t_{i_0 j_0}^t - S_{k_0}^t \Delta g_{i_0 j_0}^t \qquad (6)$$

$$C_{l_0} = \sigma_0^2 \begin{bmatrix} k_1 C_{\Delta g} & 0 \\ 0 & k_2 C_{x^0} \end{bmatrix} \qquad (7)$$

From which P can me computed as the inverse of C_l

$$x = \begin{bmatrix} g_i^{t_0} \\ \dot{g}_i \\ g_j^{t_0} \\ \dot{g}_j \\ D_k^t \\ S_k^t \end{bmatrix} \tag{8}$$

3.3.2. Modules

Each module contains part of the source code and should be executed sequentially from module 1 to module 6. The software was written this way to insure computational efficiency, which makes it particularly powerful as it can run even on small computer. Obviously, the author of GRAVET did not make use of the above notations when writing the software. The symbols used, thought slightly different, are self-explanatory. Some of them are given in TABLE 4

Table 4: Symbols used in GRAVNET to represent different symbols from the mathematical model

Literature Symbol	Software Symbol	Description
g_i^{t0}	G	Gravity
$\dot{g}_i$	GDOT	Rate of change of gravity
D_k^t	DRIFT	Instrumental drift
Δt_{ij}^t	DT	Diff in time btw measurements at the 2 stations
S_k^t	SCALE	Instrument Scale
Δg_{ij}^t	DG	Gravity difference
$(t - t0)$	DTY2K	Difference between current and reference epoch

The program also uses a few notations which are imperative in the description of this software;

USTN = Number of stations;
NS = Number of Instruments; and
NM = Number of ties

3.3.2.1. Module 1

Module 1 uses all input files and creates 6 intermediate files usable by other modules: OBSEQ.DAT, FCT.DAT, CL, BA, BCR, BCB and GRNET1.LOG.

A file that records events while the software runs (log file) is produced to track that status of the program and to ease debugging. The log file for module 1 is **GRNET1.LOG**

First, the software reads all input files and records all the information in a new files called **OBSEQ.DAT** in the following order – stations, instruments, ties. The number associated with each instrument is its position in the SPC file. Similarly, the number associated with each station in a tie is the station's position in the SPC file. During this process, it reads the scale factor for the errors in initial gravity and initial scales from the first line of the NX-1 and writes it into **FAC.DAT**

A file called **PROJ.REP** (where PROJ=name of input file) is created to store the number of ties, number of stations, number of instruments and a few linear combinations of these. The software uses variable CR to store the variances of delta g, drift and gdot obtained by squaring PP, SDRF and SGDOT from .TIE, .SPC and .SPC respectively and prints it in file **CL**

Next it computes the design matrices A and B using equations given above. These two matrices are printed in file **BA** in an augmented form [B | A]. B comes from only one variable (-Scale of instrument), therefore it has dimensions NM by 1. A on the other hand is a hypermatrix composed of 4 sub-matrices from 6 variables.

$$A = \begin{bmatrix} [-DT] & [\pm DTY2K] & [\pm 1] & [-DG] \end{bmatrix}$$

-DT is NM by NU since it's the product of the partial derivative of the scale (an instrumental attribute). Similarly, ±DTY2K is NM by USTN, ±1 is NM by USTN and –DG is NM by USTN. Therefore, A has dimensions NM by 2*(USTN+NS) or simply NM by NU while the augmented matrix BA has dimensions NM by NU+1. Note that for –DT and –DG each columns represents an instrument so only one column per row is filled (corresponding to the position of the instrument as given in OBSEQ). Also, each column of ±DTYK and ±1 represents a station and so 2 column per line (From station and To station) are filled according to the position of the base in the SPC file as given in OBSEQ

The software uses variable CX to store the standard deviations of initial gravity values and initial scales which, along with aforementioned CR are used to compute **BCR –** the product of the second design matrix and the covariance matrix of the observations. The last file created by module 1 is the M matrix **BCB**. This is the product of the second design and its transpose metricized by the covariance matrix of the observations.

3.3.2.2. Module 2

Module 2 uses SPECS.IN, BCB and PROJ.REP and creates M-1 and GRNET2.LOG. Recall that file BCB contains M produces by module 1. Module 2 reads this matrix, uses Cholesky Decomposition to compute its inverse and stores it in file **M-1**. The log file for module 2 is **GRNET2.LOG**.

3.3.2.3. Module 3

Module 3 uses SPECS.IN, BCR and PROJ.REP and creates CRB and GRNET3.LOG. Its sole purpose if to calculate the transpose of matrix BCR and stores it in file **CRB**. The log file for module 3 is **GRNET3.LOG**.

3.3.2.4. Module 4

Module 4 uses SPECS.IN, OBSEQ, BA, .TIE, FCT.DAT, M-1, CRB and PROJ.REP and creates L0, W, CBM, R, ADJL and GRNET4.LOG

Module 4 uses information from OBSEQ.DAT to create the observation hyper-vector which consists of relative gravity observations (delta G), initial drift, initial g-dot, initial G and initial scale (Pagiatakis & Salib, 2003). This vector is saved in file **L0.**

Next, it calculated the misclosure vector using the Equation (6) and saves it in file **W**. It goes on to form file **CBM** which contains a matrix obtained by multiplying the covariance matrix of observation, the second design matrix and the inverse of the M matrix. This constitutes the first part of the residual vector, v (see Equation (3)), the second being the misclosure vector W. The product of both produces the residual vector which is stored in **R**.

Adjusted estimated of unknowns are then computed by find the difference between the initial estimates and the residual vector and saved in file **ADJL**. The log file for module 4 is **GRNET4.LOG**.

3.3.2.5. Module 5

Module 5 uses NX-1, OBSEQ.DAT, .TIE, CL, BCR, PROJ.REP, CBM, R, ADJL and FCT.DAT, to create CRH, CXH, RES.DAT and GRNET5.LOG and modifies PROJ.REP

First, Module 5 computes the a-posteriori variance factor using residuals and covariance matrices from CL and NX-1. **PROJ.REP** is modified to include this factor. Next it computes the covariance matrix of residuals and saves it in file **CRH** and computes the covariance matrix of estimated parameters and saves it in file **CXH**. The log file for module 5 is **GRNET5.LOG**.

It now has all required info to print out file **RES**. The first block is an introductory block containing information about the project. The second block consist of adjusted gravity and g-dot initially computed and stored in file ADJL and their standard deviations computed from files CXH and CL/CRH respectively. The third block consists of adjusted instruments scaled and their standard deviations while the last block consists of adjusted drifts and their standard deviations.

3.3.2.6. Module 6

Module 6 creates STATS.DAT, NR.DAT and GRNET6.LOG. It computes the residuals, normalized residuals and saves them in **NR.DAT**. It performs a statistical analysis of the results from RES and saves it in file **STATS.DAT**. This includes distribution of residuals, chi-square goodness of fit test, chi-square test on variances list all outliers, in both the in-context and out-of-context sense. The log file for module 6 is **GRNET6.LOG**

Section 4

POSTGRAVNET

4.1 INTRODUCTION

POSTGRAVNET consists of only two modules: RESANALYSIS and PLOT.

4.2 MODULE 1 - RESANALYSIS

Residual ties provided in the STAT file post adjustment (see SECTION 3) could, upon additional analysis, be minimized without introducing bias to the solution. This is accomplished by RESANALYSIS which uses residual stations and residual ties to investigate the presence of common patterns amongst residuals, for example whether they were observed with the same instrument, or within the same project or year etc. This information is used to improve the covariance matrix of observation and obtain quality but most importantly unbiased solution.

4.3 MODULE 2 - PLOT

PLOT on the other hand is used to provide the solution in a format that can easily be plotted by commercial software such as ArcMap and Surfer. It performs simple statistical analysis of results over each excentre network, eliminates outlying solutions and computes g-dot over that network by averaging remaining solutions.

Section 5

CONCLUSION

Notice that the software package described above does not include a script to treat absolute gravity measurements. A support software whose role is to compute g-dot constraints, was also devised. This software consists of 2 modules LOADSDP_HYDROLOGY and LSSAv.2. The first module, LOADSDP-_HYDROLOGY, is used to correct absolute gravity observation for effects from ground water flow and surface water recharge that is, hydrological effects. LSSAv.2 suppresses any significant uncorrected periodic signal from the data and identifies the linear trend whose slope defines g-dot constraint and y-intercept defines gravity at reference epoch.

Interested readers can request this software package from the authors and run them sequentially to reproduce results shown here and/or produce an updated version based on newly available data and/or model**.**

APPENDIX B

G-DOT CONSTRAINTS COMPUTATION

Data obtained from Natural Resources Canada's (NRCan's) Canadian Gravity Data Base (CGDB) include 1705 absolute gravity measurements obtained from 154 absolute gravity stations on the Canadian Gravity Standardization Network (CGSN). After analysis of these observations, we notice that 99 stations (532 absolute gravity observations) are missing positional reference. Measurements from these stations are therefore removed from the set of measurements.

The first absolute gravimeter was purchased by the Canadian government in mid-1980s. At this time, field personnel had seldom been exposed to such an instrument making early observations questionable. For this reason, all observations obtained before 1990 are deemed unreliable and therefore not used in this work.

Further analysis shows that only 13 out of the remaining 55 stations have 5 or more epochs (years) of observations. Weighted Least-Squares Regressions (WLSR) normally only requires a minimum of three observations for an overestimated system but we consider a minimum of 5 in this work to ensure high accuracy.

Preliminary analysis shows that only measurements from 5 absolute stations define an observable linear pattern; usually after suppressing one or more periodic signal using LSSA. These stations are therefore the only ones used to constrain our network and include Calgary, Churchill, Nanoose, Ucluelet and Victoria. Below we describe how g-dot at each of these stations is obtained. According to field data, absolute gravity measurements were corrected for all systematic errors (tides and ocean tide loading). The technique used for such correction was unclear so we decided to also analyse each time series for periodic signals. Due to the non-uniformly distributed nature of the data, LSSA was used.

CALGARY

6 absolute gravity measurements were observed at Calgary station after 1990. Preliminary analysis shows that 1 of these observations is an outlier as it is significantly off the linear trend defined by the other measurements. The remaining 5 observations observed between 2002 and 2008 are plotted against time and shown in Figure 1.

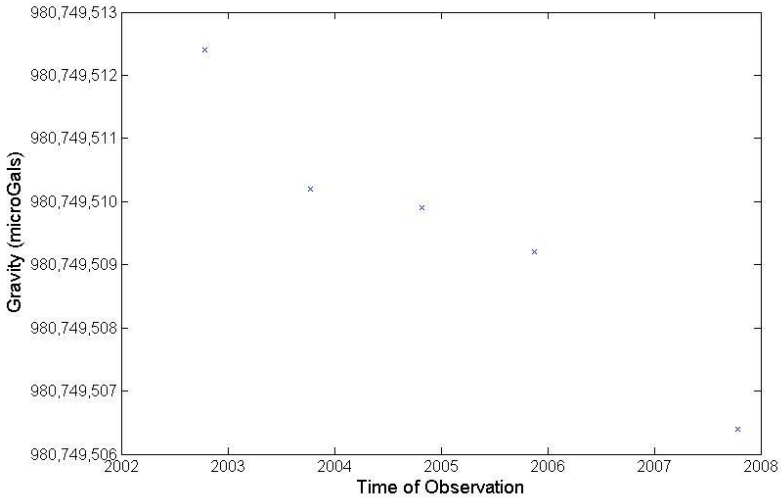

Figure 1: Five absolute gravity observations obtained over Calgary Station

Upon analysing the series using LSSA, no significant signal is observed. WLSR is used to determine the line of best fit (in the Least-Square sense using weights). Results are shown in Figure 2.

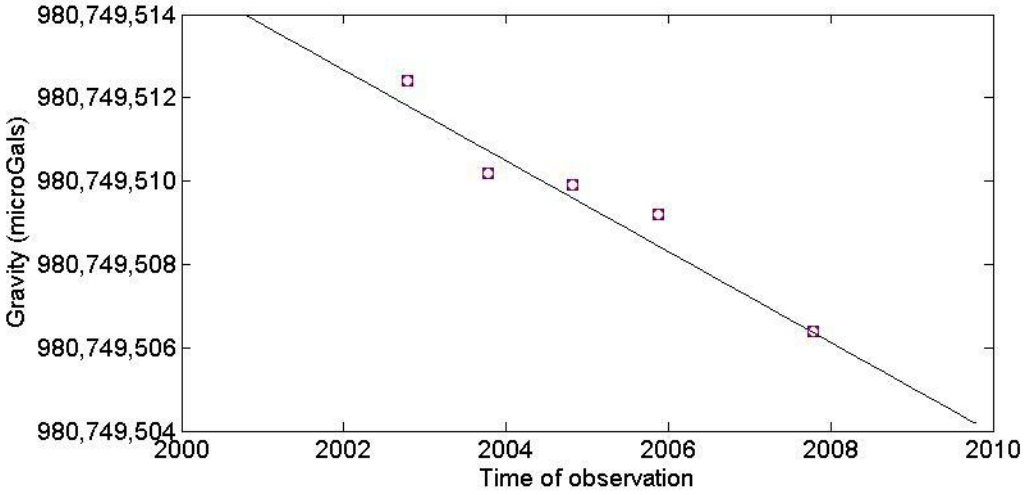

Figure 2: Plot of absolute gravity observations (red circles in blue squares), and Weighted Least-Squares fit (black line) against time for Calgary station.

Figure 2 shows that Weighted Least-Squares fit of absolute gravity measurements defines a downward sloping line (negative g-dot) representing uplift in areas around Calgary. Results are summarized below

No of years of observation	= 5 years
G-dot	= -1.09 μGal

Standard deviation of g-dot	= 0.026 µGal
A-posteriori variance factor	= 0.34
R^2	= 0.94

R^2 shows a very good fit although the a-posteriori variance factor shows a poor fit of the data. The difference between these two factors is due to the fact that standard deviations are taken into account when describing the nature of the fit using a-posteriori which is not the case when R^2 is used.

CHURCHILL

23 absolute gravity measurements were observed at Churchill station after 1990. Preliminary analysis shows that 6 of these measurements are outlier as they are significantly off the linear trend created by majority of the measurements. The remaining 17 observations observed between 1990 and 2004 are plotted against time and shown in Figure 3 below.

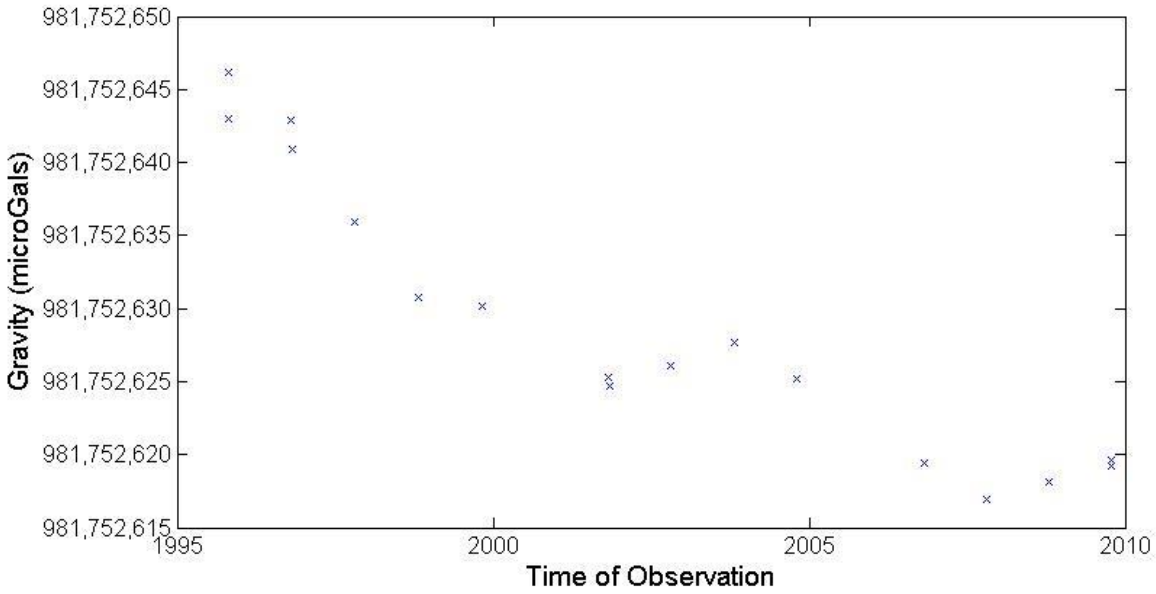

Figure 3: Seventeen absolute gravity observations obtained over Churchill Station

Upon analysing the series using LSSA, one significant signal is observed with period 1.00 years and amplitude 46.89 µGal. After suppressing this signal, WLSR is used to determine the line of best fit from corrected observations. Results are shown in Figure 4.

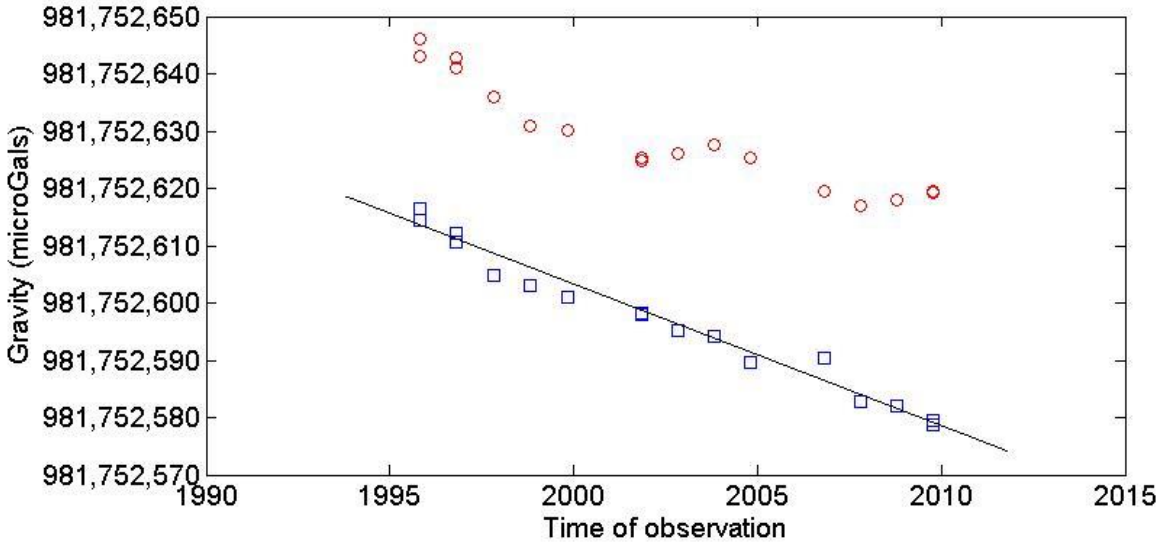

Figure 4: Plot of absolute gravity observations (red circles), corrected absolute gravity observations (blue squares) and Weighted Least-Squares fit (black line) against time for Churchill station.

Figure 4 shows that corrected absolute gravity observations at Churchill show a significant improvement from uncorrected observations that is, they define a more linear pattern. Weighted Least-Squares fit of corrected data shows a downward sloping line (negative g-dot) representing uplift in areas around Churchill. Results are summarized below

No of years of observation	= 14 years
G-dot	= -2.47 µGal
Standard deviation of g-dot	= 0.15 µGal
A-posteriori variance factor	= 1.00
R^2	= 0.97

Both R^2 and a-posteriori variance factor show a very good linear fit.

NANOOSE

37 absolute gravity measurements were observed at Nanoose station after 1990. Preliminary analysis shows that 5 of these observations are outlier as they are significantly off the linear trend created by majority of these measurements. The remaining 32 observations observed between 1997 and 2007 are plotted against time and shown in Figure 5 below.

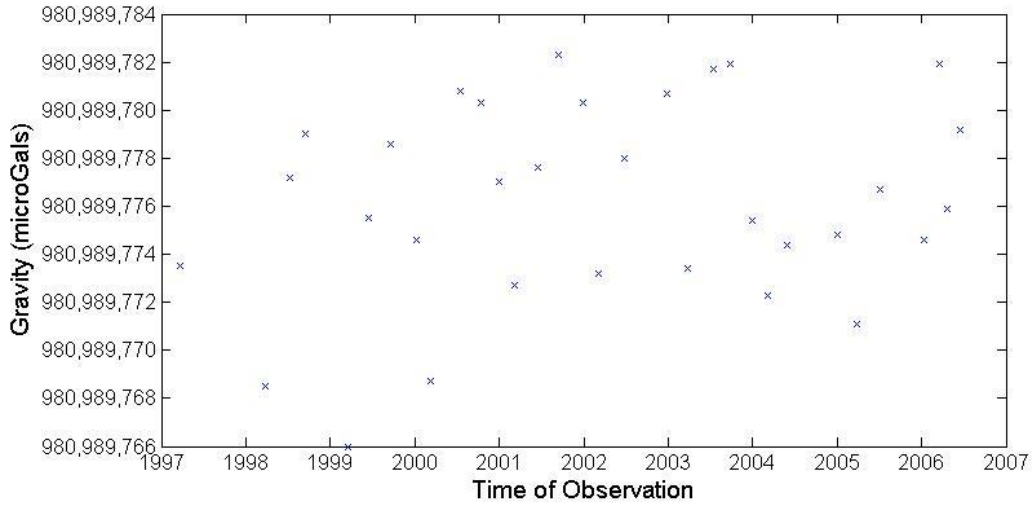

Figure 5: Thirty-two absolute gravity observations obtained over Nanoose Station

Upon analysing the series using LSSA, two significant signals are observed, one with period 1.00 years and amplitude 4.80 µGal and the other with period 5.42 years and amplitude 2.34 µGal. After suppressing these 2 signals, WLSR is used to determine the line of best fit from corrected observations. Results are shown in Figure 6.

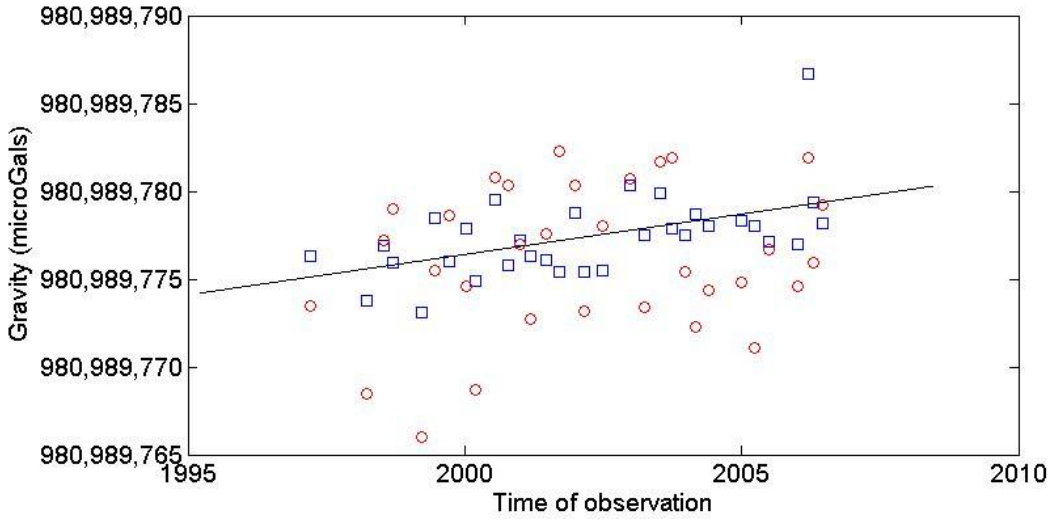

Figure 6: Plot of absolute gravity observations (red circles), corrected absolute gravity observations (blue squares) and Weighted Least-Squares fit (black line) against time for Nanoose station.

Figure 6 shows that corrected absolute gravity observations at Nanoose show a significant improvement from uncorrected observations that is, they define a more linear pattern. Weighted Least-Squares fit of

corrected data shows an upward sloping line (positive g-dot) representing subsidence in areas around Nanoose. Results are summarized below

No of years of observation	= 9 years
G-dot	= 0.46 µGal
Standard deviation of g-dot	= 0.12 µGal
A-posteriori variance factor	= 1.5
R^2	= 0.29

R^2 and a-posteriori variance factor both show a good fit. The difference between these two factors is due to the fact that weights (or rather standard deviations) are taken into account when describing the nature of the fit using a-posteriori which is not the case when R^2 is used.

UCLUELET

63 absolute gravity measurements were observed at Ucluelet station after 1990. Preliminary analysis shows that 2 of these observations are outlier. The remaining 61 observations observed between 1996 and 2008 are plotted against time and shown in Figure 7 below.

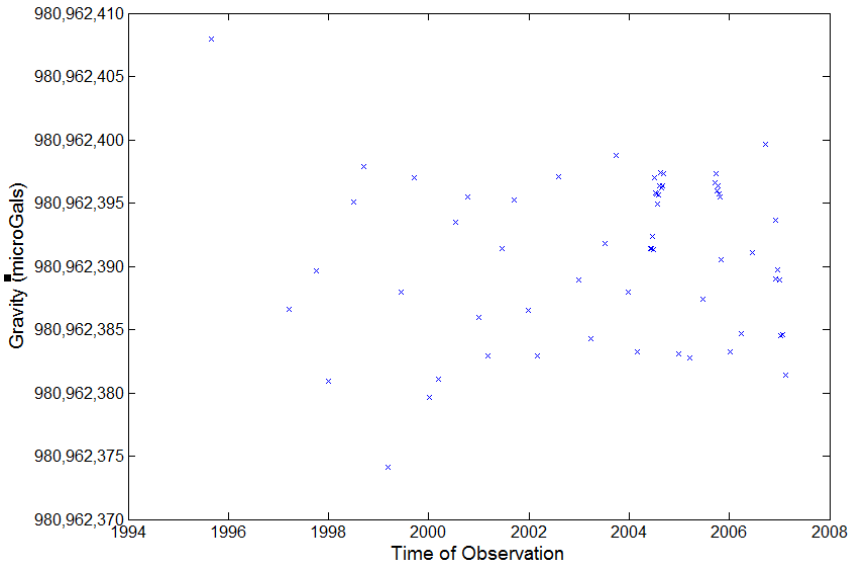

Figure 7: Sixty-one absolute gravity observations obtained over Ucluelet Station

Upon analysing the series using LSSA, one significant signal is observed with period 1.01 years and amplitude 70µGal. After suppressing this signal, WLSR is used to determine the line of best fit. Results are shown in Figure 8.

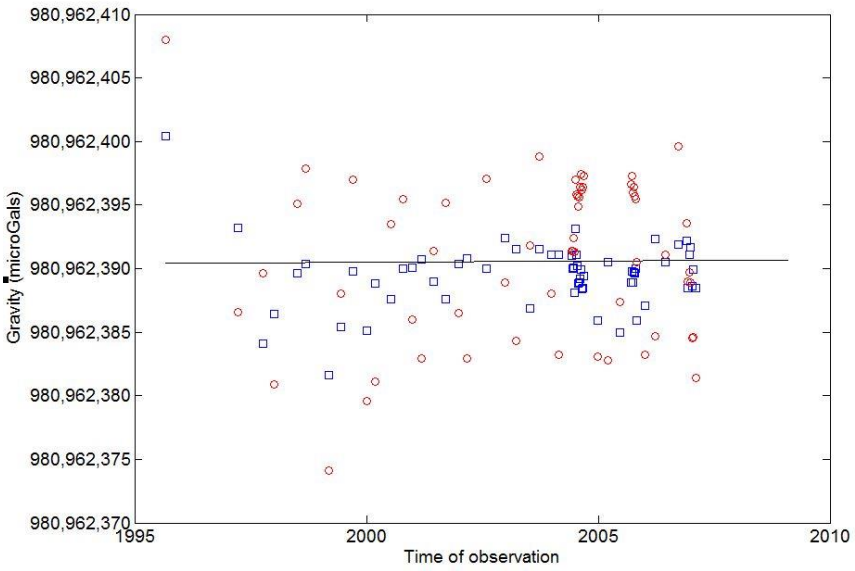

Figure 8: Plot of absolute gravity observations (red circles in blue squares) and Weighted Least-Squares fit (black line) against time for Ucluelet station.

Figure 8 shows that corrected absolute gravity observations at Ucluelet show a significant improvement from uncorrected observations that is, they define a more linear pattern. Weighted Least-Squares fit of this time series shows an upward sloping line (positive g-dot) representing subsidence in areas around Ucluelet. Results are summarized below

No of years of observation	= 10 years
G-dot	= 0.02 µGal
Standard deviation of g-dot	= 0.08 µGal
A-posteriori variance factor	= 2.29
R^2	= 0.00

Both R^2 and a-posteriori variance factor shows very a poor fit of the data. No additional information was available to further investigate.

VICTORIA

147 absolute gravity measurements were observed at Victoria station after 1990. Preliminary analysis shows that 3 of these observations are outlier as they are significantly off the linear trend. The remaining 144 measurements obtained between 1990 and 2004 are plotted against time and shown in Figure 9 below.

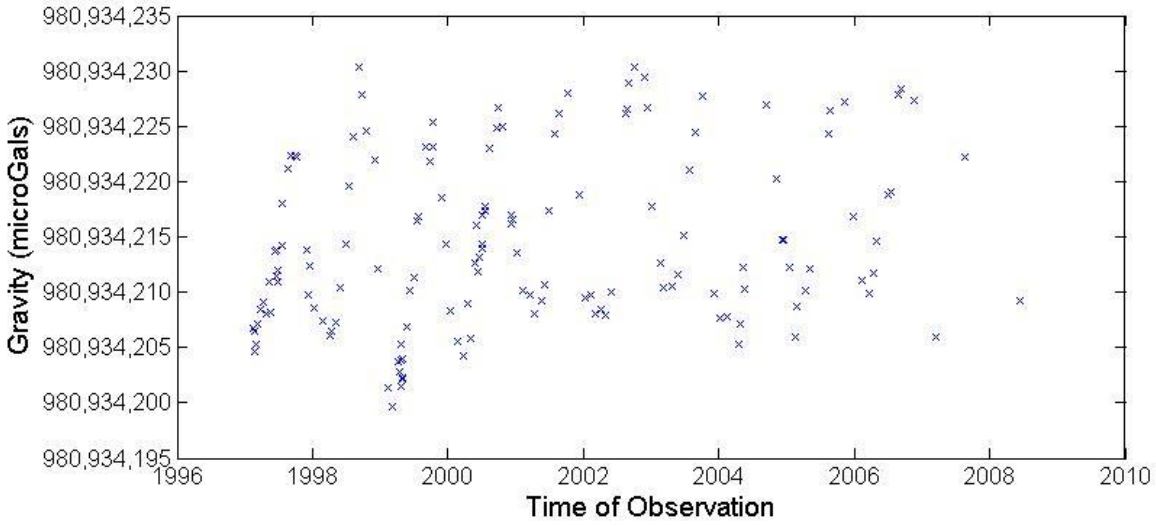

Figure 9: One hundred and forty-four absolute gravity observations obtained over Victoria Station

Upon analysing the series using LSSA, one significant signal is observed with period 1.00 years and amplitude 9.77 µGal. After suppressing this signal, WLSR is used to determine the line of best fit. Results are shown in Figure 10.

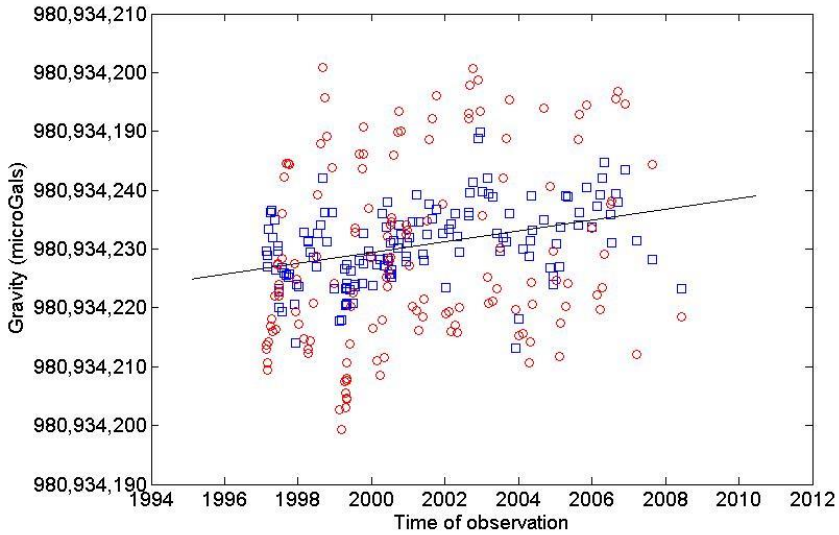

Figure 10: Plot of absolute gravity observations (red circles), corrected absolute gravity observations (blue squares) and Weighted Least-Squares fit (black line) against time for Victoria station.

Figure 10 shows that corrected absolute gravity observations at Victoria show a significant improvement from uncorrected observations that is, they define a more linear pattern. Weighted Least-Squares fit of corrected data shows an upward sloping line (positive g-dot) representing subsidence in areas around Victoria. Results are summarized below

No of years of observation	= 11 years
G-dot	= 0.46 µGal
Standard deviation of g-dot	= 0.05 µGal
A-posteriori variance factor	= 3.08
R^2	= 0.17

R^2 and the a-posteriori variance factor show a poor fit of the data.

APPENDIX C

ASSIGNING STANDARD DEVIATIONS TO OBSERVATIONS

In order to assign reliable standard deviation, each instrument (instrument code) was assigned a factor, representing the standard deviation of observations obtained within an hour. This factor was doubled for observations obtained within 12 to 24 hours. Linear variation was assumed for ties observed within 1 to 12 hours. This was rule of thumb used by Pagiatakis & Salib (2003) and hence adopted here. Ties observed in over 24hours were assigned a standard deviation of 500μGal. These overnight ties usually necessitated flying the instrument from one station to another, probably causing perturbations within the instrument, hence the huge number. This can be summarized in the following piecewise function

$$std\_dev = \begin{Bmatrix} factor & for & \Delta t < 1 \\ \left[\frac{1}{11}\Delta t + \frac{10}{11}\right] * factor & for & 1 < \Delta t < 12 \\ 2 * factor & for & 12 < \Delta t < 24 \\ 500 & for & \Delta t > 24 \end{Bmatrix}$$

Where Δt represents time of observation in hours, time interval between reading 1 and reading 2.

Instruments used in the adjustment of the Canadian network were assigned the same factors. 156 of such instruments were found and are given, along with the factors in the table below. On the other hand, all other instruments we assigned factors based on the type of instrument or its letter code

- D instruments were assigned a factor of 19μGal
- S and X instruments were assigned a factor of 28 μGal
- C and L instruments were assigned a factor of 21μGal
- G instruments were assigned a factor of 60μGal for ties observed in 1950 and 40μGal for ties observed in 1980 - linear variation was assumed between and beyond the two extremes.

#	Instrument	Factor (uGal)
1	C0132.H	0.021
2	D0006.B	0.019
3	D0006.C	0.019
4	D0006.E	0.019
5	D0027.B	0.019
6	D0027.D	0.019
7	D0028.A	0.019
8	D0028.B	0.019
9	D0110.B	0.019
10	G0007.B	0.046
11	G0007.C	0.046
12	G0007.D	0.042
13	G0007.E	0.046
14	G0007.F	0.036
15	G0009.A	0.044
16	G0009.B	0.036
17	G0009.C	0.041
18	G0009.D	0.035
19	G0009.E	0.021
20	G0028.A	0.037
21	G0028.B	0.043
22	G0028.C	0.025
23	G0028.D	0.024
24	G0028.E	0.027
25	G0038.A	0.058
26	G0039.A	0.041
27	G0039.C	0.024
28	G0074.A	0.027
29	G0074.B	0.038
30	G0074.C	0.036
31	G0074.D	0.031
32	G0074.E	0.022
33	G0074.F	0.022
34	G0074.G	0.019
35	G0074.H	0.018
36	G0074.I	0.019
37	G0074.K	0.019
38	G0074.L	0.017
39	G0074.M	0.025
40	G0075.B	0.046

#	Instrument	Factor (uGal)
41	G0075.C	0.042
42	G0075.D	0.046
43	G0075.E	0.045
44	G0075.F	0.036
45	G0075.G	0.036
46	G0075.H	0.041
47	G0075.J	0.023
48	G0075.K	0.023
49	G0088.B	0.039
50	G0088.C	0.040
51	G0088.D	0.025
52	G0109.A	0.023
53	G0112.B	0.041
54	G0172.C	0.041
55	G0172.D	0.041
56	G0172.E	0.027
57	G0172.F	0.023
58	G0172.G	0.023
59	G0172.H	0.026
60	G0172.I	0.021
61	G0172.J	0.024
62	G0173.A	0.036
63	G0173.B	0.041
64	G0173.C	0.036
65	G0173.D	0.036
66	G0173.E	0.024
67	G0173.F	0.024
68	G0173.G	0.024
69	G0173.H	0.025
70	G0234.A	0.023
71	G0237.A	0.026
72	G0255.B	0.041
73	G0255.C	0.036
74	G0255.D	0.042
75	G0255.E	0.041
76	G0255.F	0.024
77	G0255.G	0.024
78	G0255.H	0.021
79	G0255.I	0.019
80	G0256.A	0.039

#	Instrument	Factor (uGal)
81	G0256.C	0.041
82	G0256.D	0.027
83	G0256.E	0.024
84	G0256.F	0.021
85	G0256.G	0.021
86	G0278.A	0.039
87	G0278.B	0.042
88	G0278.D	0.041
89	G0278.E	0.041
90	G0278.F	0.023
91	G0278.G	0.024
92	G0278.H	0.024
93	G0278.I	0.022
94	G0278.J	0.025
95	G0278.K	0.025
96	G0282.A	0.036
97	G0291.A	0.033
98	G0291.B	0.022
99	G0291.C	0.018
100	G0291.D	0.020
101	G0291.E	0.020
102	G0291.H	0.018
103	G0291.I	0.017
104	G0294.B	0.043
105	G0294.C	0.024
106	G0294.D	0.024
107	G0329.A	0.037
108	G0329.B	0.041
109	G0333.A	0.042
110	G0386.B	0.035
111	G0393.A	0.024
112	G0416.A	0.041
113	G0417.A	0.042
114	G0417.C	0.021
115	G0431.A	0.033
116	G0431.C	0.021
117	G0431.D	0.018
118	G0431.E	0.019
119	G0431.F	0.019
120	G0431.G	0.019

#	Instrument	Factor (uGal)
121	G0444.B	0.040
122	G0444.C	0.025
123	G0444.D	0.022
124	G0444.E	0.021
125	G0444.F	0.019
126	G0498.B	0.041
127	G0498.C	0.021
128	G0498.D	0.021
129	G0498.E	0.021
130	G0504.A	0.024
131	G0504.B	0.024
132	G0586.A	0.024
133	G0611.A	0.023
134	G0617.A	0.024
135	G0626.A	0.023
136	G0626.B	0.024
137	G0727.A	0.019
138	G0790.A	0.024
139	G0790.B	0.024
140	G0790.C	0.023
141	G0790.D	0.024
142	G0790.F	0.025
143	G0792.A	0.020
144	G0932.A	0.023
145	G0932.B	0.021
146	G0932.E	0.023
147	L0001.A	0.021
148	S0056.F	0.028
149	X0054.B	0.022
150	X0054.C	0.024
151	X0054.G	0.012
152	X0054.I	0.025
153	X0141.A	0.023
154	X0197.B	0.012
155	X0197.C	0.024
156	X0197.D	0.025

APPENDIX D

RESIDUAL ANALYSIS

An analysis of residual outliers is conducted in an attempt to reduce the number of outliers and improved the g-dot solution. This report provides a summary of our findings and conclusions drawn as a results.

Residual outliers are analyzed based on a few characteristics including class of residual ties, instrument used, project and year of observation, and location of residual ties.

Base Class – More excentre stations appear in residual ties than any other base class. Also, more excentre stations are used in the network than any other. Consequently, there is a uniform distribution of residual station per number of station in each base class. Therefore, NO correlation observed between base class and residual ties.

Tie Class – There are more primary residual ties than secondary residual ties but there is a lot more primary ties than there are secondary ties giving secondary ties a higher (~double) proportion of residual ties to all ties. In fact, 42% of all residual ties are secondary ties (260 out of 625). This is problematic, further investigation is performed later. Secondary ties are tie involved at least 1 secondary station while in primary ties, no secondary station is involved.

Type of Tie – For A = Alaska station, C = Canada station, G = Greenland station, U = USA station, X = Constraint station, there are slightly more UU ties than CCs. Surprisingly, there are 37% more CC residuals outliers than UUs. This is probably due to the fact that CC ties include a lot of secondary ties.

INSTRUMENT TYPE

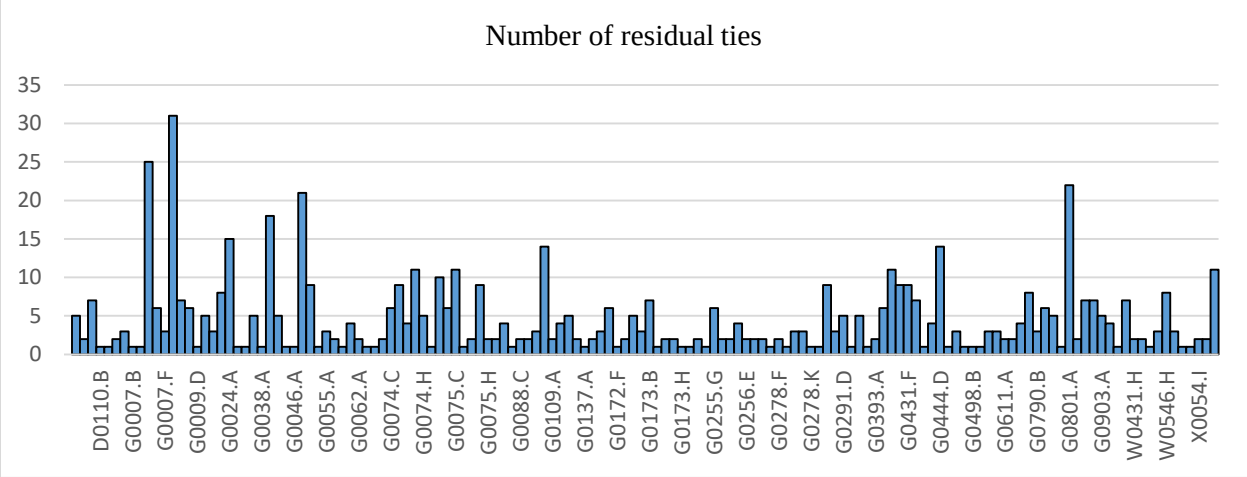

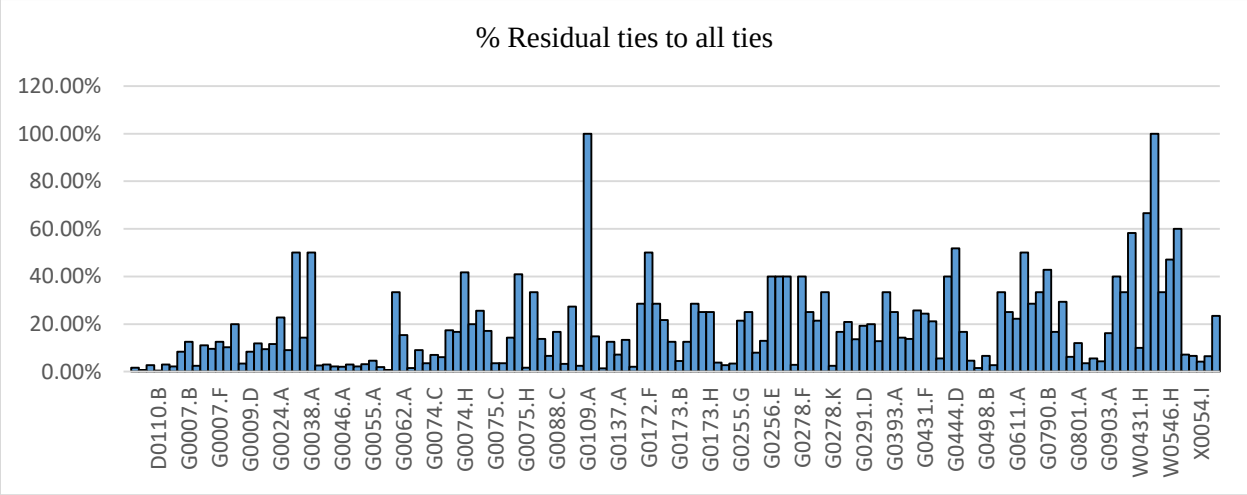

The 7 most recurring instruments (major peaks) in residual ties each form less than 25% the number of ties with which they were observed. The 8th, G0444.D was used to observe 27 ties, 14 of which are residual (i.e. 52% of ties observed with it are residual).

Rule of Thumb: An instrument was deemed questionable and required further evaluation if at least 5 residual ties were observed with it and at least 40% of all its ties were residual. Instruments requiring further analysis included:

- G0444.D
- G0075.G
- W0546.H
- W0431.A
- G0074.H

RESIDUAL ANALYSIS – **OBSEVATION YEAR**

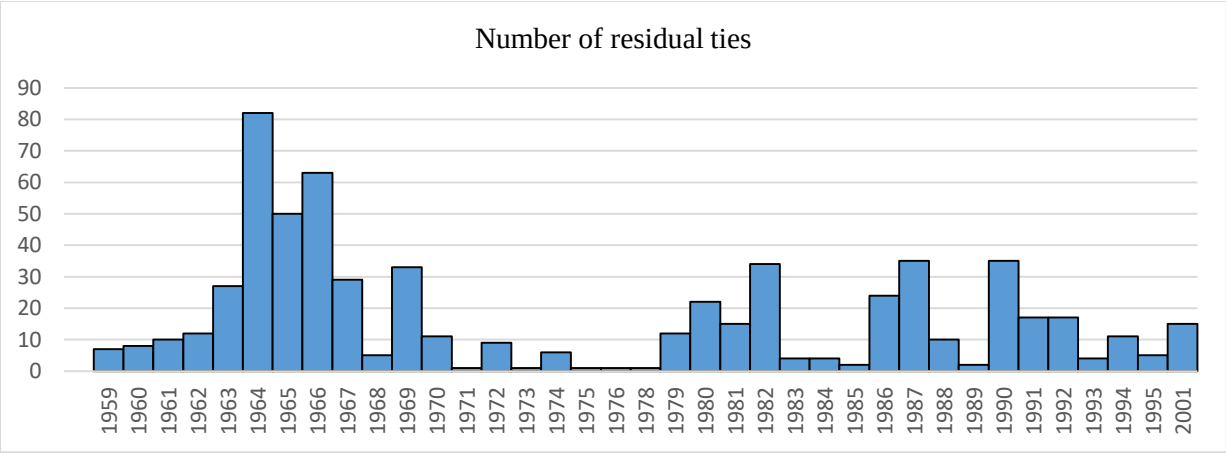

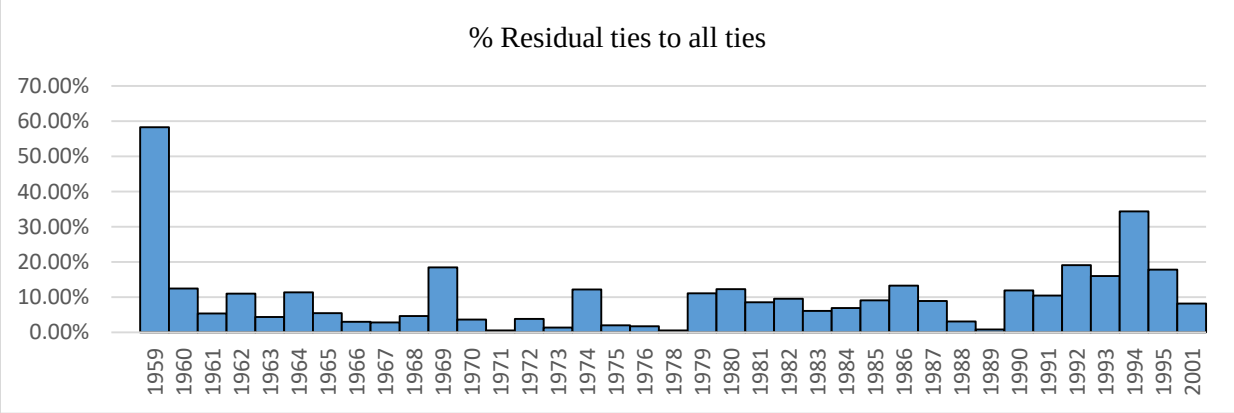

The years 1963 to 1967 together form 251 residual ties; that is about 40% of all residual ties. Similarly, 5337 tie were observed from 1963 to 1967 that is about 53% of all ties. Though the ratio of residual ties to all ties for each of these years was low, they are still worrisome and need to be looked at.

Rule of Thumb: A year was also deemed questionable if at least 5 residual ties were observed that year and at least 30% of all ties observed that year were residual. Two years were deemed questionable

- 1959
- 1994

RESIDUAL ANALYSIS – **PROJECT**

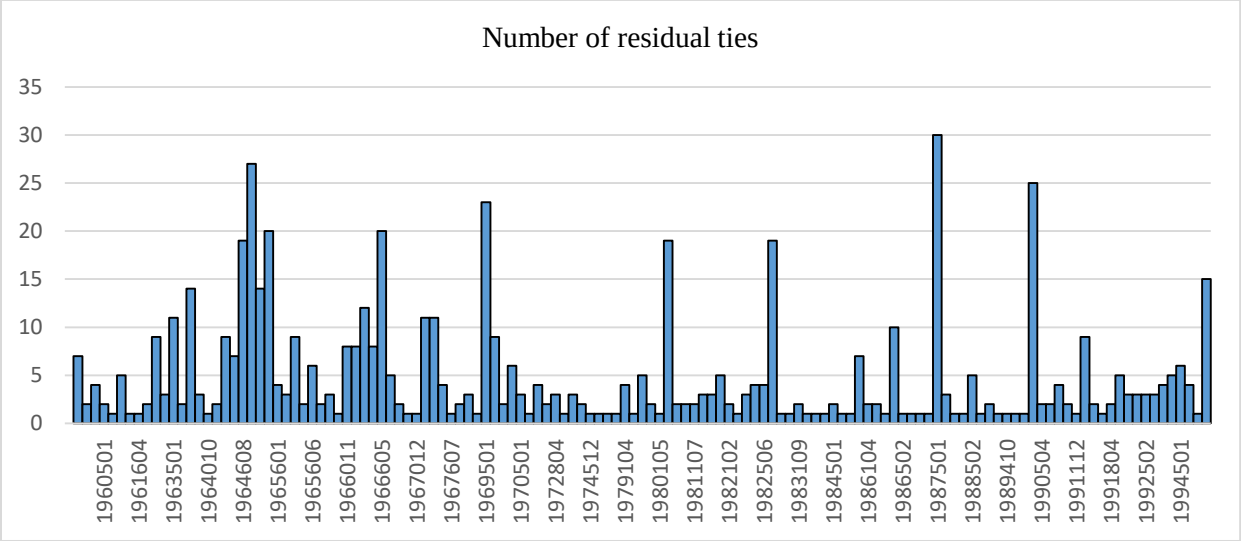

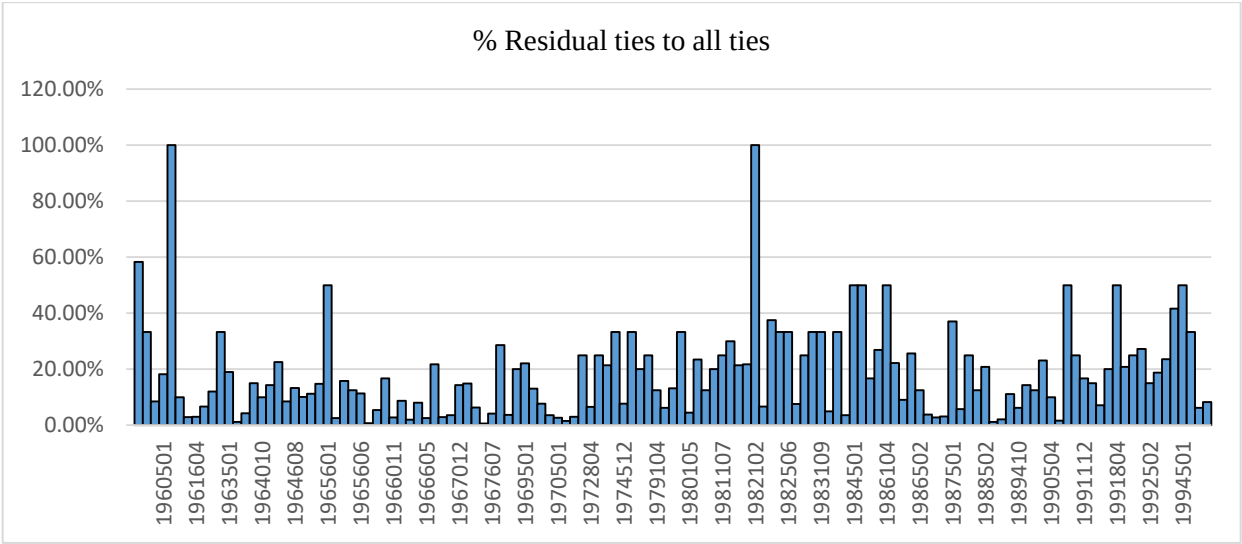

The most significant project is 1987501. It has more residual ties (30) that any other project. In addition, these residual ties make up over 37% of its ties.

Other questionable projects include

- 1959002 – 7 residuals of its 12 ties (58% residual ties). This is the oldest project on our network.
- 1994501 – 6 residuals of its 12 ties (50% residual ties).
- 1994104 – 5 residuals of its 12 ties (42% residual ties).

Note that the last 2 projects were carried out in the year 1994. Recall from above that 1994 was starred as questionable. Same with the first project which was carried out in questionable year1959

YEAR **1959**, PROJECT **1959002** & INSTRUMENT **W0431.A**

Facts:

- 1959 is the oldest year of observation
- 12 observations were taken this year, 7 of which were residuals – 58%
- ALL these observations, hence residuals, were observed with instrument W0431.A. These were the only observations taken with this instrument.
- ALL these observations, hence residuals, were from project 1959002. These were the only observations taken within this project.
- ALL these observations, hence residuals, were CC ties.
- ALL these observations, hence residuals, were secondary ties.

Analysis:

- Standard deviations for all 12 ties in mGal were as follows 0.035, 0.028, 0.035, 0.028, 0.192, 0.221, 0.145, 0.166, 0.233, 0.200, 0.187 and 0.163

Conclusion:

Notice that the first few standard deviations are less than 50µGals. It is not surprising that these are also the ties that appear amongst residuals after the adjustment. We conclude that these are not realistic standard deviations for secondary ties observed in the late 1950s with woorden instruments. ALL ties observed with the woorden instruments should have a standard deviation of at least 200µGals. This was already implemented on new ties and will now be implemented on CC ties. Correcting this produces 14 les residuals than before.

YEAR **1994** & PROJECTS **1994104** and **1994501**

Facts:

- 32 observations were taken this year, 11 of which were residuals – 34%
- ALL 1994 residuals, were from project **1994104** and **1994501**. These were the only residuals from these projects.
- 24 observations came from project **1994104** and **1994501**, 8 others came from projects 1994503 and 1994504.
- ALL 1994 residuals, were **CC** ties. 26 observations were **CC** ties, 6 were **GG** ties.
- ALL 1994 residuals, were **secondary** ties**.** 26 observations were **secondary** ties, 6 were **primary** ties**.**
- Distribution of residuals according to instruments is as shown on the right. Note that none of these instruments appear in the list of questionable instruments (see "residual analysis – instrument type" above)

Analysis:

- Standard deviations for all 32 ties in milliGals were as follows 0.008, 0.008, 0.008, 0.008, 0.008, 0.009, 0.009, 0.011, 0.012, 0.012, 0.012, 0.013, 0.013, 0.013, 0.013, 0.013, 0.013, 0.013, 0.013, 0.015, 0.020, 0.024, 0.025, 0.025, 0.047, 0.055, 0.119, 0.200, 0.200, 0.200, 0.200, and 0.350.
- Notice that the numbers are very low for **secondary** ties (ignoring a few, the average is roughly 15µGals).
- Note the 28 secondary CC ties have standard deviations of less than 0.015mGals – **20** of these ties were observed in 1994.

Conclusion:

Down weighing secondary ties did not produce significant change to the g-dot solution. There is therefore no correlation between residual outliers and year 1994, projects 1994104 and project 1994501 ties.

INSTRUMENTS: **G0444.D, G0075.G. W0546.H, W0431.A** & **G0074.H**

Facts:

- A total of 90 ties were observed by these 5 instruments, 43 of which are flagged residuals post adjustment.
    - G0444.D - 14 residuals from 27 ties (52%). Instruments used on 5 diff projects (amongst which 1987501), 4 from which we have residuals. ALL CC and CX secondary ties and primary (only 2) ties. Used in 1984, 1986 & 1987
    - G0075.G - 9 residuals from 22 ties (41%). Used only on project 1969501 and in 1969. CC, UU, AA & UC. Mostly primary ties, with a few secondary ties.
    - W0546.H - 8 residuals from 17 ties (47%). Used only on project 1967501 and in 1967. All primary UU, AA and UC ties and residuals.
    - W0431.A - 7 residuals from 12 ties (58%). Used only on project 1959002 and in 1959. All secondary CC ties and residuals.
    - G0074.H - 5 residuals from 12 ties (42%). Instruments used on 4 diff projects (amongst which 1987501), 2 from which we have residuals. ALL CC primary and secondary ties. Used in 1984, 1987 & 1988.

Conclusion:

Down weighing all ties from these instruments by 10 and 15% did not produce significant change to the g-dot solution both individually and collectively. There is therefore no correlation between residual outliers and ties from these 5 instrument.

PROJECT **1987501**

Facts:

- 81 observations taken under this project, 30 of which were residuals – 37%. This was the project with the largest number of residual ties.
- ALL observations, hence residuals, were obtained in 1987
- ALL project 1987501 observations, hence residuals, were **CC** ties.
- ALL project 1987501 observations, hence residuals, were **secondary** ties**.**
- Distribution of residuals according to instruments is as shown on the right. Note that **TWO (2)** of these instruments appear in the list of questionable instruments (see "residual analysis – instrument type" above), i.e., G0074.H and G0444.D

Conclusion:

Down weighing project 1987501 ties did not produce significant change to the g-dot solution. There is therefore no correlation between residual outliers and project 1987501 ties.

YEARS: **1963** to **1967**

No additional information available to treat this ties. We therefore conclude that there exist no correlation between residual outliers and ties observed between the years 1963 to 1967.

CANADA-CANADA TIES

No additional information available to treat this ties. We therefore conclude that that there exist no correlation between residual outliers and Canada-Canada ties.

SECONDARY TIES

We analyze instruments, projects, years and base classes for this set of residual outliers and discovered no correlations. We conclude that there exist no correlation between residual outliers and secondary ties and that the large number of secondary tie outliers is due to the fact that measurements to secondary stations

were of lower quality compared to other measurements on the network. The major peaks in instruments, projects or years are those already analyzed above

CONCLUSION

A low residual outlier count is a good indicator that realistic weights were assigned to the measurements. We therefore made an effort to eliminate residual outliers by relating them to a particular instrument, project, base class or year. Unfortunately, no clear correlation is observed between these characteristics and residual outliers. Consequently no further action is taken to reduce the number of outliers. Though tedious and time consuming, these tests prove to being very beneficial in verifying the quality of the solution. It is important to note that not a single observation is eliminated from the final adjustment.